Oleksandr Puchko

Multipoint Transmission Scheme for HSDPA

JYVÄSKYLÄN YLIOPISTO

Oleksandr Puchko

Multipoint Transmission Scheme for HSDPA

Esitetään Jyväskylän yliopiston informaatioteknologian tiedekunnan suostumuksella
julkisesti tarkastettavaksi yliopiston Agora-rakennuksen Lea Pulkkisen salissa
joulukuun 11. päivänä 2013 kello 12.

Academic dissertation to be publicly discussed, by permission of
the Faculty of Information Technology of the University of Jyväskylä,
in building Agora, Lea Pulkkinen´s hall, on December 11, 2013 at 12 o'clock noon.

UNIVERSITY OF JYVÄSKYLÄ

JYVÄSKYLÄ 2013

Multipoint Transmission Scheme for HSDPA

Oleksandr Puchko

Multipoint Transmission Scheme for HSDPA

UNIVERSITY OF JYVÄSKYLÄ

ABSTRACT

This thesis presents one of the multipoint transmission schemes for HSDPA, a scheme referred to as HS-SFN. This scheme can increase the peak data rate for the UEs in the softer handover area, or UEs that are located in the border between two cells belonging to the same Node B. The study also considers the techniques that can increase the performance of HS-SFN, such as the enhanced type3 receiver, phase adjustment and common intra-site scheduler. The HS-SFN study is carried by means of extensive system-level simulations employing a semi-static network simulation tool for HSDPA. The simulation tool includes detailed modeling of propagation model, radio resource management algorithms, physical layer and a part of the upper layers of HSDPA radio access network.

Keywords: Multipoint transmission , HS-SFN, Multiflow, Type3 receiver, phase adjustment, HSDPA, system performance, simulations

Author   Oleksandr Puchko
                     Department of Mathematical Information Technology
                     University of Jyväskylä
                     Finland

Supervisors   Professor Timo Hämäläinen
                     Department of Mathematical Information Technology
                     University of Jyväskylä
                     Finland

                     Dr. Alexander Sayenko
                     CTO, Industrial Environment
                     Nokia Siemens Networks,
                     Espoo, Finland

Reviewers   Professor Yevgeni Koucheryavy
                     Department of Electronics and Communication Engi-
                     neering
                     Tampere University of Technology
                     Finland

                     Professor Nickolay Smirnov
                     General Technical Department 2
                     Moscow Technical University of Communications and
                     Informatics
                     Russia

Opponent   Docent, Dr. Sergey Balandin
                     Tampere University of Technology
                     Finland

ACKNOWLEDGEMENTS

GLOSSARY

3GPP	3rd Generation Partnership Project
AMC	Adaptive modulation and coding scheme
C/I	Carrier to Interference ratio
CDMA	Code Division Multiple Access
CN	Core Network
CoMP	Coordinated Multipoint Transmission
CQI	Channel Quality Indicator
CS	Circuit Switched
CT	Core and Terminals
DL	Downlink
EDR	Estimated Data Rate
FDD	Frequency Division Duplexing
GGSN	Gateway GPRS Support Node
GMSC	Gateway Mobile Services Switching Centre
GPRS	General Packet Radio Service
GSM	Global System for Mobile Communications
HARQ	Hybrid Automatic Repeat Request
HLR	Home Location Register
HS-DDTX	High-Speed Data Discontinuous Transmission
HS-DSCH	High-Speed Downlink Shared Channel
HS-SFN	High-Speed Single Frequency Network
HSDPA	High-Speed Downlink Packet Access
ITU	International Telecommunication Union
LMMSE	Linear Minimum Mean Square Error
MAI	Multiple Access Interference
Max C/I	Maximum carrier to interference ratio
ME	Mobile Equipment
MIMO	Multiple Input Multiple Output
MSC	Mobile Services Switching Centre
OVSF	Orthogonal Variable Spreading Factor
PA	Phase Adjustment
PS	Packet Switched

QAM	Quadrature Amplitude Modulation
QoS	Quality of service
QPSK	Quadrature phase-shift keying
RAN	Radio Access Network
RNC	Radio Network Controller
RRM	Radio Resource Management
RX	Receive
SA	System Architecture
SI	Study Item
SINR	Signal to Interference plus Noise Ratio
SGSN	Serving GPRS Support Node
TB	Transmit Block
TDD	Time Division Duplexing
TSG	Technical Specification group
TTI	Transmission Time Interval
UE	User Equipment
UMTS	Universal Mobile Telecommunications System
USIM	UMTS Subscriber Identity Module
UTRAN	Universal Terrestrial Radio Access Network
VLR	Visitor Location Register
WCDMA	Wideband Code Division Multiple Access
WG	Working Group

LIST OF FIGURES

LIST OF TABLES

CONTENTS

1   INTRODUCTION

The development of wireless communication systems has been traditionally associated with improving the peak rate of individual users and increasing the overall system throughput. At the same time, it has become more and more evident that the cell edge performance is equally important. Quite a number of mobile users actually may stay at the cell edge area for fairly long periods of time generating or downloading significant amounts of data. The most typical example of such a scenario is mobile subscription used with a wireless modem in an office or home environment. Users at the cell borders are usually subject to low signal level due to strong path loss caused by the long distance to Node B or because their location is not in the cell's antenna beam direction. They also suffer from high interference from other sites in the network, resulting in aggregate signal energy reduction of up to dozens of decibels. As the center cell terminals enjoy good signal quality, the overall fairness of the network in uneven channel conditions declines. Failing to deploy techniques to help mobile users at the cell edge may lead to unfairness and/or inability to ensure the minimum QoS requirements as mandated by the subscription type.

1.1   Multipoint Transmission Schemes and related research work

The idea of solving the cell edge problem by coordinating transmission from several Node Bs is not novel for LTE-Advance technology, however for the HSPA this idea is quite new. The research on CoMP, as this multipoint transmission technique is referred to, was initiated under the LTE-Advance technology in March 2008 at the level of a study item (SI). In March 2010, the technology was specified in E-UTRA [3GPo], but after that the research was suspended until December 2010. Starting from 2011 many studies were published on CoMP in LTE-A, including [SKM+10], [XMX10] and [BZGA10]. Finally, LTE COMP was standardized in Rel-11 [3GPp].

Similar multipoint transmission techniques have been researched under

HSPA technology from December 2010, because enhancements for WCDMA based HSDPA are especially of interest for operators as the next generation mobile networks, such as LTE, are just starting to be rolled out, whereas HSPA is largest wireless mobile ecosystem that will remain the largest one for many years. The main concept of the multipoint transmission schemes for HSDPA, as the name tells, is to coordinate transmission of data from two or several cells to one UE simultaneously. Research on multipoint transmission schemes for HSDPA was started under the 3GPP in December 2010, as an official SI was initiated in January 2011 [3GPj], and in March 2011 two main schemes were proposed for further investigation: HS-SFN, the main topic of this thesis, and Multiflow. In the latter, data is also transmitted from two cells; however, the downlink transport block contains different data and can be transmitted independently. One additional scheme, HS-DDTX, is also explained in the following subsection.

1.1.1 High-Speed Data Discontinuous Transmission

High-speed data discontinuous transmission is one of the possible multipoint transmission schemes. The main idea behind this scheme is to remove the second best interferer by stopping the transmission from it. The simple theoretical equation for HS-DDTX transmission may be expressed as :

$$C/I = \frac{0.7 P_{own}}{\sum_{i=1}^{N} P_i - P_{own} - 0.7 P_{2nd}} \tag{1}$$

where i is cell number and N is the total number of cells. In this equation the power for control and pilot channels is assumed to be 30% while 70% is left for the data channel. This scheme was investigated in parallel with HS-SFN, but the gains from it was much lower compare to HS-SFN, because HS-SFN, in addition to the removal of interference for the own cell, can also bring gains from signals combining. The removal of interference for other cells, that happens only in HS-DDTX, has marginal effect on the results.

1.1.2 Multiflow

Multiflow is another of the possible multipoint transmission schemes. Multiflow can help cell edge UEs as they are able to receive data from two transmitting cells, located either in the same or different sites. In addition to almost doubled the peak data rate, Multiflow can increases the fairness by two ways. Firstly, low and medium throughput UEs at cell edge areas are able to receive data from two transmitting cells, located either on the same site or on different sites. In theory, these UEs may even double their throughput if the channel conditions to both cells are in balance. Secondly, load balancing between the cells is achieved, improving the cell edge UE's throughput and the utilization rate of the whole network.

As data blocks can be transmitted from two cells to a single user concurrently, the coexistent transmissions may highly interfere with each other if they

are scrambled with different codes. In order to mitigate this issue, the UE can use a type3i receiver with antenna diversity (and different RF receiver chains), which provides interference cancellation with a sub-chip level equalizer. This type of receiver is capable of calculating channel impulse response matrices from nearby interfering cells, thus minimizing the negative effect to aggregate Signal-to-Interference-plus-Noise ratio (SINR). [NKV07]

Gain mechanisms

The gain mechanism for UEs in the network with enabled Multiflow is two-fold. First, utilization of the second data stream increases per-UE data rates. The amount of extra throughput depends on the received signal strength ratio of the links and load levels of the cells. Second, Multiflow directly helps users at the cell borders: they are able to finish their data transfer events faster, offering increased opportunities to resource utilization for other users in the network. Since cell-edge users usually remain in the network for quite a long time due to high signal losses and inter-cell interference, reduction of their activity time in the network improves the system fairness.

A Multiflow-capable UE may be allocated resources from both cells in an Multiflow active set independently, which thereupon increases the utilization rate of low-load cells while enhancing scheduling opportunities for UEs in high-loaded cells. In consequence of the increased degree of freedom in scheduling, load balancing is a significant derivative of the multi-cell transmission concepts.

Flow control and signaling

A Multiflow-capable UE may receive different transport blocks over separate data flows, which means the HS-DSCH data needs to be divided for each cell participating in the transmission. At the receiver, an inverse operation is performed for merging the flows. There are two distinctive options for the location of the data split and combining and their adequacy is determined by the supported multi-cell Tx operation.

Intra-site Multiflow enables the use of fast data flow split on the MAC-ehs layer at the Node B, whereas for inter-site operation the split needs to be performed on the RLC layer in the Radio Network Controller (RNC) - see Figure 1. In HSDPA, there is no direct link for communication between Node Bs, thus the split operation in RNC is the only option for excluding a possible core network operation for inter-site Node Bs. [3GPc]

At the receiver side, two MAC-ehs entities are needed for the RLC PDU reception of the primary and secondary transmission, in case of inter-site Multiflow. Similarly, one MAC-ehs entity is sufficient if only intra-site Multiflow is supported by the network.

RNC is responsible for enabling and disabling Multiflow on user-by-user basis. It informs the UEs about the cells they should monitor and instructs them to produce correct Channel Quality Indication (CQI) feedback messages. The CQI feedback for the Multiflow operation generally follows the structure that was already defined for the multi-carrier HSDPA. It is the responsibility of the Node B scheduler to decide, based on the feedback messages, which cells may
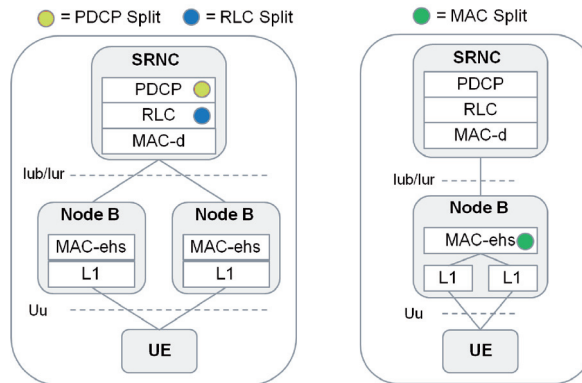
FIGURE 1   Data flow split options for Multiflow

participate in a Multiflow transmission. As for the other operations, higher-layer (L2, L3) signaling will support the activation of Multiflow as well as data flow control. In addition, Hybrid Automatic Repeat Request (HARQ) on the physical layer requires dedicated messaging between a UE and each participating cell.[dAKH$^+$09][3GPe]

1.2   3GPP

The 3GPP forum [3GPa] was created at the end of 1998 by the USA, Europe, South Korea and Japan (China joined soon after) with the intention to introduce a new single global standard for mobile communication based on the WCDMA technology. Figure 2 shows a timeline, which indicates release dates, including not only for the already existing releases, but also for releases that are expected to take place before June 2014.
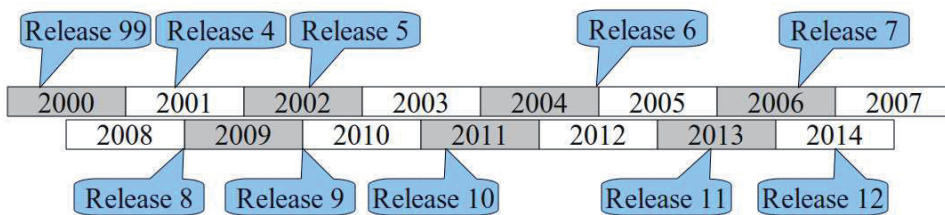
FIGURE 2   3GPP release timeline

The structure of the 3GPP forum is as follows:

– Technical Specification group(TSG) Radio Access Network (RAN), with the main focus on the radio interface, internal interfaces between Node B and

RNC, and interface from RNC to CN.
- TSG core and terminals (CT), with the main focuses including the core network, signaling between terminals and core network.
- TSG services and system architecture (SA), with the main focuses on the services and overall system architecture.
- TSG GSM/EDGE RAN (GERAN), with the main focuses the same as those of TSG RAN for the GSM/GPRS/EDGE-based radio interface.

Each TSG is divided into several working groups (WG). For example, TSG RAN has the following WGs:

- TSG RAN WG1 - physical layer or layer 1.
- TSG RAN WG2 - Layer 2 and 3.
- TSG RAN WG3 - RAN internal interfaces.
- TSG RAN WG4 - performance and radio frequency requirements.
- TSG RAN WG5 - terminal testing.

To understand this study better, it is good to keep in mind that it covers mostly the RAN1 aspects and a bit of RAN2.

1.3 Main contribution and outline

This work addresses the cell edge performance issues; in particular, it examines how to increase the peak data rate for UEs allocated at the cell edge. This work has been carried out under the project with Nokia Siemens Networks and some of its results were included into the 3GPP technical report on the multi-point transmission schemes [3GPd]. Based on the studies of this thesis, one patent was submitted in cooperation with researchers from Nokia Siemens Networks [HSH+12]. Almost all the results were previously published as articles while the studies on multipoint transmission schemes progressed. The main concept and first results are provided in [HPHC11]. Articles [PZH+11] and [PZH+12] present additional techniques, the so-called enhanced equalizer or enhanced type3 receiver and phase adjustment that can increase the performance in the use of HS-SFN. The work presented in [Puc12] in a way finalizes the HS-SFN study by providing extended results for HS-SFN with all the additional techniques under the different ITU channel models. One article [HPHC12] was written about another multipoint transmission scheme for HSDPA, so-called Multiflow. This thesis extends the previous research topics by adding more theoretical information, including explanation of combined intra-site scheduler, type3i receiver, and results analysis, including consideration of PedestrianA, PedestrianB and VehicularA ITU channel models. In addition to that, theoretical comparison of HS-SFN and Multiflow as well as new results of HS-SFN performance with six-sector site deployment were carried out in this thesis.

The rest of this thesis is structured as follows: Chapter 2 provides an introduction to the architecture of UMTS as well as to the concept and basic features of HSDPA. In addition to that, various UE receiver structures such as type3 and type3i, with their mathematical models are presented. The chapter also considers three main scheduling algorithms. Chapter 3 presents the main concept of the HS-SFN with additional techniques, including the enhanced type3 receiver, phase adjustment and common intra-site scheduler or so called combined scheduler, that can increase HS-SFN performance. In Chapter 4, two different simulators that were used in this thesis are presented together with the results achieved with them. Finally, Chapter 5 concludes this thesis.

2 HIGH SPEED DOWNLINK PACKET ACCESS

The main concept of HSDPA has been well described in [Hol06] and in [KPW$^+$03, PDF$^+$01]. A more detailed explanation of the physical layer aspects can be found in the 3GPP specification [3GPr] . This chapter presents the basic architecture of HSDPA as well as its particular features that were used in this study. The general structure of UMTS is presented in Subsection 2.1. Other key features of HSDPA such as HSDPA channels, link adaptation and HARQ are presented, respectively, in Subsections 2.2, 2.3 and 2.4. Subsections 2.5 and 2.6 present some well-known types of schedulers and receivers. These features are highly important for this dissertation: based on the knowledge of these, new types of schedulers for the multipoint transmission scheme performance were investigated and a new type of receiver was created especially for high-speed single frequency network scheme.

2.1 UMTS architecture

UMTS is a complete system architecture that was designed for flexible delivery of any type of services, where each new service does not require particular network optimization. Other important issues regarding UMTS are the backwards compatible handsets and signaling to support intermode (TDD to FDD and vice versa) and intersystem handoffs (UMTS to GSM or UMTS to LTE). UMTS network can be divided into three logical domains:

- UE that interfaces with the user;
- UTRAN that handles all radio-related functionalities;
- Core network (CN) that is responsible for transport functions, including switching and routing calls and data as well as tracking users.

Each of these logical domains can also be divided to smaller elements, as can be seen from Figure 3 that represents a UMTS architecture, where:
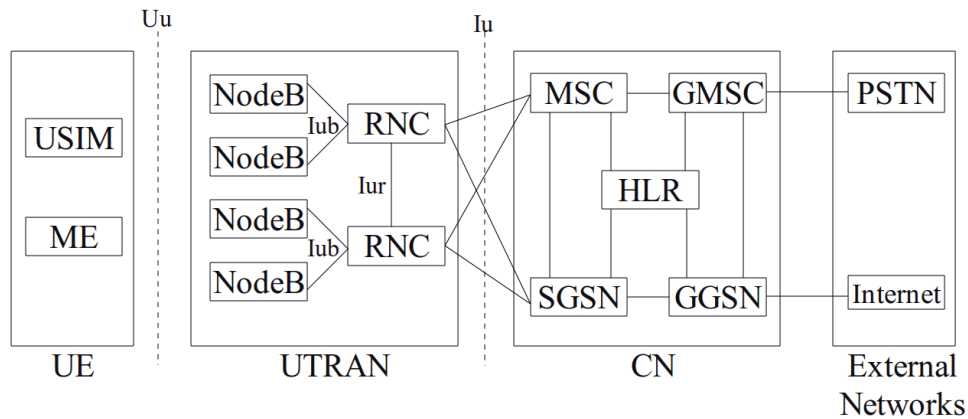
FIGURE 3   UMTS architecture

- Mobile Equipment (ME) - is a single or multimode terminal used for radio communication.
- UMTS Subscriber Identity Module (USIM) - is a smart card that holds the subscriber identity, subscribed services, authentication and encryption keys.
- Node B performs the air interface processing (channel coding, rate adaptation, spreading, synchronization, power control) and responsible for Radio Resource Management (RRM). It also can operate a group of antennas.
- Radio Network Controller (RNC) - controls the operation of multiple Node Bs, managing resources such as allocating capacity for data transmissions and providing signaling (call set-up, handoffs etc).
- Home Location Register (HLR) - is a database located in the user's home system. It stores the master copy of the user's service profile. The HLR also stores the UE location on the level of Mobile Services Switching Centre (MSC) and Serving General Packet Radio Service (GPRS) Support Node (SGSN).
- MSC/Visitor Location Register(VLR) - is the switch and database that serves the UE in its current location for Circuit Switched (CS) services. The MSC function is used to switch the CS transactions, and the VLR function holds a copy of the visiting user's service profile as well as more precise information on the UE's location within the serving system.
- Gateway MSC (GMSC) - is the switch at the point where UMTS is connected to external CS networks. All incoming and outgoing CS connections go through GMSC.
- SGSN - is similar to MSC/VLR, but it is used for Packet Switched (PS) services. The part of the network that is accessed via the SGSN is often referred to as the PS domain.
- Gateway GPRS Support Node (GGSN) - has a functionality close to that of GMSC but in relation to PS services.

TABLE 1   Differences between HS-DSCH and DCH

Feature	DCH	HS-DSCH
Spreading factor	Variable, 4-512	Fixed, 16
Fast power control	Yes	No
Soft handover support	Yes	No
Multi-code operation	Yes	Yes, extended
Adaptive modulation and coding	No	Yes
Physical layer retransmissions	No	Yes
Node B based scheduling	No	Yes
Link adaptation	No	Yes
TTI length	10,20,40 or 80 ms	2ms
Modulation	QPSK	QPSK,16QAM or 64QAM

2.2   HSDPA channels

This section presents the overview of HSDPA channels and compares them with the channels from WCDMA. As for the transport layer, the HSDPA has a High Speed Downlink Shared Channel (HS-DSCH) which is the common transport channel, i.e. it is shared by all UEs within a cell, while WCDMA has a Dedicated Channel (DCH) for each UE. The differences between these channels are shown in Table 1. [Hol07]

Depending on the transmitted bits the HS-DSCH can be mapped to the High Speed Physical Downlink Shared Channel (HS-PDSCH) for data bits and to the High Speed Shared Control Channel (HS-SCCH) for control bits. [3GPq] The third channel is the High Speed-Dedicated Physical Control Channel (HS-DPCCH) and it is the associated channel in the uplink. All these channels are explained below.

HS-PDSCH is the physical channel used for transmitting data bits. It does not transport any signaling bits. HS-PDSCH has a fixed SF equal to 16, and it does not have fast power control mechanism. Instead, HS-PDSCH can use three different types of modulations: QPSK, 16-QAM or 64-QAM. HS-PDSCH has 16 spreading codes; however, one code is allocated for the common channels HS-SCCH and only 15 codes at most can be allocated for real data. The final number of codes allocated for data is dependent on the UE (supporting 5, 10, or 15 codes).[3GPs]

HS-SCCH is the downlink control channel. This channel arrives 2 slots before the HS-PDSCH. The HS-SCCH channel transports the signaling data associated to the transport channel. Basically, HS-SCCH indicates to the UE how to read HS-PDSCH. HS-SCCH is divided into two parts. The first part contains the UE identity, modulation used in HS-PDSCH, and coding information. The

second part transports information, such as HARQ information, or redundancy information. This physical channel uses QPSK modulation, and its SF is equal to 128. Unlike HS-PDSCH, HS-SCCH can be power controlled. Nevertheless, it is a vendor-specific solution. Networks are configured with one HS-SCCH channel if HSDPA is time-multiplex based. However, if HSDPA scheduling is code-multiplex based, the network will need to be configured with more than one HS-SCCH channel. According to the standard, UE can monitor up to four HS-SCCH channels per a carrier.

The HS-DPCCH channel is an uplink channel used for signaling purposes. The modulation scheme for this channel is BPSK, and the spreading factor is 256; thus, this channel has a bit rate of 15 Kbps. Moreover, the HS-DPCCH channel has a fixed power offset relative to DPCCH and DPCCH is power controlled. The signaling information sent through this channel is related to ACK/NACK, and to CQIs. Based on this feedback, Node B will be able to perform link adaptation, scheduling decisions and retransmission of erroneous information.

2.3   Link adaptation

In cellular communication systems, the quality of a signal received by a UE depends on the number of factors: the distance between the serving and interfering Node Bs, path loss, log-normal slow fading (shadowing), fast fading and noise. In order to improve system capacity, peak data rate and coverage reliability, the signal transmitted to and by a particular user is modified to account for the signal quality variation through a process commonly referred to as link adaptation. Traditionally, CDMA systems have used fast power control as the preferred method for link adaptation.[3GPb]

The main feature of this technique is its ability to give a proportionally larger part of the total available cell power to links with bad channel conditions, as Figure 4 shows [PS07]. It provides similar QoS to all UEs in the cell which have different channel qualities. However, not all of the available output power is fully used because some power has to be reserved for downlink connection that might need more power if channel conditions become degraded. This reserve power cannot be used to increase the system throughput. That's why its power control is not the most efficient in the sense of allocating available resources. [ERI99]

As was mentioned in the previous subsection, HS-PDSCH does not use fast power control for link adaptation, and the spreading factor is fixed to 16 [Hol07]. HSDPA, on the other hand, uses the link adaptation that selects proper Transmit Block(TB) sizes, coding rates and modulation to match the channel conditions. This is known as the Adaptive Modulations and Coding scheme(AMC). Proper usage of AMC requires the measuring of channel quality by UE and reporting it to Node B. For this purpose, the 3GPP introduced a new technique called Channel Quality Indicator (CQI).[3GPr]

Besides QPSK modulation, which is used by WCDMA 3GPP Release 99, HS-
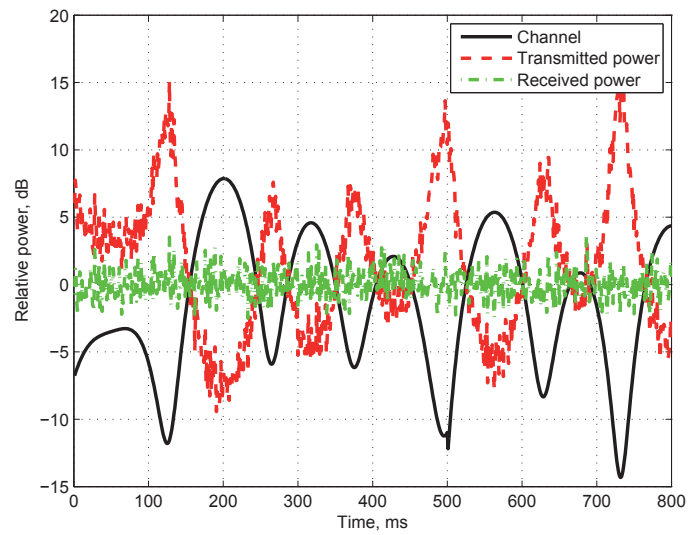
FIGURE 4   Example of fast power control in WCDMA
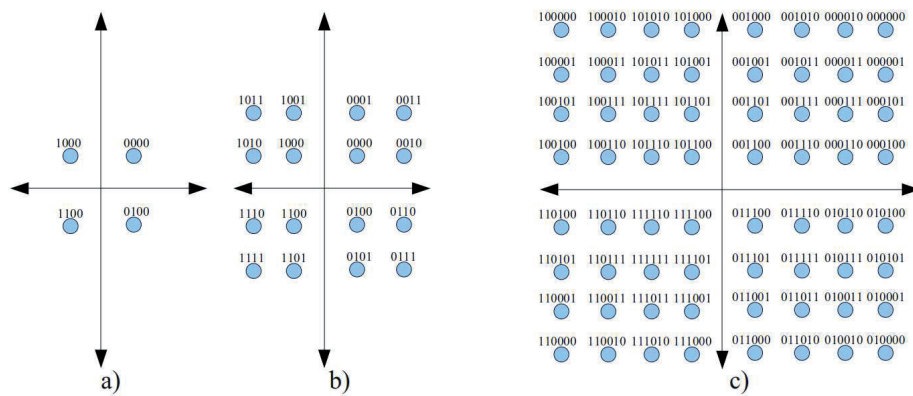
FIGURE 5   Constellations of QPSK, 16QAM and 64QAM modulations

DPA is able to use 16 QAM to provide a higher data rate [3GPt] . And from 3GPP
Release 7 a new modulation scheme known as 64QAM was standardized [3GPt].
In case of QPSK modulation, the modulation alphabet consists of four different
signaling alternatives (Figure 5(a)) that allow transmission of up to 2 bits of infor-
mation during each modulation-symbol interval. With 16QAM modulation, 16
different signaling alternatives are available (Figure 5(b)), that is, 4 bits of infor-
mation per symbol interval. Finally 64QAM modulation allows transmitting of
up to 6 bits per symbol and has 64 different signaling alternatives (Figure 5(c)).

2.4   HARQ

Link adaptation, which was described previously, and channel dependent schedul-
ing, which will be explained later, are the two main features of HSDPA. These are
achieved through proper data processing before data transmission and allow the
exploitation of wireless channel variations. However, radio-link quality is sus-
ceptible to random variations, and it is hard or almost impossible to perfectly
adapt to instantaneous radio-link variations. Therefore, it is very common to
receive erroneous data packets. Hybrid ARQ, also known as HARQ, is a very ef-
ficient technique that employs a coding scheme through which some frame errors
can be corrected [DPSB10].

The advantage of this is reduction in the average number of transmissions
although each transmission carries redundant information. In HARQ, a subset
of all errors is corrected using Forward Error Correction (FEC) bits, which are
redundantly added to the existing Error Detection (ED) bits. In poor signal con-
ditions, HARQ outperforms ARQ, but, in good signal conditions, HARQ has a
noticeable performance decrease. Basically, HARQ falls into two categories: Type
I and Type II. Type I is the simplest form: the sender encodes the message through
adding both ED and FEC information before transmission; the receiver first de-
codes the error-correction code to determine channel quality and then decides
whether a retransmission is needed based on the channel quality. If the chan-
nel quality is acceptable, all transmission errors are correctable and the received
data block can be obtained error free. When the channel does not have a proper
quality, the received data block is rejected and a retransmission request is sent
to the sender. Type II applies a more complex operation than Type I. The sender
sends the original message plus ED codes without FEC information, if the first
transmission is received error free. If an error is detected by the receiver, then
FEC is added to the sent data along with the pre-existing ED. It is also possible
to combine two consecutive error-free transmissions when none of the two sent
messages has errors [DPSB10].

Both chase combining and incremental redundancy are supported by the
HSDPA standards. Chase combining offers diversity gain and is simple in terms
of implementation, while incremental redundancy generally demonstrates a bet-
ter performance than chase combining, though at the cost of increased complex-
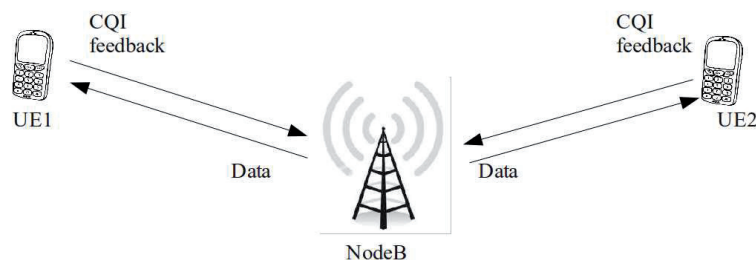
FIGURE 6   Main principle of Node B scheduling

ity and implementation overhead. It has been shown that redundancy in wireless transmission can significantly enhance throughput and improve performance [Gol05].

In [FPD01], it has been shown that in a HARQ Type II system, incremental redundancy substantially outperforms chase combining. However, there are situations where incremental redundancy cannot be a significantly better choice than chase combining. It is possible to achieve the highest gains for high channel-coding rates and high modulation orders, but concerning low Modulation and Coding Schemes (MCS), incremental redundancy does not yield considerable link-level performance. Moreover, [FPD01] shows that in a system which utilizes link adaptation using Incremental Redundancy, large gains cannot be obtained if link adaptation errors are at a low level. Also, as for fading channels, there are some cases where incremental redundancy demonstrates poorer performance than chase combining.

2.5 Scheduling

Starting from Release 5, the scheduler is not located in RNC as it was in Release 4; it is located at the Node B, which minimizes the delays for the scheduling process. Furthermore, each HSDPA-capable UE continuously transmits CQI to the Node B. Based on this information and on the type of scheduler in close cooperation with link adaptation and HARQ, the scheduler can allocate HS-PDSCH resources to the UE with data in the buffer in each TTI, as shown in Figure 6.

Although scheduling algorithms are very important, they are not standardized by the 3GPP. That gives an interesting topic to research for the academic and the industrial world. Indeed, many papers have been written about different types of scheduling algorithms. For example, in [MKW07], the authors propose a new scheduling algorithm for Real Time (RT) traffic and compare it to previously investigated algorithms for RT and Non-Real Time (NRT). The scheduling algorithm primarily depends on the QoS classes and services. The main difference between these classes is the balance between transmission delay and reliability.

There are three basic types of scheduling algorithms which are explained in this subsection. However, there are other specific scheduling algorithms, including the Modified Largest Weighted Delay First (M-LWDF) [AKR$^+$01] and in the Expo-Linear (EL) [GP06] algorithm. One of the standalone scheduling algorithms is the Maximum Carrier to Interference ratio (Max C/I) or maximum SINR or maximum throughput algorithm. The main principle of this scheduling algorithm with many names is to allocate HS-PDSCH resources to the user with the highest CQI. On one hand, this scheduling algorithm would always have the best throughput, on the other, there are no fairness in the resource allocation between the users, and the users with lower CQI may never be scheduled. The second standalone scheduling algorithm is known as round-robin. A round-robin scheduler provides the highest fairness in the resource allocation between the users by scheduling each user with equal fairness their CQI. However, its overall throughput might be small. The third scheduling algorithm is the proportional fair scheduler. It was initially proposed in [Hol00] and further analyzed in [Hol01] and [JPP00]. This scheduler takes into account CQI of the users for upcoming transmission as well as the amount of previously transmitted bits, and calculates proportional fair metrics of the users to provide the best throughput and fairness for the resource allocation. The PFmetric for user k at TTI n can be calculated as:

$$P_k[n] = \frac{EDR_k[n]}{T_k}, \tag{2}$$

where $P_k[n]$ is the proportional fair metric for the user k for the next TTI n, $EDR_k[n]$ is the estimated data rate for the user k in the next TTI n and T_k is the average delivered user throughput from previous TTIs.

The average delivered user throughput is calculated as:

$$T_k = (1 - \alpha) \cdot N_k + \alpha \cdot EDR_k[n-1], \tag{3}$$

where N_k is the average user throughput from the past, $EDR_k[n-1]$ is the data rate from the previous TTI, and α is the forgetting factor.

Forgetting factor is a very important parameter for proportional fair scheduling. According to the value of the forgetting factor, the proportional fair scheduler can allocate resources to achieve either better throughput or better fairness. The examples of these three scheduling algorithms are presented in Figure 7.

The figure shows that, with the Max C/I scheduling algorithm, the UE with the highest throughput will always be scheduled. In case of round-robin, UEs will be equally scheduled over TTIs. The example with proportional fair scheduler is empty because it can vary depending on the forgetting factor.
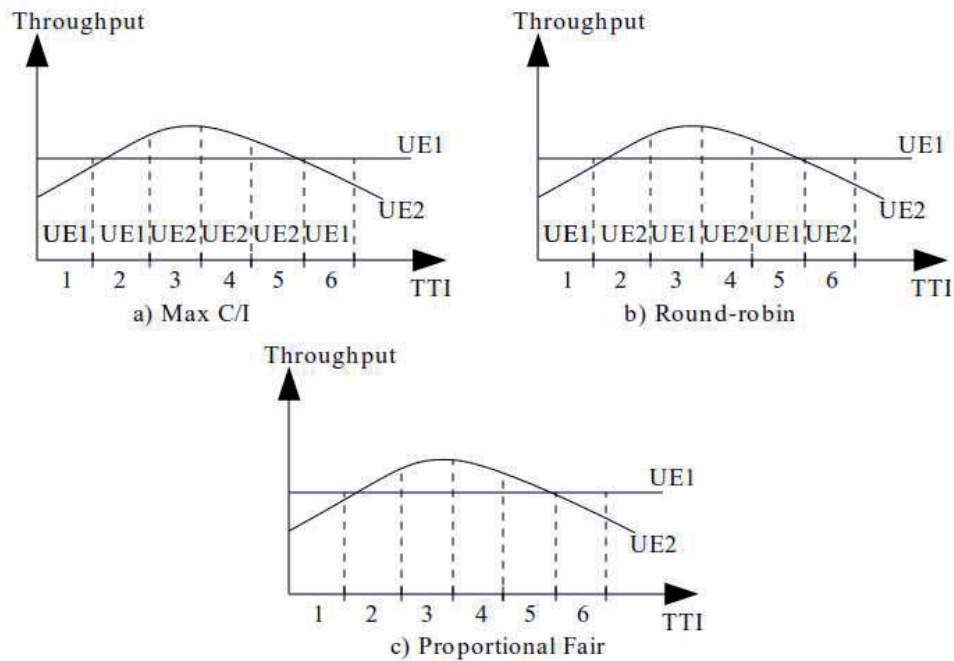
FIGURE 7   Types of scheduling algorithms

2.6   Receiver

Different types of receivers have come under research. Some of them can decrease the impact of multipath propagation, and some of them can even be aware of interference from other cells. Table 2 shows a receivers according to the 3GPP specification [3GPm].

TABLE 2   Types of Receivers

3GPP Name	Reference Receiver
Type0	RAKE
Type1	Diversity receiver (RAKE)
Type2	Equalizer
Type2i	Equalizer with interference awareness
Type3	Diversity equalizer
Type3i	Diversity equalizer with interference awareness
TypeM	Multiple-Input Multiple-Output

Not all of these receivers are used in this study: some of them are too old, mainly fit to be taken into account in the simulation as legacy user equipment. Type3 and type3i are considered in this thesis. The enhanced type3 receiver, spe-

cially developed for the HS-SFN transmission scheme, is explained later in this work.

2.6.1 Signal model

According to [NKLR05], transmission from a cell assumes that there is one Tx antenna each cell in Node B and N_{Rx} RX antennas at UE. The received chip sequence equals to

$$\mathbf{r}(m) = \mathbf{H}^T \mathbf{s}(m) + \mathbf{n}(m), \tag{4}$$

where $\mathbf{s}(m)$ is the transmitted chip stream (5) and $\mathbf{n}(m)$ is the noise vector.

$$\mathbf{s}(m) = [\mathbf{s}(m+F+L-D), \ldots, \mathbf{s}(m), \ldots, \mathbf{s}(m-D)]^T, \tag{5}$$

$$0 \leq D \leq F. \tag{6}$$

In (5) L is the delay spread of the channel normalized to the chip interval, D is the delay parameter satisfying inequality (6) and F is the length of the linear filter $\mathbf{w}$ that the receiver uses in the filtering of $\mathbf{r}$ to obtain the estimate $\tilde{\mathbf{s}}$ for the transmitted chip sequence $\mathbf{s}$:

$$\tilde{\mathbf{s}}(m) = \mathbf{w} \cdot \mathbf{r}(m). \tag{7}$$

Multiplication of the channel coefficient matrix $\mathbf{H}^T$ in (4) models the convolution with the impulse response of the channel. $\mathbf{H}$ is the $(F+L) \times (F \cdot N_{Rx})$ matrix given by the following equation:

$$\mathbf{H} = \begin{bmatrix} \mathbf{h} & 0 & 0 & \ldots & 0 \\ 0 & \mathbf{h} & 0 & \ldots & 0 \\ 0 & 0 & \mathbf{h} & \ldots & 0 \\ \vdots & \vdots & \vdots & \ddots & \vdots \\ 0 & 0 & 0 & \ldots & \mathbf{h} \end{bmatrix}^T, \tag{8}$$

where $\mathbf{h}$ is the $N_{Rx} \cdot (L+1)$ channel impulse response matrix defined by

$$\mathbf{h} = \begin{bmatrix} \mathbf{h}_1(0) & \mathbf{h}_1(1) & \ldots & \mathbf{h}_1(L) \\ \mathbf{h}_2(0) & \mathbf{h}_2(1) & \ldots & \mathbf{h}_2(L) \\ \vdots & \vdots & \ddots & \vdots \\ \mathbf{h}_{N_{Rx}}(0) & \mathbf{h}_{N_{Rx}}(1) & \ldots & \mathbf{h}_{N_{Rx}}(L) \end{bmatrix}. \tag{9}$$

Here $\mathbf{h}_i(l)$ is the channel impulse of ith Rx-antenna at the delay l.

2.6.2 Type3

The type3 receiver is also known as LMMSE equalizer with receiver diversity. It can be used in frequency-selective channels to make the channel flat again and restore the orthogonality lost due to time-shift between the signals [Nih08]. The
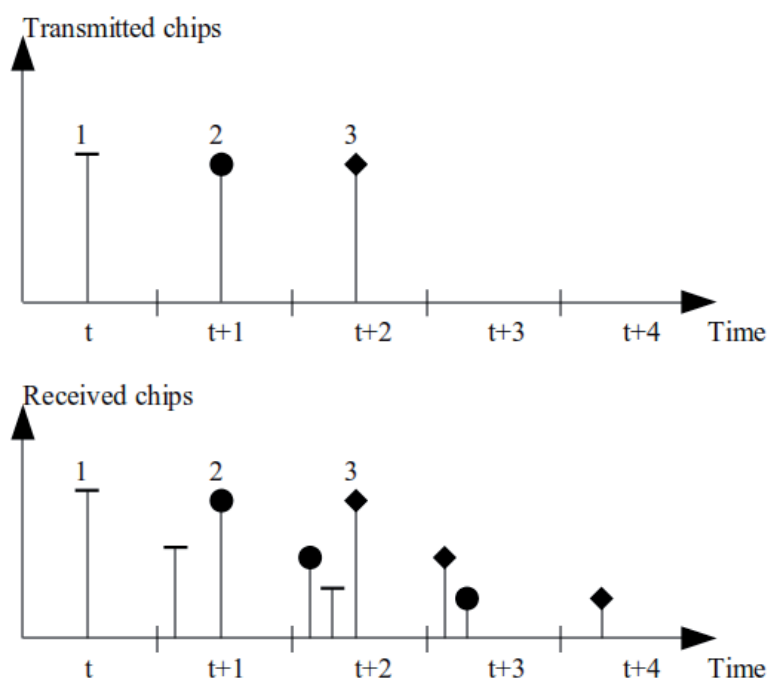
FIGURE 8   Multiple access interference

type3 receiver helps to avoid intra-cell interference or so-called multiple access interference, which is referred to in this study as own interference.

Intra-cell interference

WCDMA uses Orthogonal Variable Spreading Factor (OVSF) Codes to spread user data in both the uplink and the downlink[3GPl]. Like signals with different frequencies or times, orthogonal signals do not create any interference with each other. However cross-correlation between OVSF codes can rise considerably if there is a delay shift between them.

Intra-cell interference is a type of the interference that comes from the serving (own) cell. It emanates from the multipath propagation of the own signal as presented in Figure 8.

Type3 receiver coefficient calculation

The main concept of type3 receiver is to restore the orthogonality by equalizing the received signal from the own cell at a chip level before despreading as shown in Figure 9 . Equalization take place via an adaptive calculation of the receiver coefficient.[DAO01]

To calculate the receiver coefficient vector $\mathbf{w}$ of length $N_{Rx} \cdot F$ the following quadratic cost function should be minimized:

$$F(\mathbf{w}) = E\left\{\left|\mathbf{w}^T\mathbf{r}(m) - \mathbf{s}(m - \tau)\right|\right\}, \tag{10}$$
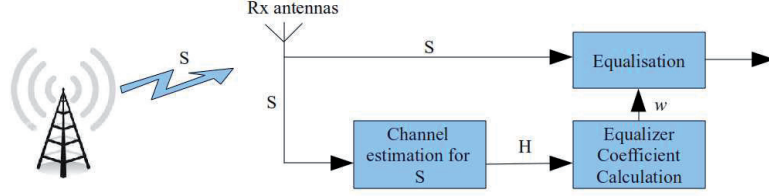
FIGURE 9   Type3 Receiver

which is the distance between the received chip sequence $\mathbf{r}(m)$ equalized and the $(m - \tau)$-th transmitted chip $\mathbf{s}(m - \tau)$ for a given value of delay $\tau \in \{-F + D + 1, -F + D + 2, \ldots, D + L\}$.

The value of $\mathbf{w}$ which minimizes the cost function $F(\mathbf{w})$ can be found by deriving (10) with respect to $\mathbf{w}^T$ [Bra83]:

$$\frac{\partial F}{\partial \mathbf{w}^T} = 0. \tag{11}$$

After rearranging the equation (11) can be rewritten as:

$$\left(\mathbf{H}^T \mathbf{H}^* + \mathbf{C}_w\right) \mathbf{w}^* - \left(\mathbf{H}^T \delta_\tau\right) = 0, \tag{12}$$

where $\mathbf{C}_w$ is the white noise autocorrelation matrix, and δ_τ is a zero vector with the unit on the position τ. Therefore, the type3 receiver coefficient is equal to

$$\mathbf{w} = \left(\mathbf{H}^H \mathbf{H} + \mathbf{C}_w\right)^{-1} \mathbf{H}^H \delta_\tau. \tag{13}$$

According to the [KZL00] and [KZ00] the equation for type3 receiver coefficient calculation can be expressed as:

$$\mathbf{w} = \mathbf{C}_w^{-1} \mathbf{H}^H (\mathbf{H} \mathbf{C}_w^{-1} \mathbf{H}^H + \mathbf{I})^{-1} \delta_\tau. \tag{14}$$

Equations (13) and (14) present the same calculation but in another form. Both of these equation can be used for calculation of type3 receiver coefficient.

2.6.3   Type3i

The type3i receiver is also known as Diversity LMMSE equalizer with interference awareness. This receiver attempts to cancel the interference from users operating in the neighboring cells. This type of interference is also referred to as inter-cell interference. In type3, only the channel from the own sector is assumed to be known, and interference from another cell is modelled as AWGN or so-called white interference. In type3i some amount of the strongest interfering sectors, referred to as like-colored interference, is assumed to be known. This type of receiver was already well investigated in [NKV07] and [3GPm].

Inter-cell interference

As the name tells, inter-cell interference is interference from other cells or Node Bs. It might appear in the network if two cells use the same frequency and time, and the scrambling codes that are used for separation signals from these cells are not orthogonal.

Type3i receiver coefficient calculation

According to [3GPm], the receiver coefficient vector $\mathbf{w}$ is calculated using the inverse of the covariance matrix $\mathbf{C}_{rr}$ as shown below (15).

$$\mathbf{w} = \mathbf{C}_{rr}^{-1}(\mathbf{M}_0)^H \delta_D, \tag{15}$$

where $\mathbf{M}_0$ is the $(F \cdot N_{Rx}) \times (F + L)$ matrix that is defined as:

$$\mathbf{M_0} = \begin{bmatrix} (\mathbf{H}_{0,1})^H \\ \vdots \\ (\mathbf{H}_{0,N_{Rx}})^H \end{bmatrix}, \tag{16}$$

where $\mathbf{H}_{0,i}$ is the channel impulse response matrix of ith Rx-antenna from the serving cell. From (15), the $(FN_{Rx}) \times (FN_{Rx})$ covariance matrix $\mathbf{C}_{rr}$ is defined as:

$$\mathbf{C}_{rr} = P_0\mathbf{M}_0(\mathbf{M}_0)^H + \sum_{j=1}^{N_{BS,all}} P_j\mathbf{M}_j(\mathbf{M}_j)^H + \mathbf{I}, \tag{17}$$

where $\mathbf{I}$ is the $F \times F$ white noise interference matrix of the receiver antenna i, which is defined by:

$$\mathbf{I}_i = \begin{bmatrix} \sigma_i^2 & \cdots & 0 \\ 0 & \ddots & 0 \\ \vdots & 0 & \sigma_i^2 \end{bmatrix}, \tag{18}$$

where σ_i^2 is the noise power of the receiver antenna i.

Equation (17) takes into account a maximum number of Node Bs as interferers. However, this is not very optimal: although this large number of interferers will increase the complexity of the receiver, it will not significantly increase interference cancelation. Research on the optimal number of interferers has been carried out by different companies including Nokia, Qualcomm, Motorola and Cingular in [3GPi], [3GPh], [3GPf] and [3GPg]. Some of the results, which were generated by these companies, show the contribution of the eight strongest interfering cells to the total interference in the system in Figure 10. These results show that the five strongest interferers contribute a large portion of the total interference. That is why only the five strongest interferers are used in the simulations of this study.
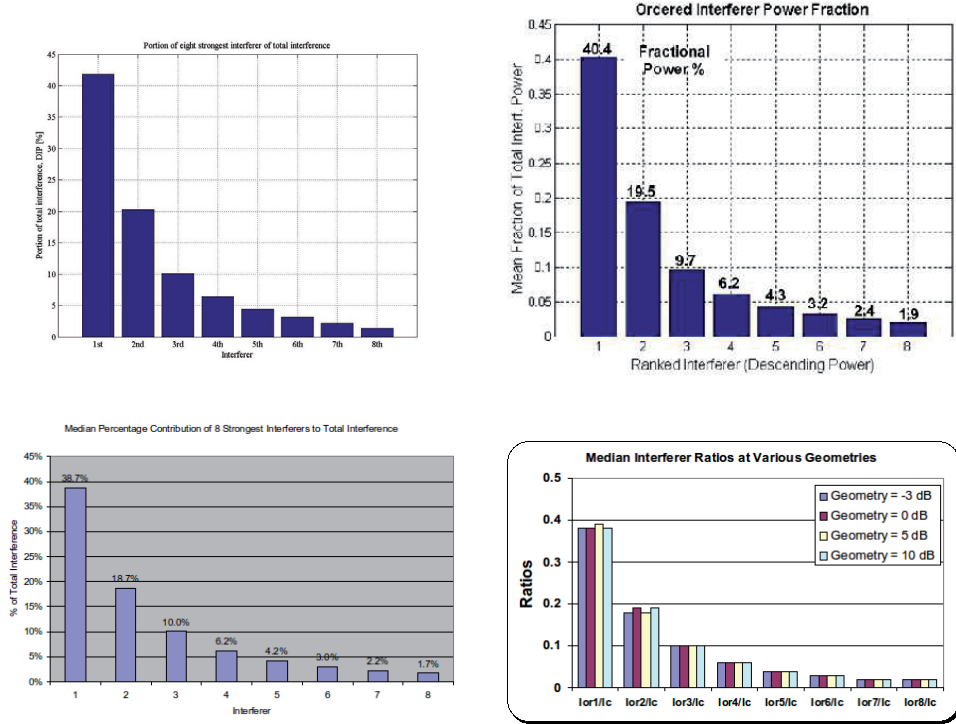
FIGURE 10   Investigation of the type3i receiver

2.6.4   C/I calculation

In order to account for inter-cell interference, intra-cell multipath interference, and equalization, we may express the C/I, according to [3GPm], more accurately as

$$C/I = \frac{P_{data} \cdot \left| \mathbf{w}^T \mathbf{H}^T \delta \right|^2}{I_{own} + I_{col} + I_{thermal}},$$ (19)

where the total interference consists of three logically different interferences: own interference or so-called Multiple Access Interference (MAI) (20), colored interference (21) and thermal noise (22).

$$I_{own} = P_0 \mathbf{w}^T \mathbf{H}^T \hat{\delta} \mathbf{H}^* \mathbf{w}^*,$$ (20)

$$I_{col} = \sum_{j=1}^{N_{BS,all}} P_j \mathbf{w}^T \mathbf{H}_j^T \mathbf{H}_j^* \mathbf{w}^*,$$ (21)

$$I_{thermal} = \mathbf{C}_{thermal},$$ (22)

where:

H is the channel impulse response matrix;
w is the receiver weight vector;
δ is the delay of the receiver;
$\mathbf{C}_{thermal}$ is the thermal noise matrix;
P_j is the power received from j Node B.

2.7 Summary

This chapter has presented the main architecture of HSDPA as well as specific features that were used for this study. However, other features, like MIMO and handover in physical layer and, a lot more in the higher layers, were dropped from this thesis not due to fact that they are unimportant, but due to the fact that it was not used in this study.

3 HIGH-SPEED SINGLE FREQUENCY NETWORK

Unlike the Multiflow multipoint transmission scheme mentioned in [3GPj], in HS-SFN, the *same* downlink (DL) data is transmitted on the HS-PDSCH channel from two cells by using the same carrier frequency and scrambling code in both cells. Data transmission is TTI-aligned, so that the signals are combining over the air at the UE receiver, as presented in Figure 11, [HPHC11]. The Figure 11 shows transmissions of two TTIs from cells A and B that belong to the same Node B, where different colors represent different scrambling codes and crosshatching depicts different channel impulse responses. The strict TTI alignment and a requirement to transmit exactly the same data pose a further constraint, namely that the HS-SFN technique is most likely limited to the intra-site scenario, i.e. cells belonging to this cooperative transmission are under the control of the same
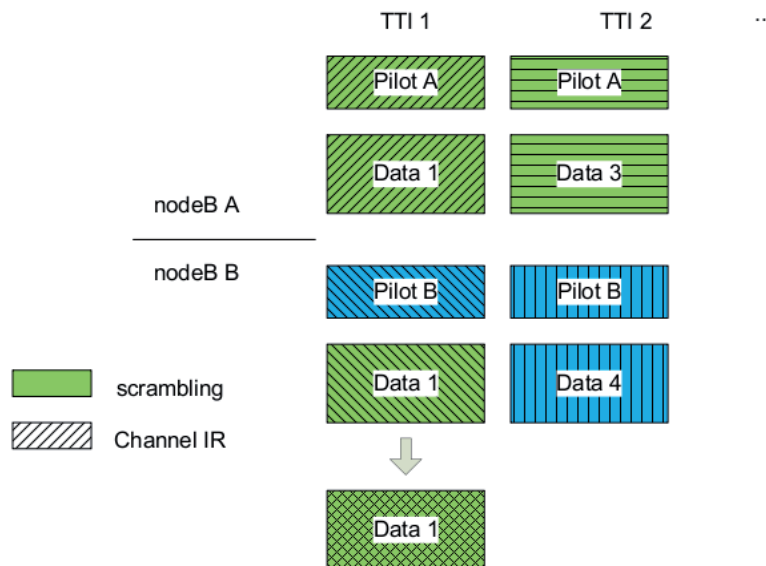

FIGURE 11   HS-SFN data signal formation

system module. It is, however, worth mentioning that recent advances in core network architectures and, in particular, remote radio head deployment makes it possible to run HS-SFN outside the classical three-sector site scenarios.

The main gain of the HS-SFN usage derives from combining the two strongest signals: the strongest signal coming from the serving Node B and the second one coming from the neighboring sector. At the same time, this can reduce considerably the interference from the second cell as it starts to assist in data transmission. Equation (23) shows s simplified version of enhanced C/I with HS-SFN:

$$C/I = \frac{0.7P_{own} + 0.7P_{2nd}}{\sum_{i=0}^{N} P_i - P_{own} - 0.7P_{2nd}},$$

(23)

where i is the i-th cell and N the total number of cells. It is assumed that 70% of power is used for data channel (HS-PDSCH) and 30% is left for control (pilots and signaling) channel overhead.

Besides the TTI-level synchronization, the receiver should be able to deal with assisted transmission. Another challenge is that the combining of two signals can have either positive or negative due to uncorrelated fast fading. This problem is solved if the data transmissions from the two cells are adjusted in such a manner that the signals arrive in phase.

3.1 Signal model

The signal model for HS-SFN transmission is very similar to the signal model for the transmission from only one sector, which was described in 2.6.1. That is why only the difference between these signal models will be described in this section. During HS-SFN assisted transmission, only the data part of the signal uses the same scrambling. However, both cells still use their own scrambling for control channels which still need to be received by other legacy UEs. As a result, expression (4) is converted to:

$$\mathbf{r}_c(m) = \mathbf{H}_0^T s_0(m) + \mathbf{H}_1^T s_1(m) + \mathbf{n}(m).$$

(24)

In turn, in expression (24), $\mathbf{s}(m)$ can be divided into control and data parts, so that:

$$\mathbf{r}_c(m) = \mathbf{H}_0^T (d(m) + c_0(m)) + \mathbf{H}_1^T (d(m) + c_1(m)) + \mathbf{n}(m),$$

(25)

where $\mathbf{H}_{0,1}$ is the channel coefficient matrix for serving ($\mathbf{H}_0$) and assisting ($\mathbf{H}_1$) cells, $\mathbf{d}(m)$ is the data part of the signal, and $\mathbf{c}_{0,1}(m)$ is the control part of the serving and assisting cell.

Since the data parts of the signals coming from the serving and assisting cells are the same, they can be combined according to equation (26):

$$\mathbf{H}_C^T = \mathbf{H}_0^T + \sqrt{\frac{L_1 P_{1,data}}{L_0 P_{0,data}}} \mathbf{H}_1^T,$$

(26)
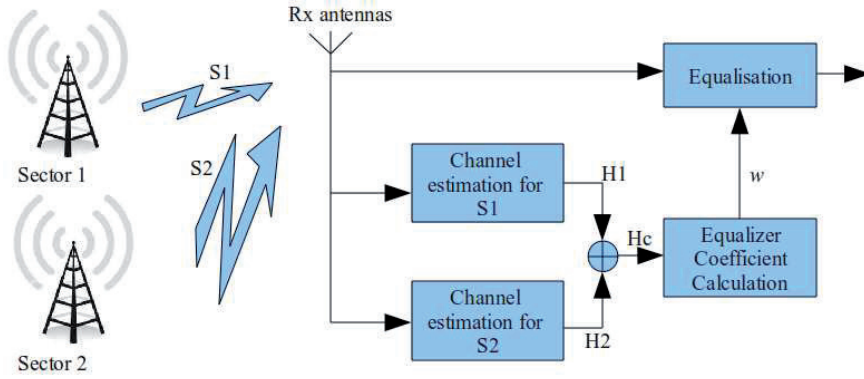
FIGURE 12   Enhanced type3 receiver

where L_j is path loss from the jth cell to UE and $P_{j,data}$ is the transmit power for HS-PDSCH of the jth cell. The serving cell is referred to by $j = 0$, and the assisting cell by $j = 1$.

Using expressions (25) and (26), the received chip sequence can be found as follows:

$$\mathbf{r}_c(m) = \mathbf{H}_C^T d(m) + \mathbf{H}_0^T c_0(m) + \mathbf{H}_1^T c_1(m) + \mathbf{n}(m). \tag{27}$$

3.2   Enhanced type3 receiver

During an HS-SFN transmission, UEs estimate the channel based on pilots transmitted in the control channel. As the pilots remain separated by scrambling also for an assisted transmission, the UE needs to estimate the two channels separately, combine the estimates, and then perform equalization of the signal, as depicted in Figure 12.

This enhanced type3 is based on the type3 receiver for standalone transmission (transmission from one cell) described in [DAO01] and [KZL00]. A comparison of type3 and enhanced type3 receivers with HS-SFN can be found in [PZH+11].

To calculate the receiver coefficient vector $\mathbf{w}$ of length $N_{Rx} \cdot F$, the following quadratic cost function should be minimized:

$$F(\mathbf{w}) = E \left\{ \left| \mathbf{w}^T r(m) - \mathbf{s}(m - \tau) \right| \right\}, \tag{28}$$

which is the distance between the received chip sequence $\mathbf{r}(m)$ equalized and the $(m - \tau)$-th transmitted chip $\mathbf{s}(m - \tau)$ for a given value of delay $\tau \in \{-F + D + 1, -F + D + 2, \dots, D + L\}$.

The received chip sequence is defined in (27), and the transmitted $(m - \tau)$-th chip in (28) is expressed as

$$\mathbf{s}(m - \tau) = \mathbf{d}(m - \tau) + \mathbf{c}(m - \tau). \tag{29}$$

Then, $\mathbf{w}$ that minimizes the cost function $F(\mathbf{w})$ can be found by deriving (28) with respect to $\mathbf{w}^T$ [Bra83]:

$$\frac{\partial F}{\partial \mathbf{w}^T} = \left(L_0 \mathbf{H}_C^T \mathbf{R}_{data} \mathbf{H}_C^* + L_0 \mathbf{H}_0^T \mathbf{R}_{ctrl} \mathbf{H}_0^* + L_1 \mathbf{H}_1^T \mathbf{R}_{ctrl} \mathbf{H}_1^* + \right.$$
$$\left. + \mathbf{R}_n\right) \mathbf{w}^* - \left(P_{data} \sqrt{L_0} \mathbf{H}_C^T \delta_\tau + P_{ctrl} \sqrt{L_0} \mathbf{H}_0^T \delta_\tau\right) = 0, \tag{30}$$

where $\mathbf{R}_{data,ctrl}$ is $(F + L - 1) \times (F + L - 1)$ the autocorrelation matrix of a signal transmitted through a data or control channel and can be found as follows:

$$\mathbf{R}_{data,ctrl} = \begin{bmatrix} P_{data,ctrl} & 0 & \cdots & 0 \\ 0 & P_{data,ctrl} & \cdots & 0 \\ \vdots & \vdots & \ddots & \vdots \\ 0 & 0 & \cdots & P_{data,ctrl} \end{bmatrix}. \tag{31}$$

Therefore, the enhanced type3 receiver coefficient is equal to

$$\mathbf{w} = \left(P_{data} L_0 \mathbf{H}_C^H \mathbf{H}_C + P_{ctrl} L_0 \mathbf{H}_0^H \mathbf{H}_0 + P_{ctrl} L_1 \mathbf{H}_1^H \mathbf{H}_1 + \right.$$
$$\left. + \mathbf{C}_n\right)^{-1} \left(P_{data} \sqrt{L_0} \mathbf{H}_C^H \delta_\tau + P_{ctrl} \sqrt{L_0} \mathbf{H}_0^H \delta_\tau\right). \tag{32}$$

Note that only a single receiver is required, leading to relative low complexity and consequently low power consumption at the UE.

3.3 C/I calculation

The same equation that was expressed in (19) can be used for both the HS-SFN C/I calculation and the C/I for standalone transmission calculation. This equation is presented also below (33) to better explain the difference in calculation of its components.

$$C/I = \frac{P_{data} \cdot \left|\mathbf{w}^T \mathbf{H}_c^T \delta\right|^2}{I_{own} + I_{col} + I_{thermal}}, \tag{33}$$

where the total interference also consists of three logically different interferences: own interference or so-called Multiple Access Interference (MAI) (34), colored interference (35), and thermal noise (36).

$$I_{own} = P_{data} w^T \mathbf{H}_c^T \hat{\delta} \mathbf{H}_c^* w^* + P_{ctrl} \mathbf{w}^T \mathbf{H}_0^T \hat{\delta} \mathbf{H}_0^* \mathbf{w}^*, \tag{34}$$

$$I_{col} = \sum_{j=1}^{N_{BS,all}} \frac{L_j P_j}{L_0 P_0} \mathbf{w}^T \mathbf{H}_j^T \mathbf{H}_j^* \mathbf{w}^*, \tag{35}$$

$$I_{thermal} = \frac{1}{L_0 P_0} \mathbf{C}_{thermal},$$ (36)

where:

$\mathbf{H}_c$ is the combined channel impulse response matrix (26);

P_{data} is the power for HS-PDSCH;

P_{ctrl} is the power for control and pilot channels;

$\mathbf{w}$ is the receiver weight vector;

δ is the delay of the receiver;

$\mathbf{C}_{thermal}$ is the thermal noise matrix;

L_j is the pathloss from UE to the jth Node B;

P_j is the transmit power of the jth Node B.

In (34), interference from the own cell was divided into the data and control parts due to the combining of the data channel impulse response matrices. In (35), if $j = 1$, then only 30% of P_j should be considered since there is no interference from that cell on the HS-PDSCH channel.

3.4 Phase adjustment

To further improve HS-SFN performance gains, the transmitted signals from serving and assisting cells can be adjusted in such a way that the signals arrive to a UE in phase. Such an approach can definitely improve performance of the HS-SFN scheme since a similar solution has been used in the HSPA and LTE systems. As with the HSPA single stream MIMO transmission[PWS$^+$07], a set of transmitting antenna weights are defined. In the case considered, this set consists of two weights: the signal transmitted through HS-PDSCH from the serving cell is multiplied by the first weight, and the one from the assisting cell by the second weight. The transmitting antenna weights are not applied to the pilot and control channels.

The first weight always remains fixed and equal to one:

$$\alpha_0 = 1.$$ (37)

The second weight provides a phase adjustment and is set to one of the following values according to the UE feedback:

$$\alpha_1 = \left\{ \frac{1+j}{\sqrt{2}}, \frac{1-j}{\sqrt{2}}, \frac{-1-j}{\sqrt{2}}, \frac{-1+j}{\sqrt{2}} \right\},$$ (38)

where j is an imaginary unit. As one can notice, the weights applied to the assisting cell's HS-PDSCH differ by ninety degrees. Thus, there are four possible sets of transmitting antenna weights and one of these sets is chosen based on the UE feedback information.

3.5 Combined Scheduler

This section introduces a different type of site scheduler for HS-SFN, the so-called combined scheduler. The main aim of the combined scheduler is to choose the best configuration taken into account metrics from all UEs in the site, with and without HS-SFN. The main concept of it is quite simple as can be seen from Figure 13. However it is hard to choose the best one in terms of improving the performance for HS-SFN UEs, with marginal impact on overall performance of the network.
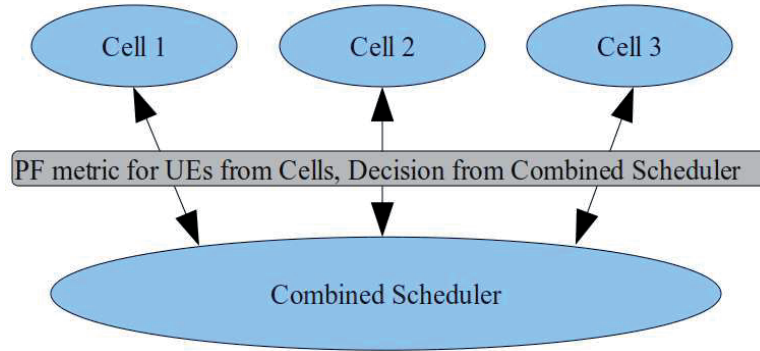

FIGURE 13   Combined scheduler architecture

To start with, each cell calculates a proportional fair metric for each UE. For HS-SFN UEs, the proportional fair metric is calculated with and without HS-SFN transmission and then the metrics are sent to the combined scheduler. The combined scheduler chooses the best combination, considering following algorithm. Let's assume, that $PFM_{XY}(n)$ is the proportional fair metric for UE n, where X and Y refer to the cell site index of 1, 2, 3 for the serving and assisting cell respectively for HS-SFN transmission. For standalone transmission, i.e. without HS-SFN, $PFM_{XY}(n)$ becomes $PFM_X(n)$, where n is the index of UE within cell X.

Firstly, the combined scheduler considers the standalone transmission of UE for each cell:

$$PFM_{standalone} = max\{PFM_1(n)\} + max\{PFM_2(n)\} + max\{PFM_3(n)\}. \quad (39)$$

Then, all the possible two-cell HS-SFN combinations are considered with the standalone scheduling from the third cell:

$$
\begin{aligned}
PFM_{12,3} &= max\{PFM_{12}(n)\} + max\{PFM_3(n)\}, \\
PFM_{13,2} &= max\{PFM_{13}(n)\} + max\{PFM_2(n)\}, \\
PFM_{21,3} &= max\{PFM_{21}(n)\} + max\{PFM_3(n)\}, \\
PFM_{23,1} &= max\{PFM_{23}(n)\} + max\{PFM_1(n)\}, \\
PFM_{31,2} &= max\{PFM_{31}(n)\} + max\{PFM_2(n)\}, \\
PFM_{32,1} &= max\{PFM_{32}(n)\} + max\{PFM_1(n)\}.
\end{aligned}
\tag{40}
$$

However, all these combinations are possible only if all cells have HS-SFN UEs as shown in Figure 14 and if some cells does not have any UE, then combinations for these cells are simply absent.
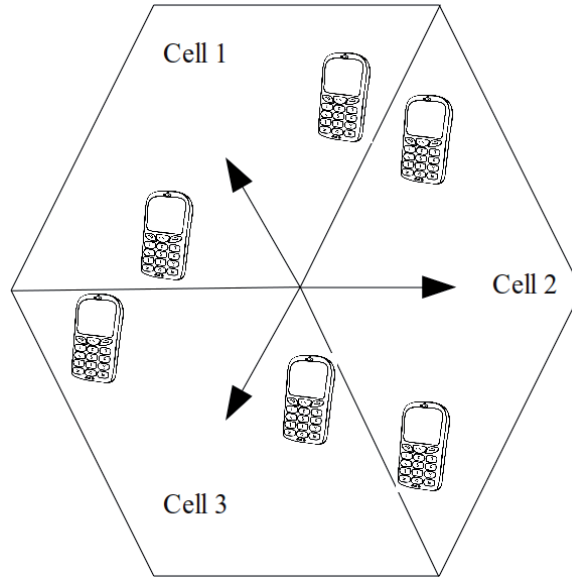
FIGURE 14   Position of UEs when all HS-SFN combinations are possible

Finally, the combined scheduler chooses the combination that maximizes the overall proportional metric:

$$
\begin{aligned}
max\{ &PFM_{standalone}, PFM_{12,3}, PFM_{13,2}, PFM_{21,3}, \\
&PFM_{23,1}, PFM_{31,2}, PFM_{32,1} \}.
\end{aligned}
\tag{41}
$$

This was the description of the proportional fair combined scheduler that was used for simulations in this work. However, by applying several additional rules this scheduler can be modified to two other schedulers. The first one is the so-called prioritized scheduler, where UEs in the softer handover area will always have a higher priority compared to the other UEs. This type of scheduler should bring the maximum gain that can be achieved from the use of HS-SFN because the HS-SFN technique is able to help UEs only in the softer handover area. But

still this gain would show a fair comparison since UEs under similar geometry conditions were prioritized. In the worst case, the prioritizing scheduler can completely block UEs in the non-softer handover area since they will not get scheduled during the presence of a softer handover UE. This can happen with the full buffer traffic model or with overloaded cells with the FTP traffic model. However, the simulations were mostly done for cells with a low or averaged load, in which the probability of this effect is too small. The second scheduler type is the so-called non-blocking scheduler, where HS-SFN transmissions take place only if the assistant cell is completely empty or does not have anything to transmit to their own UEs. This type of scheduler will bring a smaller gain from HS-SFN compared to main or prioritized schedulers, because it will limit the amount of HS-SFN transmissions. However, only this type of scheduler can guarantee a positive gain of HS-SFN for the overall performance of the network. Of course, even with this type of scheduler HS-SFN will increase the interference level for other UEs, due to additional transmission from the assisting cell, but, according to the previous simulations, the positive effect from HS-SFN is always greater than the impact due to additional interference.

3.6 Real life usage considerations

3.6.1 HS-SFN candidate selection

A straightforward approach to select candidate UEs for HS-SFN transmission is to rely upon the existing handover mechanisms and related measurements of link path strengths by the UE. Every UE maintains the active set of the strongest cells and sends measurement reports whenever changes in the link strength are detected, so that the network can decide how the active set should be adjusted.

As a part of the active set update procedure, the RNC can decide whether the HS-SFN scheme should be activated for a particular UE based on the cells' quality reported in the measurement report. It should be noted that in the 3G/HSPA architecture, the measurement reports are sent towards the RNC, whereas HS-SFN scheduling is performed by the Node B based on the CQI reports from the UE. Thus, the most preferred approach is that RNC performs a so-called synchronous change configuration where both the UE and Node B know that starting from a particular moment of time the UE will monitor the given HS-SFN assisting cell and send back related CQI reports. Similarly, it is up to the RNC to decide when the HS-SFN operation should be terminated or switched to a different assisting cell.

Once the serving cell starts to receive CQI reports on the combined channel performance from the serving and assisting cells the site-wide scheduler can make a decision in which TTIs to enable the HS-SFN transmission by instructing the assisting cell to send exactly the same data as the serving one. This concept is similar to the existent HSPA multi-carrier joint scheduling approach with the

difference that the two cells belong to different sectors and are on the same frequency.

3.6.2 Control channel considerations

As shown in Figure 11, while there is no interference on data channels in cell B, the pilot and also other control channels will remain on the native scrambling of cell B and will be subjected to higher interference by the use of scrambling A. As an example we may consider HS-SCCH which carries coding and modulation information for the UE that will be scheduled in the following TTI. The power of the HS-SCCH can be adjusted to guarantee a certain error rate at the designated UE receiver. Thus, while the interference on the HS-SCCH is raised by assisted transmissions in cell B, the C/I at the UE can be maintained by increasing the HS-SCCH power share (and decreasing that of the assisting data transmission).

Depending on the UE, the required C/I for the control channel may be from -9dB down to -12dB [3GPk]. When mapping the geometry distribution of all UEs in the network to HS-SCCH power requirements, already 90% of all UEs will be served with a share of 22% of the total transmit power on the HS-SCCH. With increased interference by HS-SFN assisted transmissions, the 90 percentile is achieved with an HS-SCCH power share of 30%. It should be noted that while the control channel power in cell B needs to be increased, it can be decreased in cell A.[HPHC11]

3.6.3 HS-SFN and HARQ

When a common scheduler is in use, also HARQ decisions can be done there. The main reason for controlling HARQ is that if scheduling and HARQ module reside separately, the scheduler is unaware of available HARQ processes and retransmission at cell level. A feasible option is to make HARQ decisions at common scheduler. If HARQ is used for initial HS-SFN transmission and a retransmission is required, the scheduler can allocate resources from both cells taking part in the transmission. This can not be guaranteed with cells doing separate scheduling since they are unaware of HARQ situation in the other cell. Common scheduler performing proportional fair scheduling may exploit HARQ decisions in its scheduling algorithm. When HS-SFN transmission is used, HARQ ACK/NACK is sent to main cell only, like with other DL transmission. With chase combining HARQ retransmission must happen with the same MCS than the initial transmission. With incremental redundancy which is used with higher MCS retransmission may happen with different MCS also. If chase combining HARQ is used then HS-SFN transmission should be used for both initial transmission and retransmission. Since chase combining HARQ has to apply the same MCS, failing to use HS-SFN in re-transmissions will not improve noticeably SINR per each retransmission (theoretically, it will be just 1.5dB versus 3dB). As opposed to that, incremental redundancy HARQ can use any MCS, so if the HS-SFN is not in use for re-transmissions, then transmission just use a more robust MCS to send those

additional parity bits. Basically there are two options for HS-SFN and HARQ: use HS-SFN for initial transmission and retransmission(chase combining HARQ) or use HS-SFN only for initial transmission (incremental redundancy).

HS-SFN for initial Tx and reTx

In this mode both initial transmissions and retransmissions are assisted. With this option the SINR remains at good level during the retransmissions. The problem is that occasionally there might not be possibility to transmit retransmissions from assisting cell. In this case the transmission will hang and in the worst case cause time-out on RLC layer retransmission.

HS-SFN for initial Tx only

In this mode only first HARQ transmission is assisted and retransmissions are performed by the main cell only. This means that the SINR for retransmission will be lower and might not be sufficient for successful reception of packet. Taking that into account, this mode would be feasible for HS-SFN-users near the BS or if their movement causes the SINR to increase enough. In that case, incremental redundancy could be possible also. This mode may be feasible if there are no free HARQ processes left. This also solves the RLC layer time-out problem. This option would be the simplest in a sense that there is no need to schedule resources for retransmission at assisting cell. The problem will be users in bad channel conditions. If same MCS has to be used for retransmission, as with chase combining, there will be a significant signal level drop and the gain from HARQ retransmission is small.

3.7 Summary

This chapter has presented main concept of HS-SFN, including the techniques, known as phase adjustment, enhanced type3 receiver and combined scheduler, that can increase the performance for the UEs in the border of the cells.

4   SIMULATION RESULTS

This chapter presents the results from the system level simulator as well as the verification results from Matlab. It also explains the simulation models with which the results were obtained.

4.1   Matlab model

Two Matlab models were created for this work. The first one was created to evaluate different HS-SFN improvements more carefully with shorter simulation time and the second one for theoretical comparison of HS-SFN and Multiflow.

The improvement in the HS-SFN performance obtained by the phase adjustment mechanism and the enhanced type3 receiver was evaluated in Matlab. A set of scripts and functions were created for deriving the signal-to-interference ratio by using for instance path gains, power of signal transmitted through HS-PDSCH and control channel. The calculation of the SINR for different values of relative path gains between the serving and the assisting cell is expressed in decibels. For each value of this ratio M simulations are run, and the impulse response matrices for serving, assisting and interfering cells are set randomly in each simulation. An average value of SINR from M simulations is calculated for each relative path gain. Basic parameters of the Matlab model are presented in Table 3 and the full description of the whole file set can be found in APPENDIX 1.

The comparison of signal-to-interference ratios for transmission in a standalone case, i.e. without a possibility of HS-SFN transmission (reference case), for HS-SFN and for HS-SFN with phase adjustment are shown in Figure 15. It can be seen that the gain from using HS-SFN is increasing with the decreasing difference between the path gains of the serving and the assisting cells. This happens because HS-SFN transmission from the assisting cell can remove 70% of interference from the second best interferer. Further, the difference between HS-SFN and HS-SFN with phase adjustment is also increasing as the difference becomes smaller in path gains. This happens due to the summing of the two signals in a

TABLE 3   Matlab verification parameters

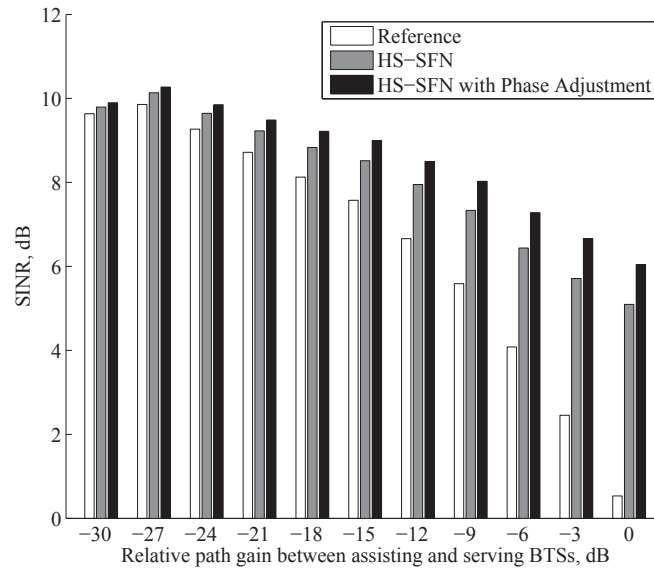| Parameter	Value
Receiver length, F	10
Number of receiver antennas, N_{Rx}	2
Number of multipath components, L	6
Relative power of the signal transmitted through HS-PDSCH, P_{data}	0.7
Relative power of the signal transmitted through control channels, P_{ctrl}	0.3
Number of interfering cells, N	56
Number of simulations, M	1000

FIGURE 15   SINR for reference and HS-SFN with and without phase adjustment cases

constructive manner only.

Figure 16 shows the C/I difference between the type3 receiver and the enhanced type3 receiver within the HS-SFN transmission. It can be seen that the difference between these receivers increases with the decreasing difference between path gains of the serving and assisting cells, which is due to the interference level of the control signal from the assisting Node B. The interference is taken into account when calculating the enhanced type3 receiver coefficients. This is not the case with the type3 receiver.

A theoretical comparison of HS-SFN and Multiflow was also done in Matlab. The Shannon equation in [MNK+07] was calibrated with the MCS distribution from a semi-static simulator and expressed as :
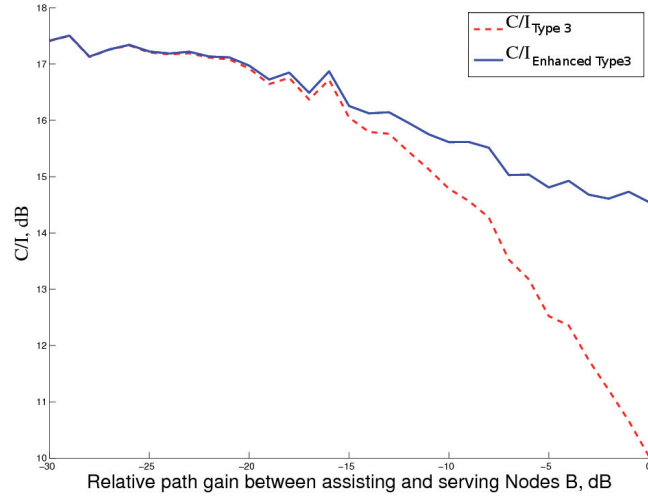
FIGURE 16   SINR for type3 and the enhanced type3 receivers under HS-SFN transmission

$$S[bits/s] = 3.84 \cdot 10^6 \cdot 0.75 \cdot log_2(1 + \text{SINR}/16). \tag{42}$$
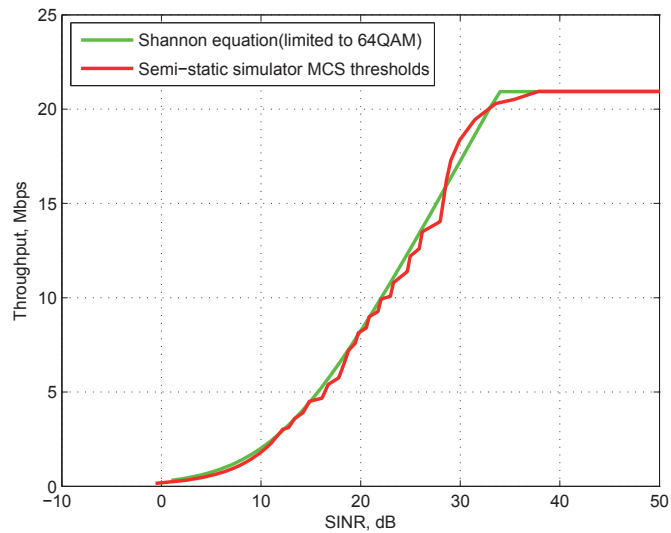

FIGURE 17   Calibration of Shannon equation

From Figure 17, it can be seen that two curves are quite similar and the upper limit is set according to the highest data rate that can be achieved with the standardized set of MCSs.
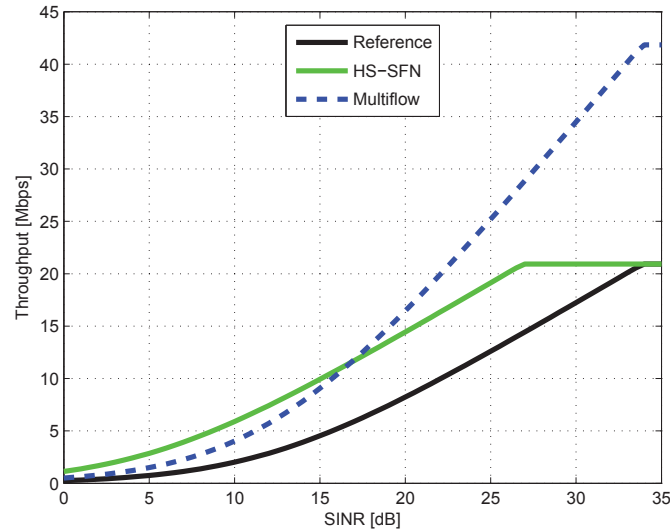
FIGURE 18   Burst rate according to the Shannon equation

Figure 18 represents the theoretical comparison of the reference case (without HS-SFN or Multiflow), HS-SFN and Multiflow. The throughput is calculated according to equation (42), where SINR values from 0 to 35 with 0.5 dB steps are passed as input. For both HS-SFN and Multiflow, it is assumed that the difference between the path gains of the serving and the assisting cells is equal to zero. According to Figure 15, the SINR in the HS-SFN case could be further increased, by several decibels, with phase adjustment and enhanced type3 receiver. With Multiflow, this theoretical throughput would be doubled since there is no difference between the path gains of the two cells. As depicted in Figure 18, Multiflow can significantly increase the throughput, especially for the UEs with high SINR. HS-SFN, however, can perform better in the lower SINR area.

4.2   System-level simulator

In this section, the system performance evaluation of the HS-SFN is presented. First, the system level simulator is described and then the results obtained with this simulator for HS-SFN are discussed in Subsections 4.2.1 - 4.2.5.

The network layout consists of 19 Node Bs, with 1 km site-to-site distance. In addition to usual 3-sector network layout, 6-sector Node Bs are simulated to increase the number of UEs in the handover area and to compare the influence on sectorization to the achieved gain from HS-SFN. The equations and parameters for 3-sector and 6-sector Node Bs [3GPn] can be found in Table 6 and the difference in the antenna pattern and network layout can be seen from Figure 19 and
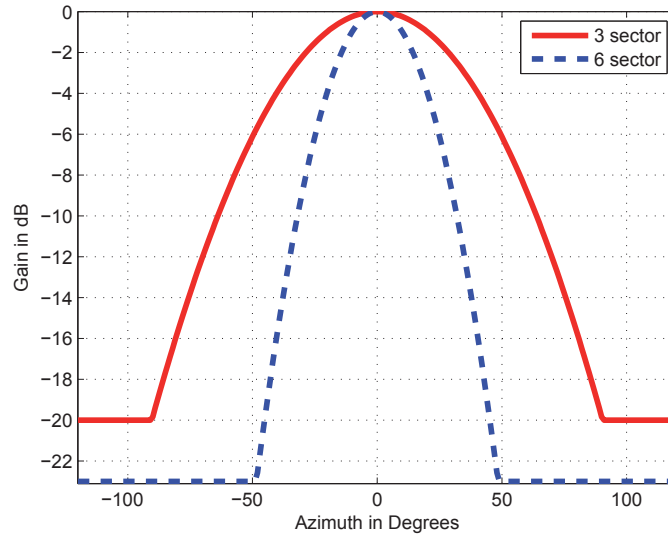
50

Figure 20.

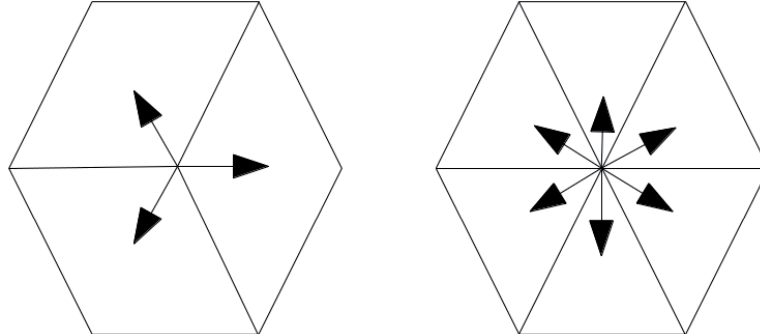FIGURE 19   Antenna pattern for 3-sector and 6-sector sites

FIGURE 20   Network layout for 3-sector and 6-sector sites

These simulations use the so-called wrap-around model: transmissions from the cells are replicated outside the existing network layout, giving a realistic interference calculation for every UE in the network and especially for the UEs at the border of the network layout. The wrap-around model as well as its simulation methodology are explained in [Hyt01], and an example of the network layout with wrap-around is presented in Figure 21. Another possible solution for proper interference calculation is provided by the so-called center-cell simulation model, where UEs are dropped to the whole network but the results are obtained only from the center cell. However, in comparison with the wraparound model, to obtain the same set of results, the simulation time will significantly increase. That is why the wrap-around model was selected for this study.
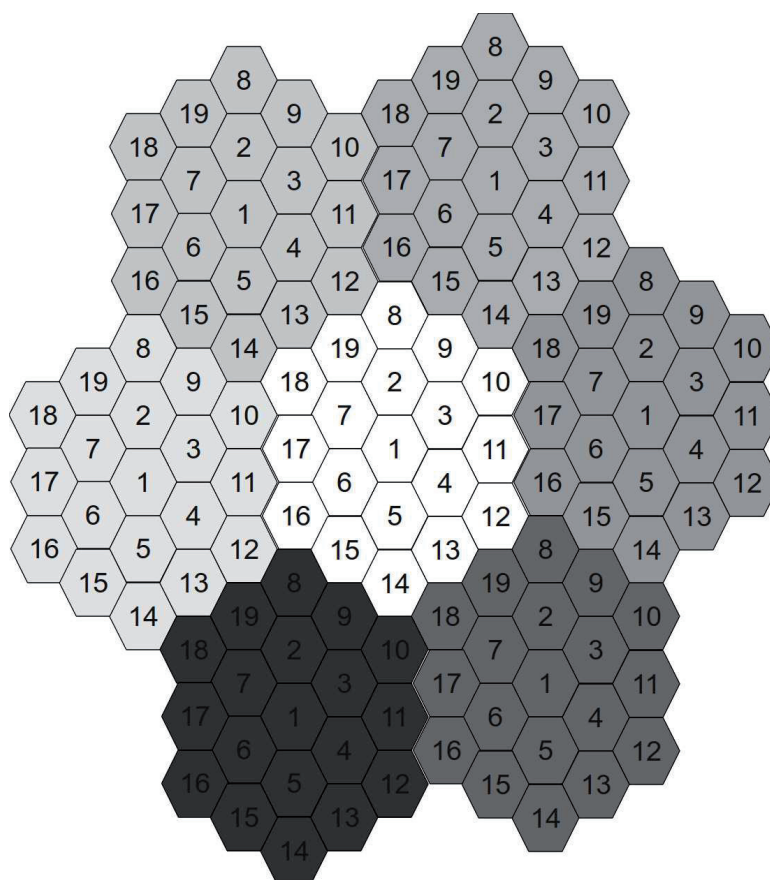
FIGURE 21   Wrap-around model with 19 Node Bs

UEs are uniformly distributed over the network, where the number of UEs per cell varies. The number of runs and number of UEs per cell has been chosen as a good balance between simulation time and accuracy of the results and presented in Table 4. The simulation time depends on the total amount UEs per network, hence with increasing the number of UEs per cell, the number of run is decreasing.

TABLE 4   Number of runs vs number of UEs per cell

Number of UEs per cell	1	2	4	8	16	32
Number of runs	106	80	27	14	7	4

The propagation model was taken from [3GPl] and defined as:

$$L = 128.1 + 37.6 log_{10}(R), \tag{43}$$

where R is the distance between UE and Node B in kilometers.

The parameters for slow fading were taken from the same document. Lognormally distributed slow fading is modeled for each UE separately when a UE enters the network with 8 dB of shadowing standard deviation and the shadowing correlation distance of 50 meters. Even though the UEs are stationary, fast fading is modeled according to the International Telecommunication Union (ITU) channel models such as PedestrianA, PedestrianB and VehicularA. However, the power delay profiles of these models were modified in the sense that the delay between paths would be equal to chip-tupled time. The modified power delay profiles presented in Table 5 and the reference for it can be found in [3GPk] and [Rec97].

TABLE 5   Power delay profiles fro ITU channel models

Number of tap	1	2	3	4	5	6
PedestrianA delay, chips	0	1	-	-	-	-
PedestrianA power, dB	0	-12.77	-	-	-	-
PedestrianB delay, chips	0	1	3	4	5	9
PedestrianB power, dB	0	-2.8	-5.97	-11.43	-10.91	-9.35
VehicularA delay, chips	0	1	2	3	4	-
VehicularA power, dB	0	-1.92	-7.31	-10.39	-10.89	-

The maximum number of HS-DSCH codes is 15, with the spreading factor of 16. The simulations were done without code-multiplexing, i.e. only one UE can be scheduled per one TTI. The maximum power of Node B is 20W; however only 14W or 70% is used for HS-PDSCH transmission. The remaining power, i.e. total overhead power, is used for the pilots and the control channel. The Signal to Interference plus Noise Ratio (SINR) is mapped to packet error probabilities using the Actual Value Interface (AVI) approach. The CQI signalling via HS-DPCCH is ideal, i.e. it always correctly decoded, however 3 TTI delays were introduced to make simulations more realistic. There are 6 parallel HARQ processes and only 4 retransmissions at most is possible per one transport block. To simplify the reviewing of the main simulation parameters, they are introduced in Table 6.

Only the second strongest interfering cell is considered as the assisting cell, with an additional requirement that this cell must belong to the same site as the main serving cell, which has an impact on choosing the candidate UE for HS-SFN. Theoretically, there is possibility to choose not only the second best interferer, but rather consider the third strongest interfering cell, which belong to the same site, as the assisting cell, if the second strongest interfering cell is belong to the different site. It will increase the number of HS-SFN candidates, however it might decrease the overall benefit from HS-SFN. According to the network layout, path loss model and Node B antenna model from Table 6, the average percentage of HS-SFN candidates for three-sector sites is 4-5% and for six-sector sites is about 6%. Since traffic load is uniformly distributed over the network, there is no need to separate the threshold value used for HS-SFN for different cells. However, for

TABLE 6   Simulation parameters

Parameter	Value
Cell Layout	Hexagonal grid, 19 Node Bs, wrap-around
Number of sectors per Node B	3, 6
Inter-site distance	1000 m
Carrier Frequency	2000 MHz
Path Loss	L=128.1 + 37.6log10(R), R in kilometers
Log Normal Fading	
Standard Deviation	8dB
Inter-Node B Correlation	0.5
Intra-Node B Correlation	1.0
Correlation Distance	50m
Max BS Antenna Gain	
3-sector site	14 dBi
6-sector site	17 dBi
2D Antenna pattern	$A(\theta) = -min(12(\theta/\theta_{3dB})^2, Am)$
for 3-sector site	$\theta_{3dB} = 70\ degrees,\ Am = 20dB$
for 6-sector site	$\theta_{3dB} = 35\ degrees,\ Am = 23dB$
Channel Model	PedA3, PedB3, VehA30
CPICH Ec/Io	-10 dB
Total Overhead power	30%
UE Antenna Gain	0 dBi
UE Noise figure	9 dB
UE Receiver type	type3, type3i and enhanced type3
Speading factor	16
Maximum Sector Transmit Power	43 dBm
Handover reporting range	3dB
Number of HARQ processes	6
Traffic	
Traffic model	Bursty Traffic Source Model
Number of UE per cell	1, 2, 4, 8, 16 and 32
File size	Fixed at 1 Mbit
Inter-arrival time	Exponential, mean = 5 seconds
Flow control on Iub	Ideal and instantaneous
CQI	Ideal with 3 TTI delay
Scheduling	
for reference scenario	Proportional Fair Scheduler
for HS-SFN scenario	Combined intra-Node B scheduler

networks with unbalanced traffic loads, a different threshold value might be used for each cell to achieve the best performance.

Two different types of schedulers were used for the non-HS-SFN and HS-SFN scenarios. One is the well-known independent proportional fair scheduler

[JPP00], where the UE probability to be scheduled depends on the proportional fair metric, which in turn depends on the achievable data rate and scheduler decisions in the previous TTIs. This type of scheduler is used for all the UEs in the reference scenario. And for the HS-SFN scenario, a common site-wide scheduler is enabled. That kind of scheduler is able to form all possible scheduling combinations and choose the combination with the highest possible total data rate for the whole site while also taking into account the proportional fair resource allocation. More precise information about site-wide scheduler can be found at 3.5.

4.2.1 HS-SFN

This subsection presents the results for HS-SFN without any additions such as phase adjustment or enhanced type3 receiver. These results represent the baseline legacy case of a UE with no HS-SFN related changes. Similar results were presented in [HPHC11]; however, after that they were regathered with the FTP traffic model, and only one scheduler approach is taken into account. HS-DDTx is dropped completely from these simulation results due to its minor benefit on the results taking into account the increasing complexity for the scheduler and signaling in the real life. The first set of results is presented as cumulative distribution function (CDF) figures for 1, 8 and 32 UEs per cell, showing the benefit of HS-SFN for cells with a low, average or high load. Two receiver types are under our consideration in this section: type3 and type3i, which were described in 2.6.2 and 2.6.2, respectively. Since HS-SFN can benefit mostly on the UEs in the softer handover area, the next figures present results for softer handover UEs and also for all UEs showing the overall system performance.

From Figure 22(a), Figure 22(b) and Figure 22(c), that show CDF for 1 UE per cell with the type3 receiver for PedestrianA, PedestrianB and VehicularA respectively, it can be seen that HS-SFN can increase the performance of the softer handover UEs. However, all UEs curves exhibit a marginal variation, that may be partly explained by different interference distributions. Regarding the usage of HS-SFN under the different channel models, there are some variations from the absolute user burst rate; however, the HS-SFN improvement looks quite similar.

The Figure 23 presents results for the type3i receiver in the same way as in the previous figures. This figure shows a similar HS-SFN benefit on the softer handover UEs and marginal differences for all the UEs.

Figure 24(a), Figure 24(b) and Figure 24(c) show CDF for 8 UE per cell with the type3 receiver for PedestrianA, PedestrianB and VehicularA, respectively. The performances of all the UEs are the similar with or without HS-SFN. The UEs in the softer handover area still have some benefit from HS-SFN, however it is decreased compared to the 1UE per cell simulation results. This can be explained by the fact that the neighboring cells with low loads often do not have their own users to schedule, thus providing opportunities for those cells to assist the serving cell. The percentage of HS-SFN TTIs are decreasing with the increasing cell load, and, in line with this, the gain from HS-SFN is decreasing. Dependency in
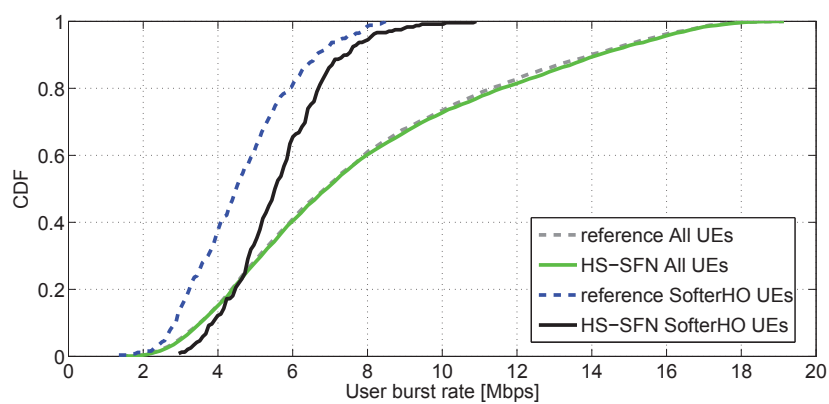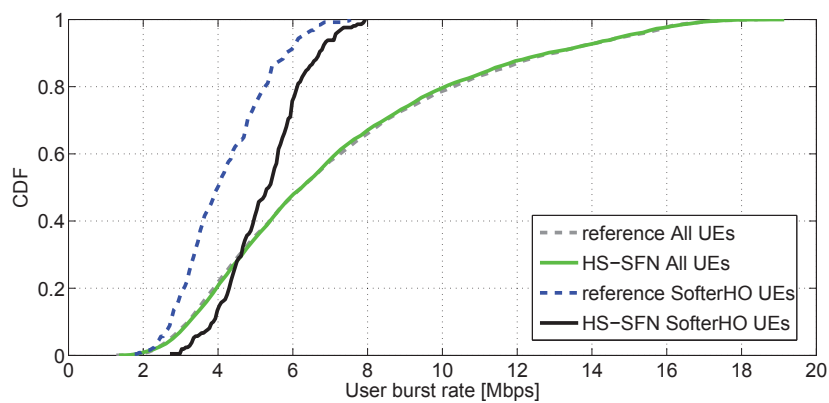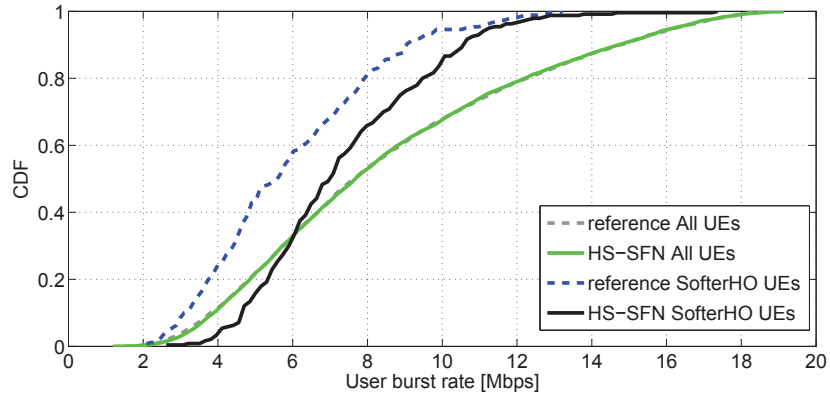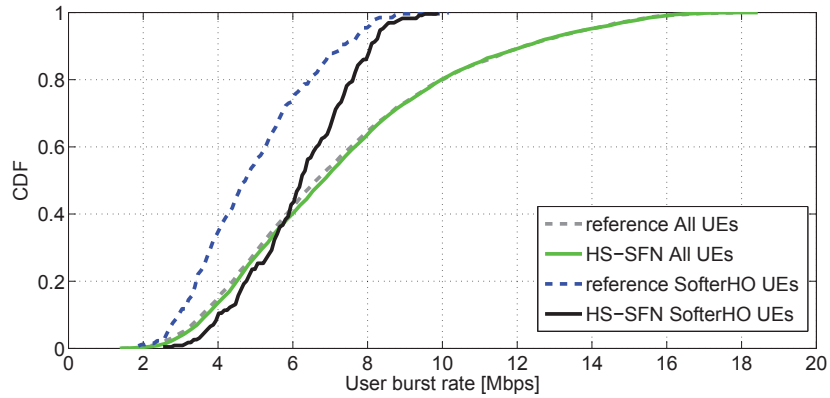
(a) Pedestrian A
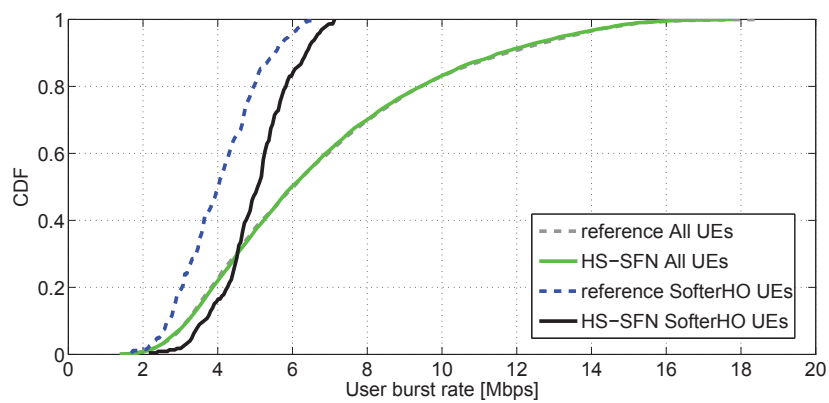
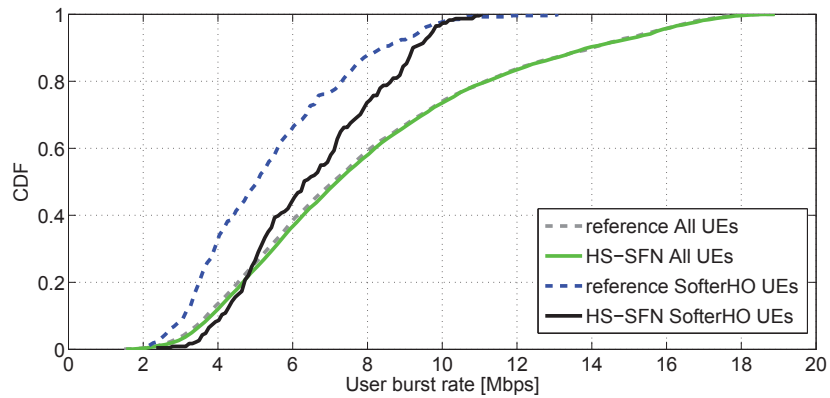(b) Pedestrian B

(c) Vehicular A

FIGURE 22   CDF of HS-SFN compared to non-HS-SFN operation for Type3 receiver and
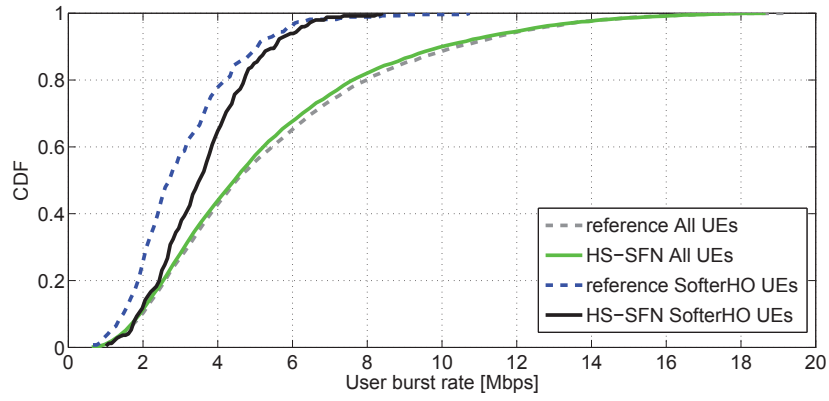1UE per cell

(a) Pedestrian A
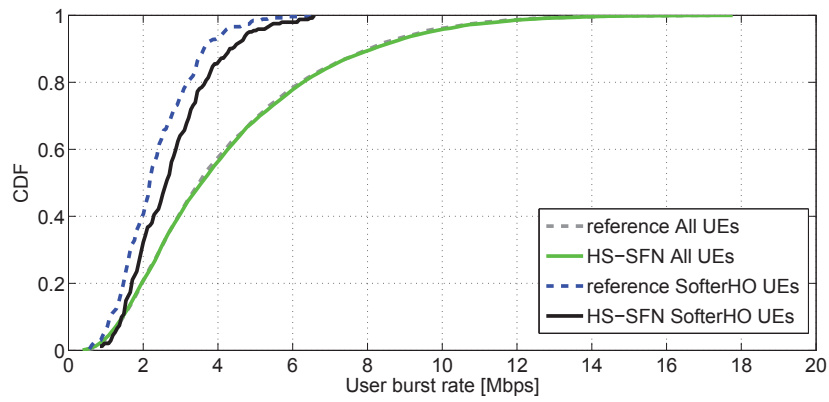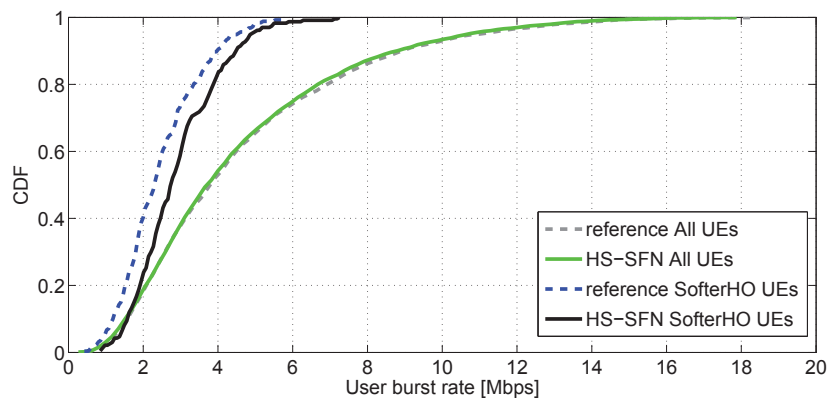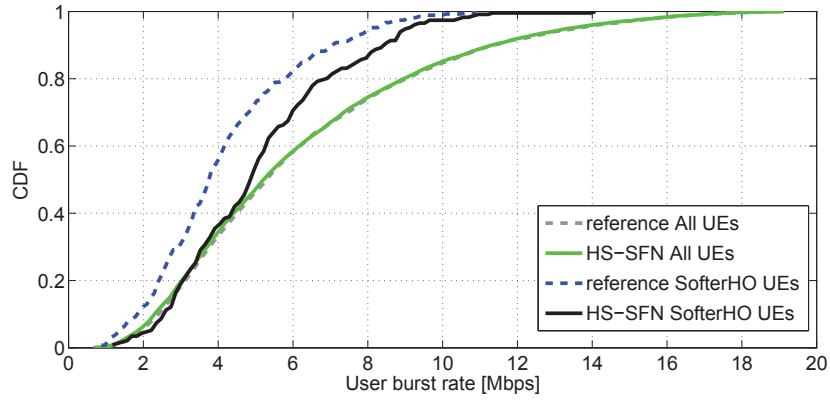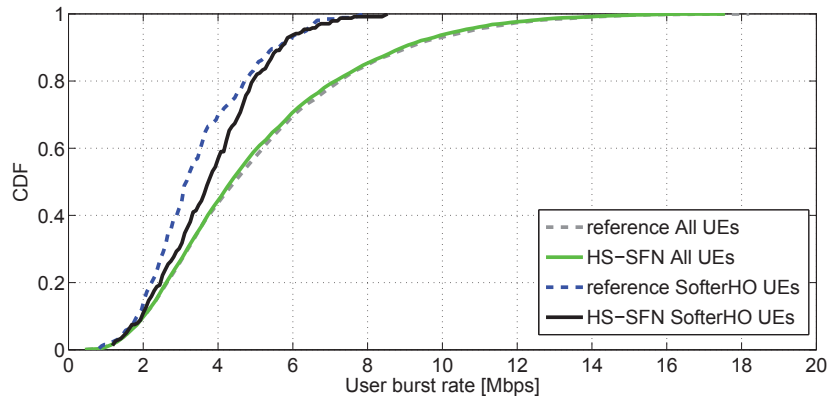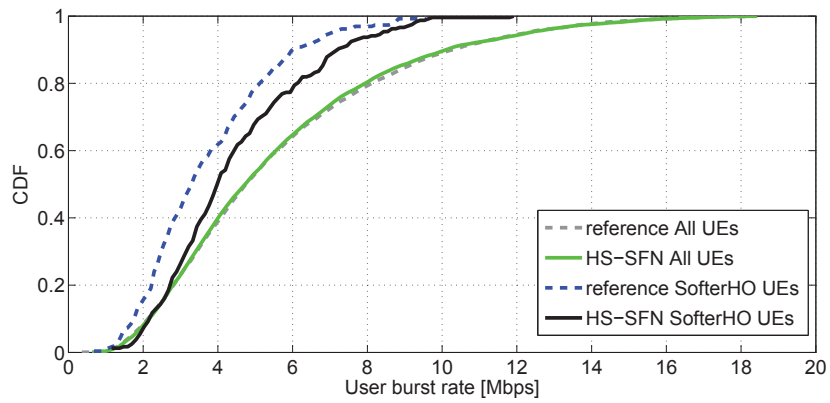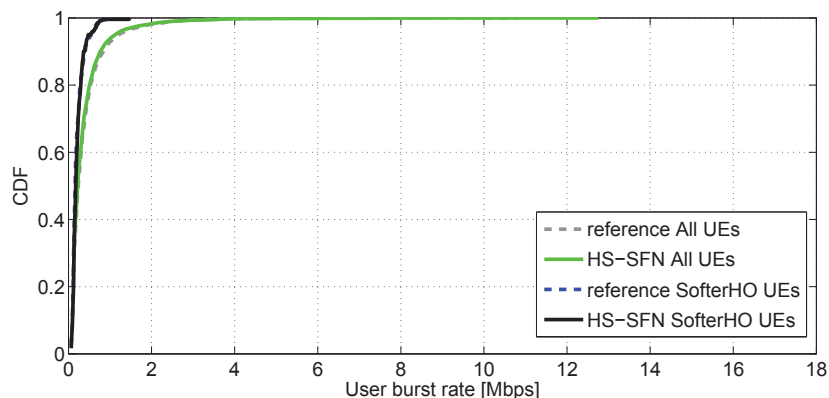

(b) Pedestrian B

(c) Vehicular A

FIGURE 23   CDF of HS-SFN compared to non-HS-SFN operation for Type3i receiver
and 1UE per cell

(a) Pedestrian A

(b) Pedestrian B

(c) Vehicular A

FIGURE 24   CDF of HS-SFN compared to non-HS-SFN operation for type3 receiver and 8UE per cell

(a) Pedestrian A
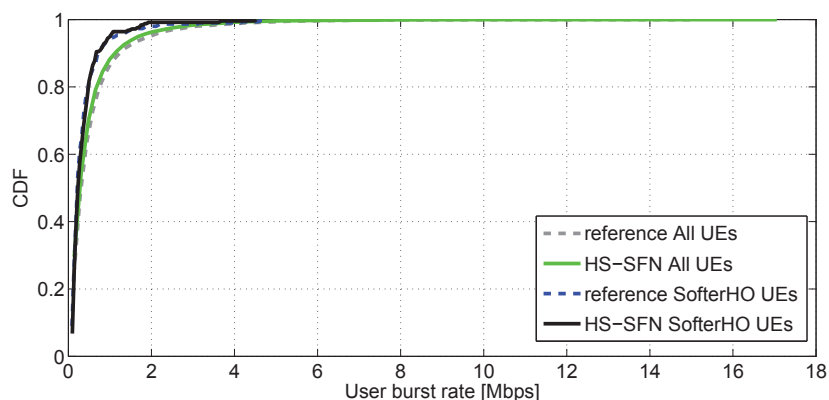

(b) Pedestrian B

(c) Vehicular A

FIGURE 25   CDF of HS-SFN compared to non-HS-SFN operation for type3i receiver and 8UE per cell

the results between different channel models looks the same as in the previous results, as well as the relation in the results between type3 and type3i receivers. Results for the type3i receiver are presented in Figure 25.

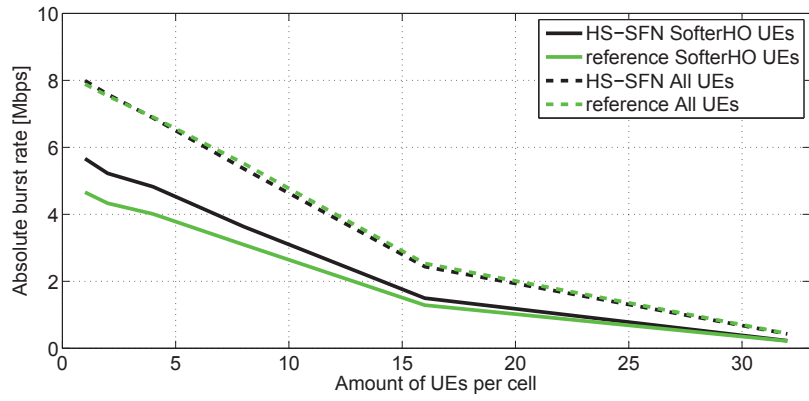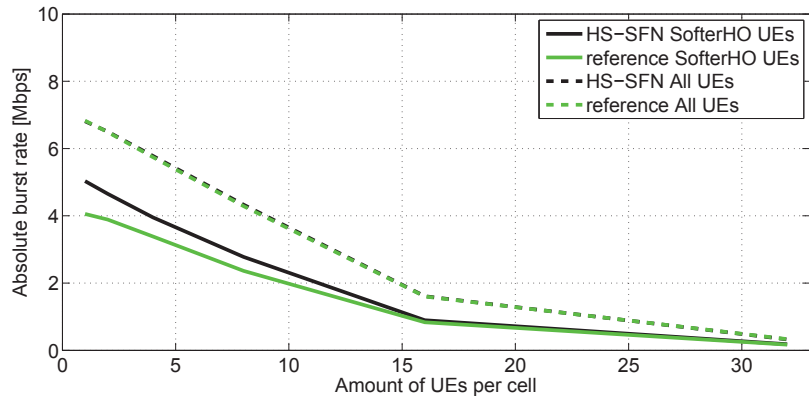(a) Type3 receiver

(b) Type3i receiver

FIGURE 26   CDF of HS-SFN compared to non-HS-SFN operation for type3 and type3i
             receivers with PedestrianA channel and 32UE per cell

The Figure 26(a) and Figure 26(b) show the results for 32 UEs per cell with type3 and type3i receivers, respectively. There is neither positive nor negative effect from HS-SFN. This can be easily explained by the rare usage of HS-SFN due to the high load in the cells, which does not allow the scheduler to assist the serving cell. The results are presented only for the Pedestrian A channel. However, the same dependence was observed in the results from other ITU channel models.
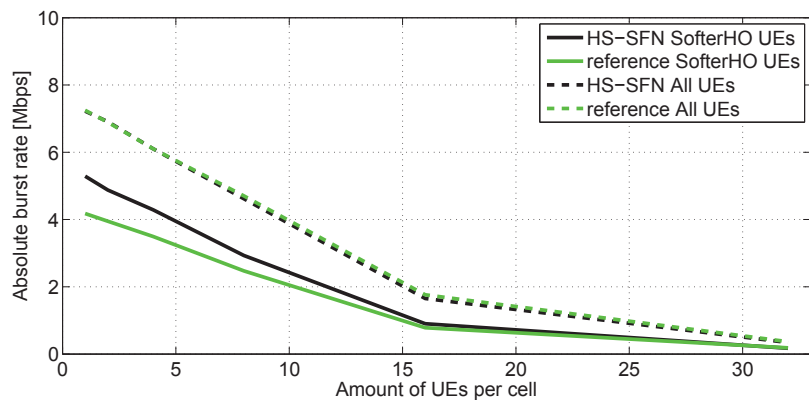
Figure 27(a), Figure 27(b) and Figure 27(c) show a quite logical dependence performance for different ITU channel models, i.e. the best performance is reached under the PedestrianA channel, a bit worse with the VehicularA and the worst with the PedestrianB. Unlike in gain comparison, that will be shown later, these
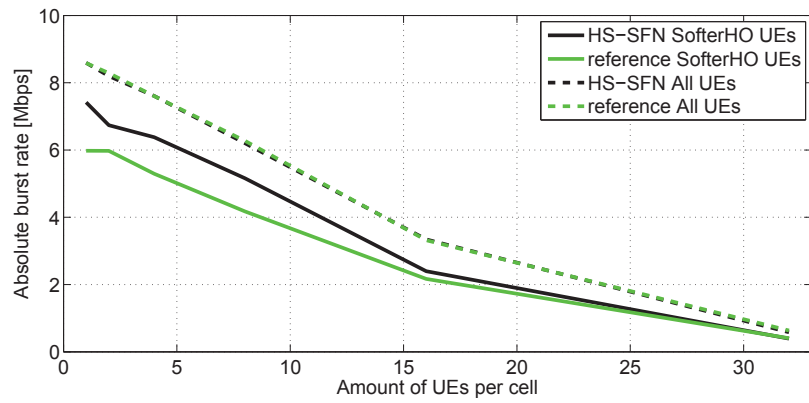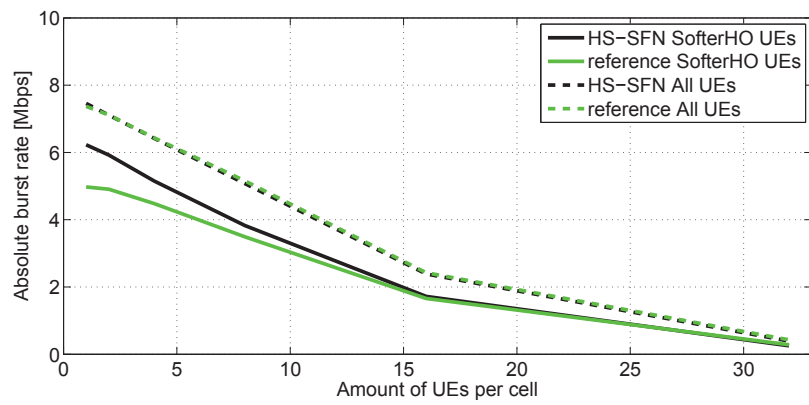
(a) Pedestrian A

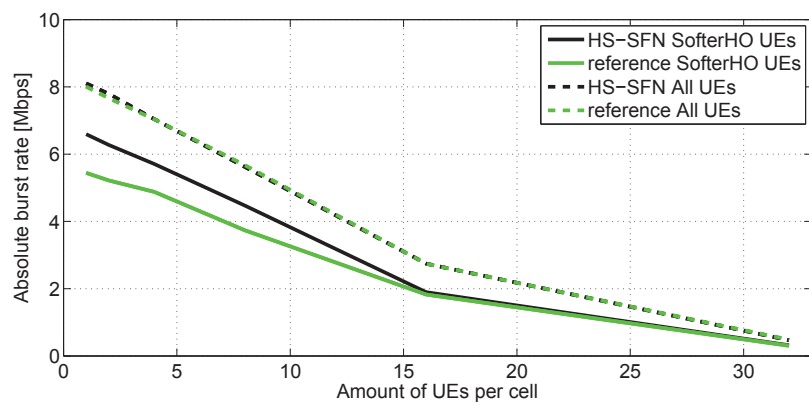(b) Pedestrian B

(c) Vehicular A

FIGURE 27   Absolute burst rate comparison of HS-SFN and reference cases for type3 receiver

(a) Pedestrian A

(b) Pedestrian B

(c) Vehicular A

FIGURE 28   Absolute burst rate comparison of HS-SFN and reference cases for type3i receiver

figures show a linearly decreasing absolute burst rate (as well as the difference of HS-SFN in relation to the reference cases) with increasing load level. Looking at Figure 27 and Figure 28 it also good to mention that the HS-SFN difference in relation to the reference cases is quite similar with the type3 and type3i receivers, despite the fact that the absolute burst rate with the type3i receiver is bigger compared with the type3 receiver.
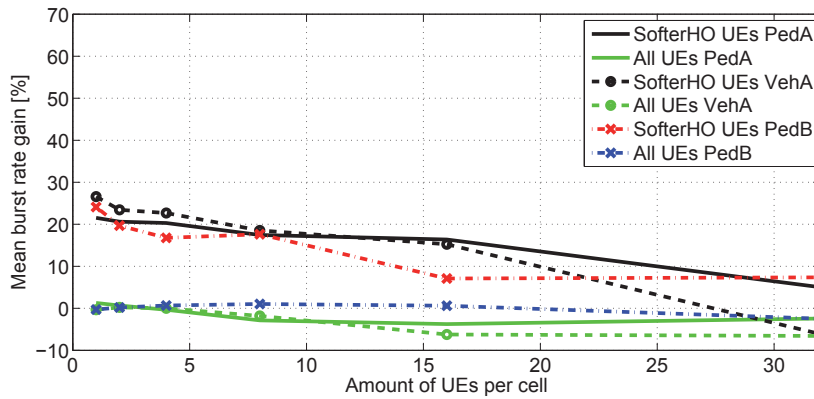

FIGURE 29   Mean burst rate gain of HS-SFN compared to non-HS-SFN operation for type3 receiver with different ITU channels
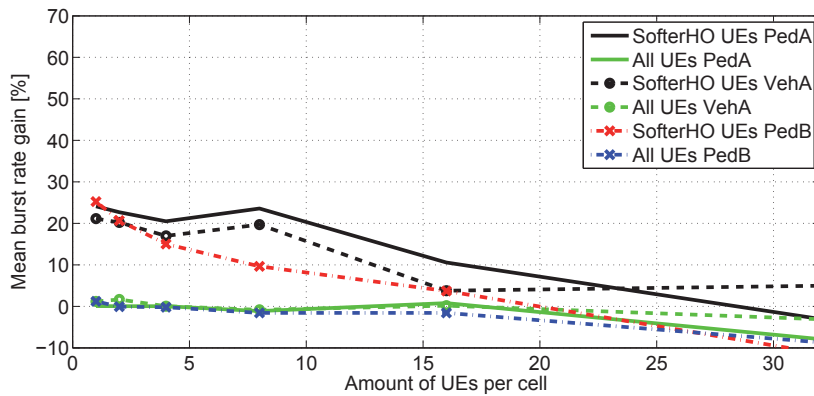

FIGURE 30   Mean burst rate gain of HS-SFN compared to non-HS-SFN operation for type3i receiver with different ITU channels

Figure 29 shows the comparison between the mean burst rate gain of an HS-SFN operation and that of a non-HS-SFN operation for all UEs and for UEs allocated to the softer handover area for the Pedestrian A, Pedestrian B and Vehicular A channels with the type3 receiver. The same results, but for the type3i receiver, are presented in Figure 30. These results show that a 20% gain can be achieved for UEs in the softer handover area with a very small overall negative gain for all the UEs in the network. The burst rate gains decrease with higher-load cells.

This may be explained by the fact that the low-load neighboring cells often do not have own users to schedule; a short-term load balancing is thus being observed there. For high-load cells, the load balancing effect disappears because without their own UEs the cells cannot make use of HS-SFN. The additional interference created by their assistance in transmission to other cells has smaller impact for the low-load than for the high-load.

$$Gain = (AbsoluteBR_{HS-SFN} / AbsoluteBR_{non-HS-SFN} - 1) \cdot 100\%. \qquad (44)$$

The gain figures also show that the decreasing gain from low to high load is not linear. This can be explained by the randomness in the simulation regarding the different UEs' position and fast fading, notwithstanding the big numbers of the simulation run. Another explanation provided in Figure 27(a) - Figure 28(c) that show the absolute burst rate for HS-SFN and the reference cases. With the increase in the load of the cell, the burst rate becomes smaller and, according to the (44), with a smaller burst rate the variation of gain becomes higher. Comparing the gain from HS-SFN under different ITU channel models from the Figure 29 and Figure 30 can be mentioned that, theoretically, HS-SFN with a PedestrianA channel should perform better than with other ITU channel models since with smaller number of taps there are more chances to achieve a bigger gain.

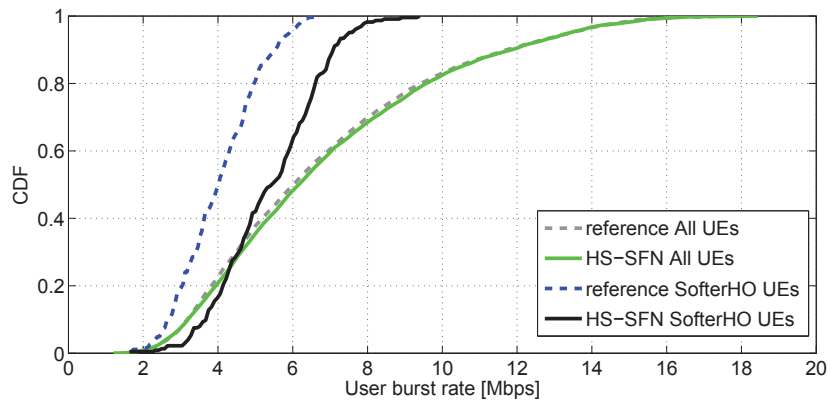### 4.2.2 HS-SFN with enhanced type3 receiver

This subsection presents the results for HS-SFN with enhanced type3 receiver as well as its comparison with the normal type3 receiver. Basically, these are extended results of the article [PZH+11], in which the results only for PedestrianA channel were presented. This study extends the results for channels with more path and with a longer delay spread, including the PedestrianB and VehicularA channel models. Additionally, in this study the results have also been gathered for the high-load cell (16 and 32 UEs per cell). The way of presenting the results here is quite similar to that in the previous section. First, the results for 1 and 8 UEs per cell are presented as CDF of user burst rate. Then a precise comparison to the type3 receiver is shown as CDF with 1 UE per cell. After that, it is the turn of absolute burst rate comparison, and finally gain comparison will finish the enhanced type3 receiver evaluation.

Figure 31(a), Figure 31(b) and Figure 31(c) present CDF curves for 1UE per cell for PedestrianA, PedestrianB and VehicularA ITU channel models respectively. These figures show that enhanced type3 receiver does not change the overall impact of HS-SFN, i.e. there is almost no difference for all UEs performance; however, UEs in the softer handover area perform better than with the type3 receiver, especially the UEs with higher burst rate. It can be seen that HS-SFN as well as the reference cases have higher burst rates with the PedestrianA channel.

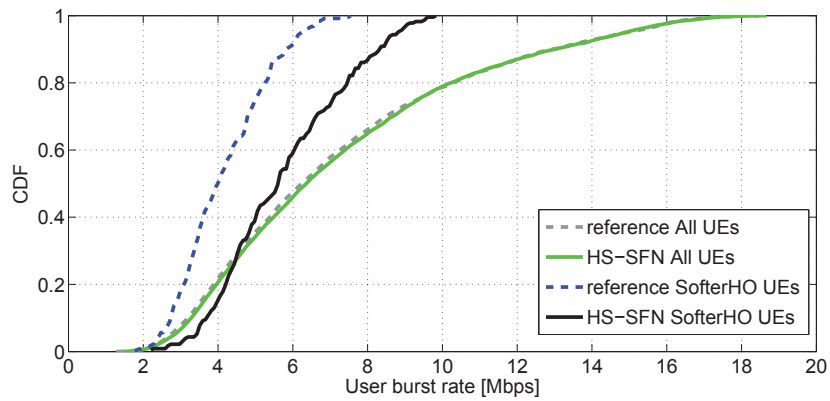Figure 32 presents the CDF curves for 8UEs per cell under different ITU channel models. The benefit from HS-SFN for 8UEs in the softer handover area is less than for 1UE per cell; however, it is still better than the results for the type3
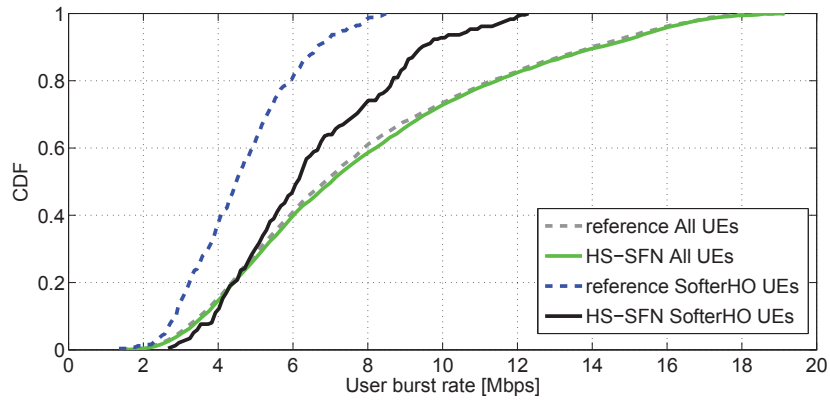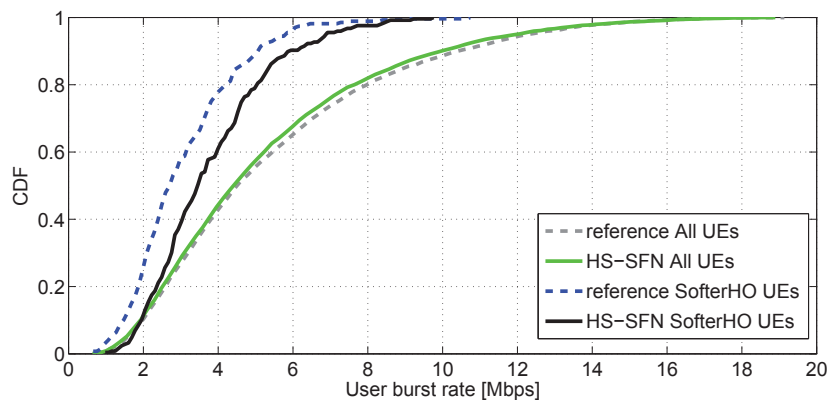
(a) Pedestrian A
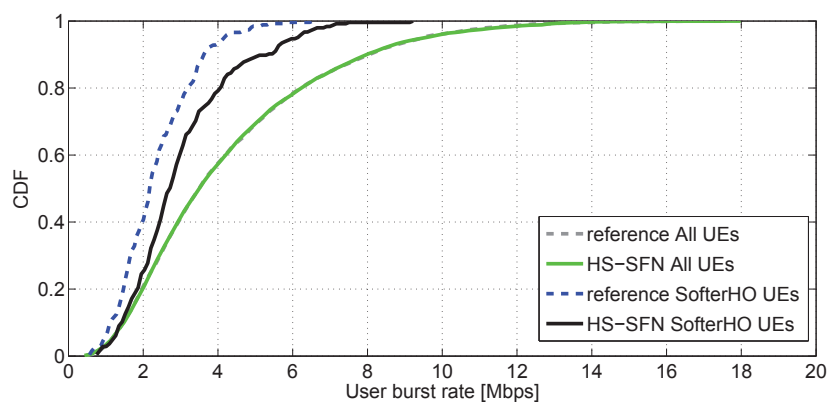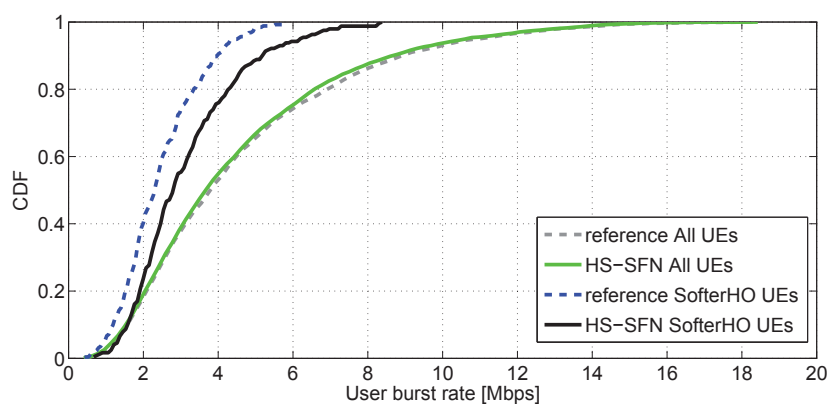
(b) Pedestrian B

(c) Vehicular A

FIGURE 31   CDF of HS-SFN compared to non-HS-SFN operation for enhanced type3
receiver and 1UE per cell

(a) Pedestrian A

(b) Pedestrian B

(c) Vehicular A

FIGURE 32   CDF of HS-SFN compared to non-HS-SFN operation for enhanced type3
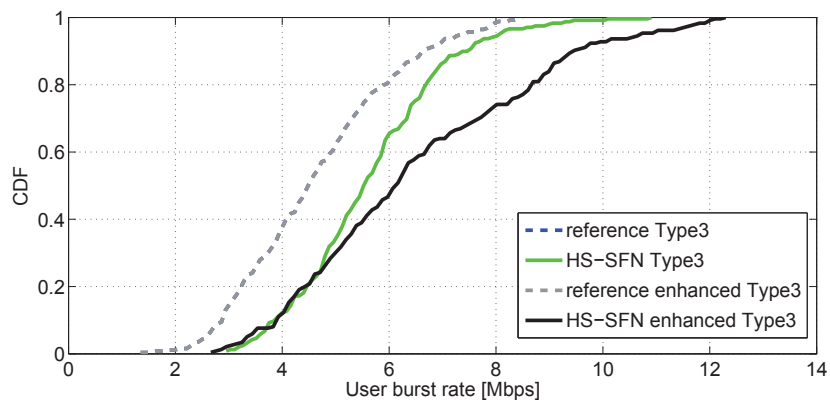receiver and 8UE per cell

receiver. An exact comparison between type3 and enhanced type3 is done only for the cases with 1UE per cell because HS-SFN has the highest benefit there, and the difference between two receivers might be seen best there. This comparison is done only for softer handover UEs and can be observed in Figure 33. This figure shows only one CDF curve for the reference cases for the type3 and enhanced type3 receivers. This is due to the results being exactly the same and overlapping each other. The enhanced type3 receiver does not increase the performance of the lowest 20% burst rate UEs and has a bigger benefit on the higher percentile portions. It can be explained by the fact, that enhanced type3 receiver decrease the own interference and UEs with low burst rate should have quite strong inter-site interference and own interference does not impact much. The smallest benefit of usage enhanced type3 compared to type3 can be observed from the results with the PedestrianB channel model.

Figure 34 presents the comparison of absolute burst rate for HS-SFN with the type3 receiver, for HS-SFN with the enhanced type3 receiver and the reference or non-HS-SFN case. As was said previously, there is no difference in the reference case between the type3 and enhanced type3 receivers: that is why only one reference case is presented in this figure. This figure shows the linearly decreasing absolute burst rate with increasing load level of the cells, pointing to the PedestrianA channel model as the best one among the channel models as it should be. Marginal improvements only can be observed with 16 and 32 UEs per cell.

Figure 35(a), Figure 35(b) and Figure 35(c) show the burst rate gains of HS-SFN transmission for the enhanced type3 receiver with the PedestrianA, PedestrianB and VehicularA channel models respectively. From these figures can be seen that a bigger improvement for the enhanced type3 receiver can be observed in low-load cell (1-4 UEs per cell), where it can provide 15 - 20% of additional gain compared to the normal type3 receiver. Comparing the differences in results between the different ITU channel models, it can be noted that the smallest gain provided results with PedestrianB. PedestrianA and VehicularA have pretty much similar gains for the 1-8UEs per cell; however, for 32 UEs the results for VehicularA show bigger gain than the results for PedestrianA. This can be explained by the very small absolute burst rate, as was explained in the previous subsection.

4.2.3 HS-SFN with phase adjustment

This subsection presents the results for HS-SFN with phase adjustment, its comparison to HS-SFN without phase adjustment and to non-HS-SFN results. The first set of the results was presented in the article [PZH$^+$12]; however, the VehicularA channel model was not included there nor the results for 32UEs per cell. In addition to the results with the type3 receiver that were presented in the article, the results with the type3i receiver are also presented in this subsection. The presentation of the earlier results was limited due to the article size restriction. In this subsection, the results are presented as follows: first, the results for 1 and 8

(a) Pedestrian A
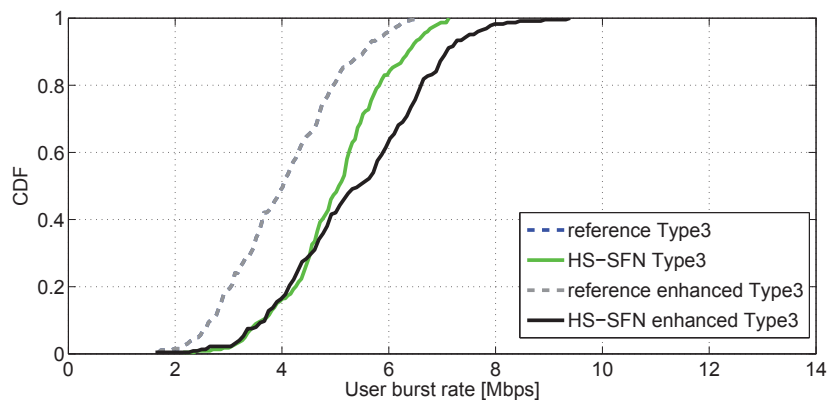
(b) Pedestrian B
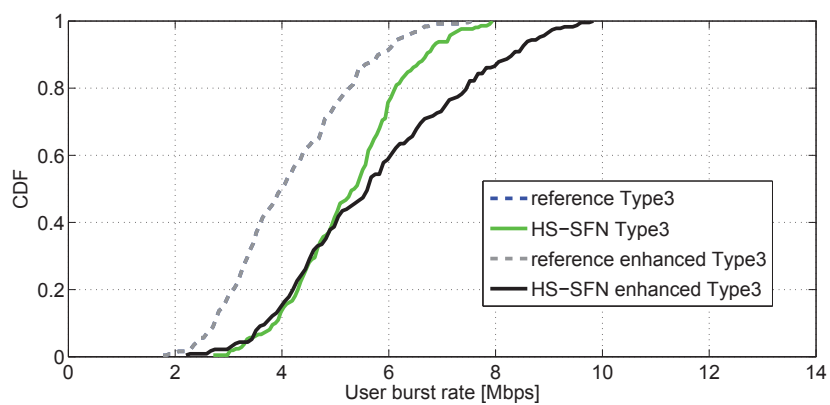
(c) Vehicular A

FIGURE 33   CDF comparison of type3 and enhanced type3 receivers under different ITU channel models for 1UE per cell

(a) Pedestrian A

(b) Pedestrian B

(c) Vehicular A

FIGURE 34   Absolute burst rate comparison of type3 and enhanced type3 receivers under different ITU channel models
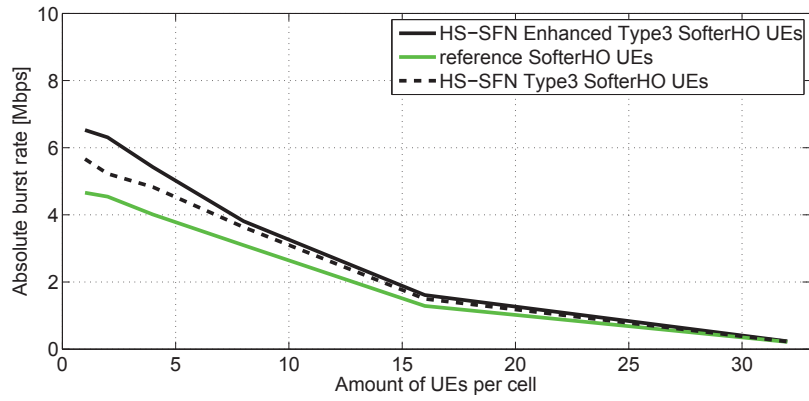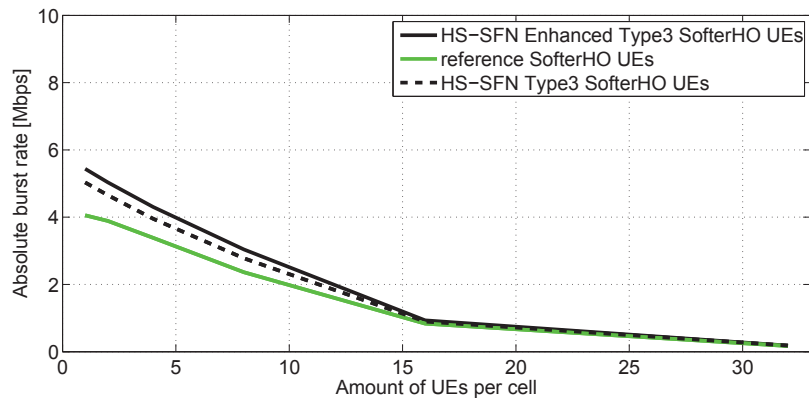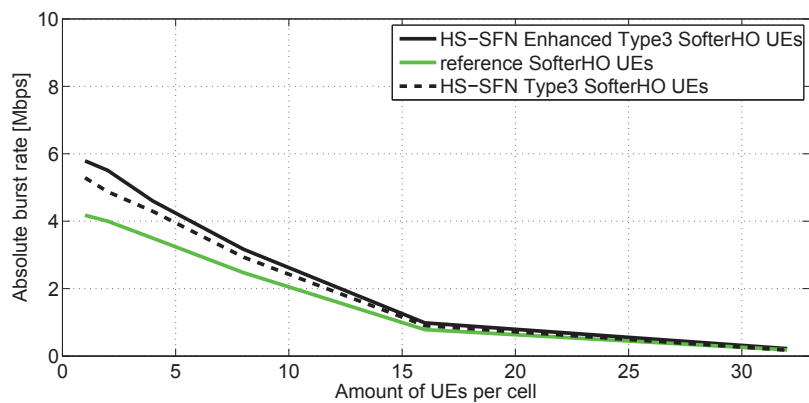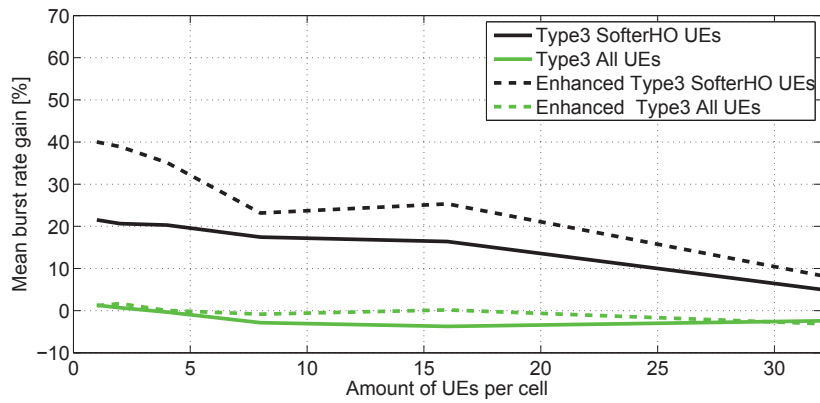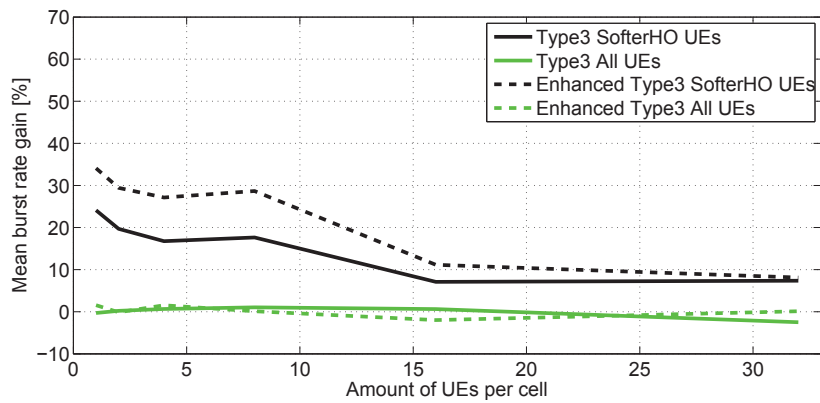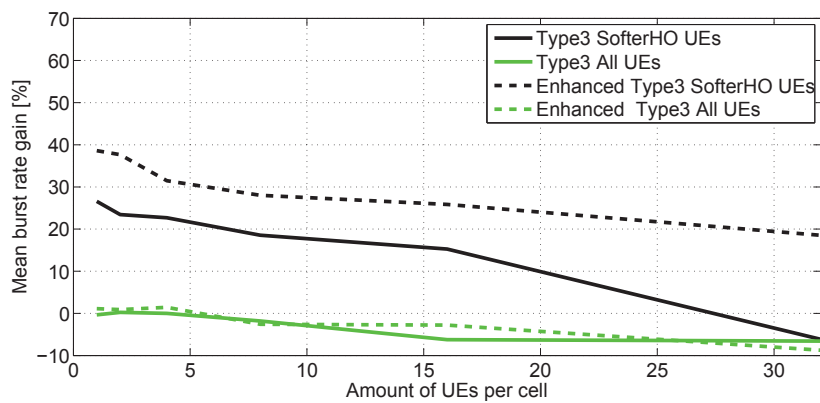
(a) Pedestrian A

(b) Pedestrian B

(c) Vehicular A

FIGURE 35 Gain comparison of type3 and enhanced type3 receivers under different ITU channel models

UEs per cell are presented as CDF of user burst rate; then the comparison of HS-SFN with and without phase adjustment are presented as CDF with 1 UE per cell. After that, an absolute burst rate comparison is shown, and the gain comparison will finalize this subsection.

Figure 36(a), Figure 36(b) and Figure 36(c) present CDF curves for 1 UE per cell with the type3 receiver for PedestrianA, PedestrianB and VehicularA, respectively. Each figure consists of the reference and HS-SFN with phase adjustment cases and shows the performance of the UEs in the softer handover area as well as the performance of all UEs. It can be seen that HS-SFN with phase adjustment can increase the performance of the softer handover UEs with a marginal variation of the performance for all UEs. However, it is worth mentioning that similar increase of performance due to HS-SFN with phase adjustment can be observed over all the percentiles of these CDF figures.

Figure 37(a), Figure 37(b) and Figure 37(c) show the CDF curves for 1 UE per cell with the type3i receiver for PedestrianA, PedestrianB and VehicularA, respectively. Roughly the same increase can be observed from HS-SFN with phase adjustment for the UEs in the softer handover area.

Figure 38(a), Figure 38(b) and Figure 38(c) show CDF for 8 UE per cell with the type3 receiver for PedestrianA, PedestrianB and VehicularA, respectively. The performance of all UEs is similar, with and without HS-SFN. The UEs in the softer handover area have a smaller benefit from HS-SFN compared to the 1UE per cell simulation results, in the similar way as in the results presented in Subsections 4.2.1 and 4.2.2. The same explanation can be applied for these results, that is, low-load neighboring cells often do not have own users to schedule and allow those cells to assist the serving cell. The results without phase adjustment for PedestrianB and VehicularA sometimes were better than PedestrianA, but with phase adjustment results for PedestrianA is the best one, because phase adjustment can perform better for channels with smaller number of taps, with PedestrianA rather than with PedestrianB or VehicularA. A better way of comparison will be given later, however. The results for the type3i receiver are presented in Figure 39(a), Figure 39(b) and Figure 39(c). The relation between the results for the type3 and type3i receivers is similar for 1UE per cell.

Figure 40(a), Figure 40(b) and Figure 40(c) present CDF comparison of HS-SFN with and without phase adjustment for the UEs in the softer handover area with the type3 receiver and for the PedestrianA, PedestrianB and VehicularA channel models, respectively. These figures show that the CDF curves for reference cases with and without phase adjustment overlap each other, which means that this technique does not effect to non-HS-SFN UEs. It is logical because no phase adjustment is possible in our model without HS-SFN, as we assume the single transmitting antenna per Node B. When the CDF curves for HS-SFN with and without phase adjustment are compared, it can be seen that phase adjustment can almost double the HS-SFN performance in terms of user burst rate. The biggest gain from phase adjustment can be reached with the PedestrianA channel. Figure 41(a), Figure 41(b) and Figure 41(c) show the same results, but for the type3i receiver. A slightly smaller benefit from the usage of phase adjustment
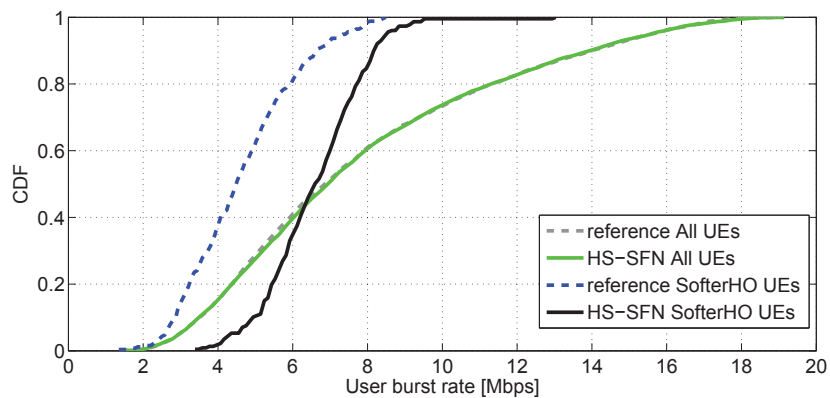
(a) Pedestrian A
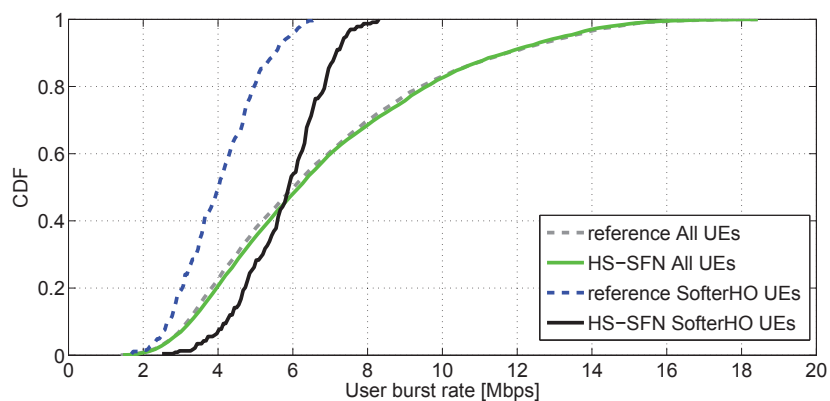
(b) Pedestrian B

(c) Vehicular A

FIGURE 36   CDF of HS-SFN with phase adjustment compared to non-HS-SFN operation for type3 receiver and 1UE per cell
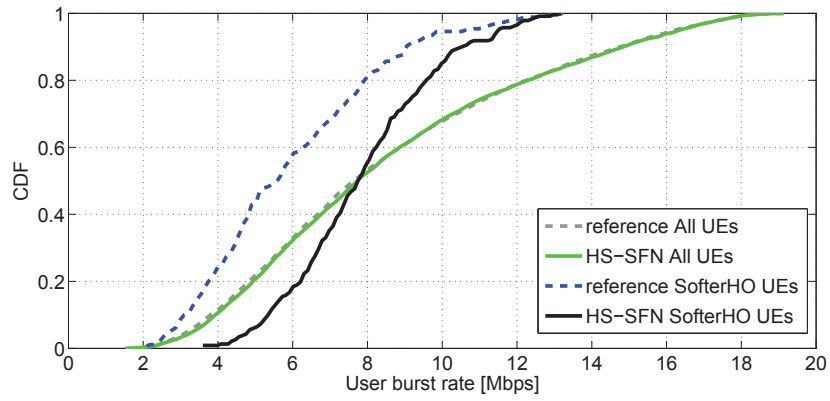
(a) Pedestrian A

(b) Pedestrian B

(c) Vehicular A

FIGURE 37   CDF of HS-SFN with phase adjustment compared to non-HS-SFN operation for type3i receiver and 1UE per cell

(a) Pedestrian A

(b) Pedestrian B

(c) Vehicular A

FIGURE 38   CDF of HS-SFN with phase adjustment compared to non-HS-SFN operation for type3 receiver and 8UE per cell

(a) Pedestrian A

(b) Pedestrian B

(c) Vehicular A

FIGURE 39   CDF of HS-SFN with phase adjustment compared to non-HS-SFN opera-
tion for type3i receiver and 8UE per cell

(a) Pedestrian A

(b) Pedestrian B

(c) Vehicular A

FIGURE 40   CDF comparison of HS-SFN with and without phase adjustment for type3 receiver and 1 UE per cell

(a) Pedestrian A

(b) Pedestrian B

(c) Vehicular A

FIGURE 41   CDF comparison of HS-SFN with and without phase adjustment for type3i
receiver and 1 UE per cell
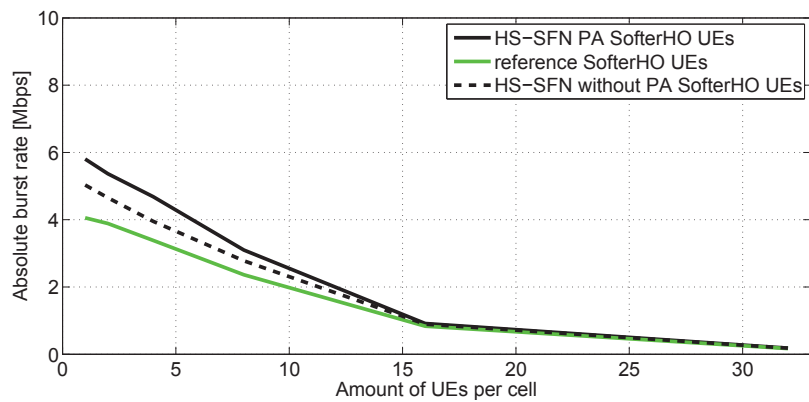
(a) Pedestrian A
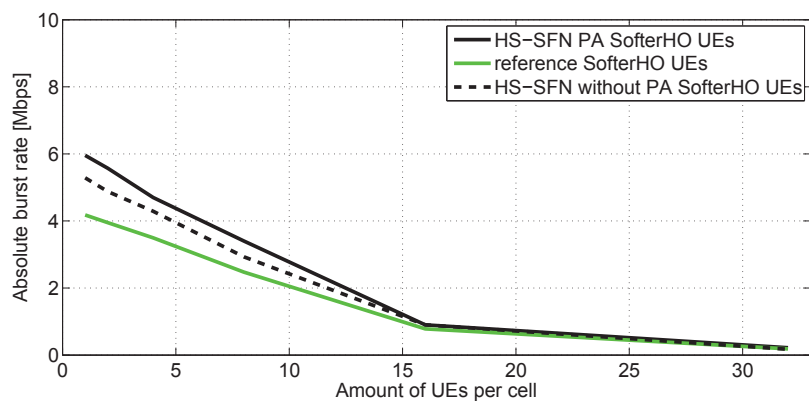
(b) Pedestrian B

(c) Vehicular A

FIGURE 42   Absolute burst rate comparison of HS-SFN with and without PA for type3 receiver
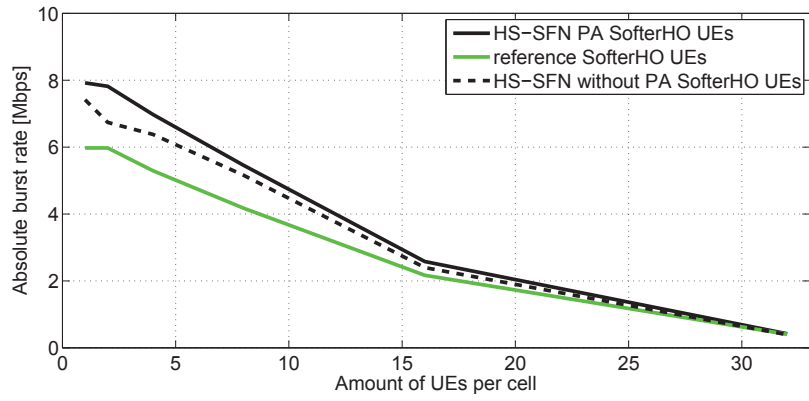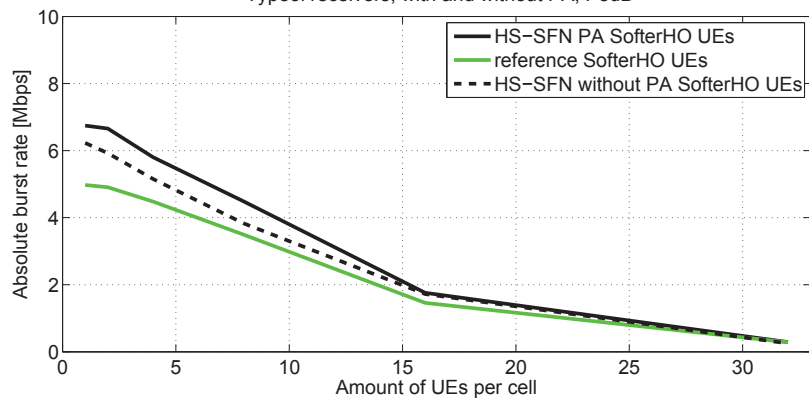
(a) Pedestrian A

(b) Pedestrian B

(c) Vehicular A

FIGURE 43   Absolute burst rate comparison of HS-SFN with and without PA for type3i
receiver
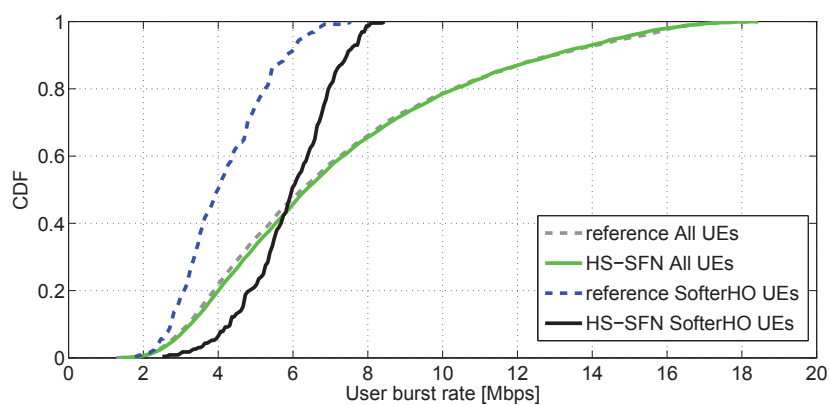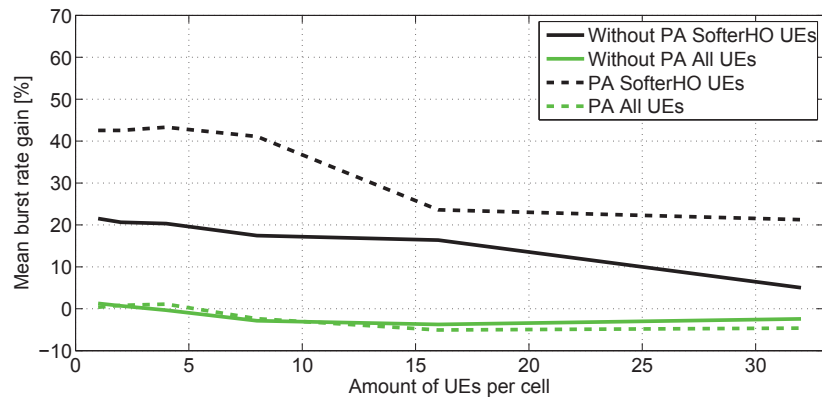
(a) Pedestrian A
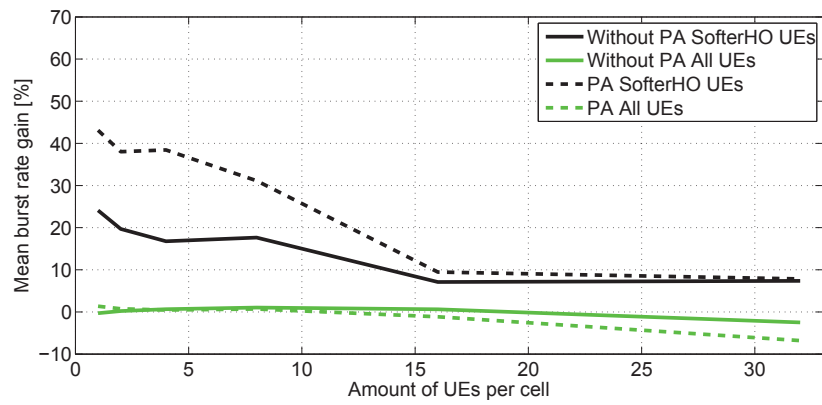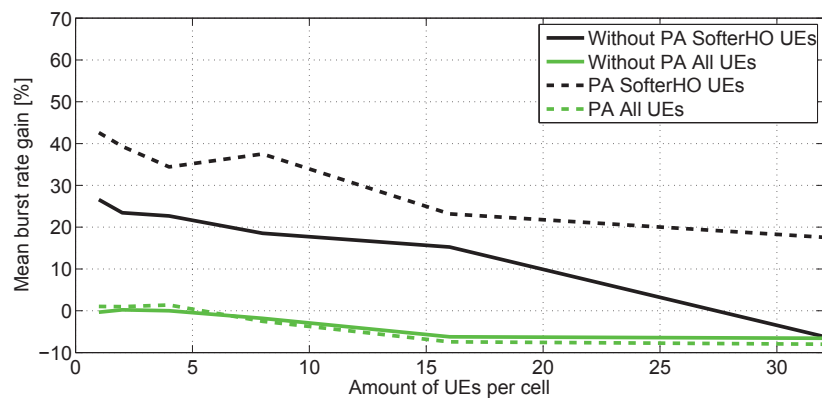
(b) Pedestrian B

(c) Vehicular A

FIGURE 44   Gain comparison of HS-SFN with and without phase adjustment for type3 receiver under different ITU channel models
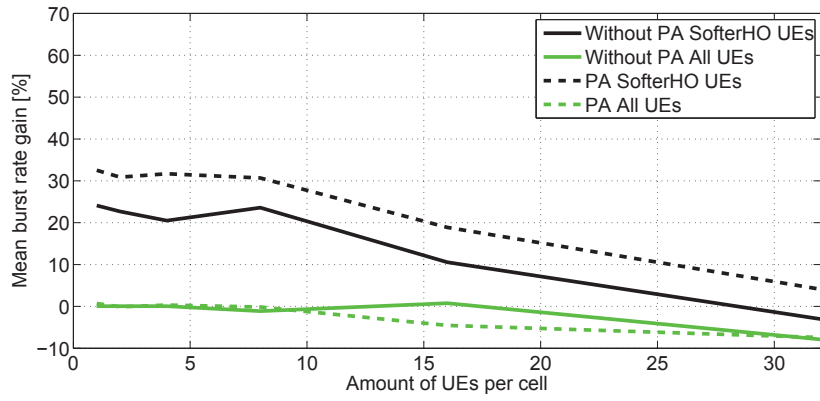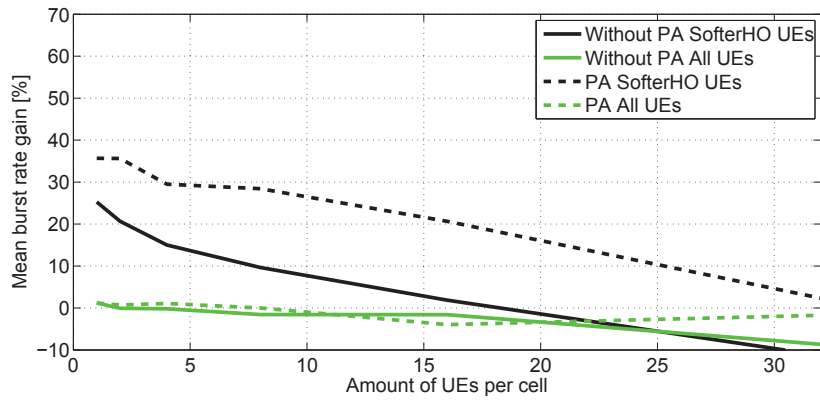
(a) Pedestrian A

(b) Pedestrian B
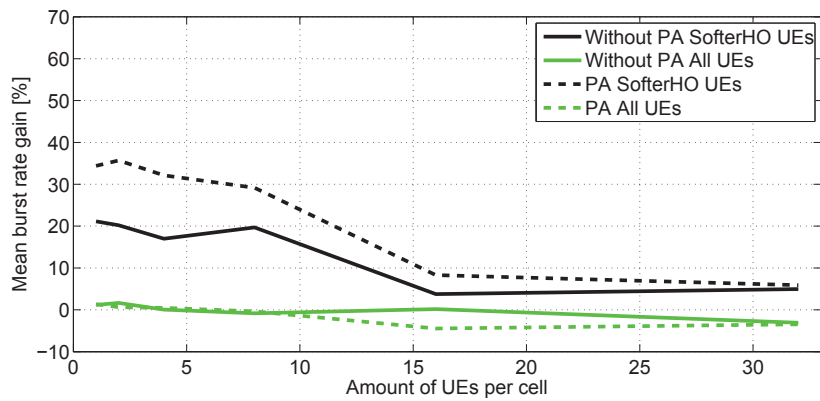
(c) Vehicular A

FIGURE 45   Gain comparison of HS-SFN with and without phase adjustment for type3i
receiver under different ITU channel models

appears compared to the type3 receiver.

Figure 42(a), Figure 42(b) and Figure 42(c) show an absolute burst rate comparison of HS-SFN transmission with and without phase adjustment for the type3 receiver under the PedestrianA, PedestrianB and VehicularA channel models, respectively, and Figure 43(a), Figure 43(b) and Figure 43(c) present the results for the type3i receiver. These figures show the similar behaviour as in figures shown in the previous subsections: i.e. there is the same dependence between different ITU channel models as well as the dependence between the type3 and type3i receivers. The results of increasing the burst rate for HS-SFN with phase adjustment compared to HS-SFN without phase adjustment will be described together with the gain consideration.

Figure 44(a), Figure 44(b) and Figure 44(c) show a burst rate gains comparison of HS-SFN transmission with and without phase adjustment for the type3 receiver under the PedestrianA, PedestrianB and VehicularA channel models, respectively. The biggest benefit from phase adjustment can be observed in the low-load and average-load cells (1-8 UEs per cell). The gain may almost be double compared to HS-SFN without phase adjustment. This can be easily explained by the fact that, in HS-SFN without phase adjustment, combining two signals can also be destructive. In this case, the scheduler will avoid this transmission. HS-SFN with phase adjustment will always produce positive gain from combining two signals, which will increase the percentage of HS-SFN transmission and therefore increase the gain from HS-SFN usage. It should be pointed out that the biggest gain from phase adjustment can be achieved under the PedestrianA channel since it has the smallest number of taps. However, phase adjustment brings additional gain also for other ITU channel models. With the increasing gain for UEs in the softer handover area the performance of all UEs decreases a bit. This can be explained by the fact that increasing HS-SFN transmission decreases the possibility of assisting cells to transmit the data to their own UEs.

4.2.4 HS-SFN with enhanced type3 receiver and phase adjustment 3 sector

This subsection presents the results for HS-SFN with phase adjustment and the enhanced type3 receiver and also a comparison of these results to HS-SFN without phase adjustment with type3 receiver (or pure HS-SFN) and to non-HS-SFN results. Similar results were presented in the article [Puc12]; however, other types of schedulers were used there as well as a different traffic model. The highest load in the article was 2Mbps with the NGMN traffic model, which can be converted to 10UEs per cell (taking into account the parameters of NGMN traffic model that was used). In this study, simulation results were obtained for up to 32UEs per cell. The structure of this subsection is similar to that of Subsection 4.2.1. First, the results for 1 and 8 UEs per cell are presented as CDF of user burst rate, after which an absolute burst rate comparison of HS-SFN with additions over pure HS-SFN and the reference cases are shown. Finally, the burst rate gain of HS-SFN with phase adjustment and the enhanced type3 receiver over the reference case is presented by figures.
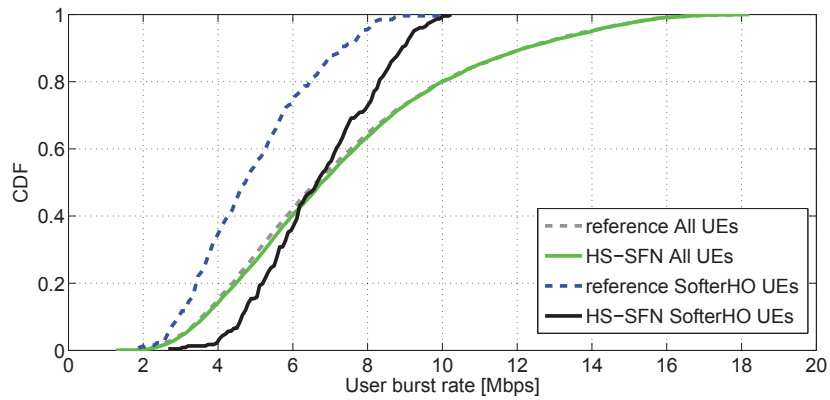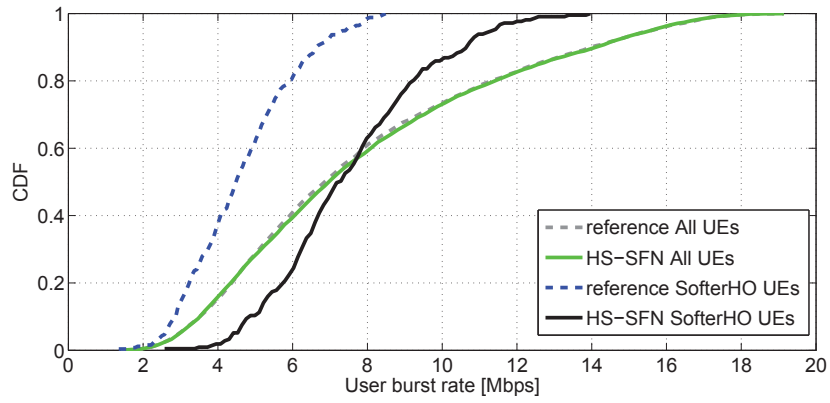
(a) Pedestrian A
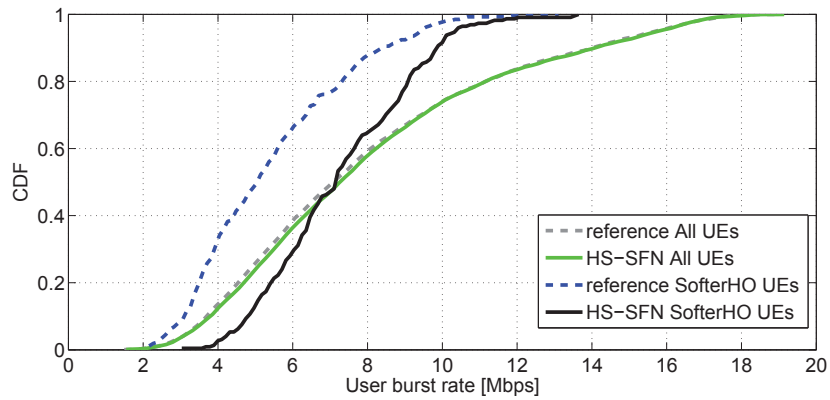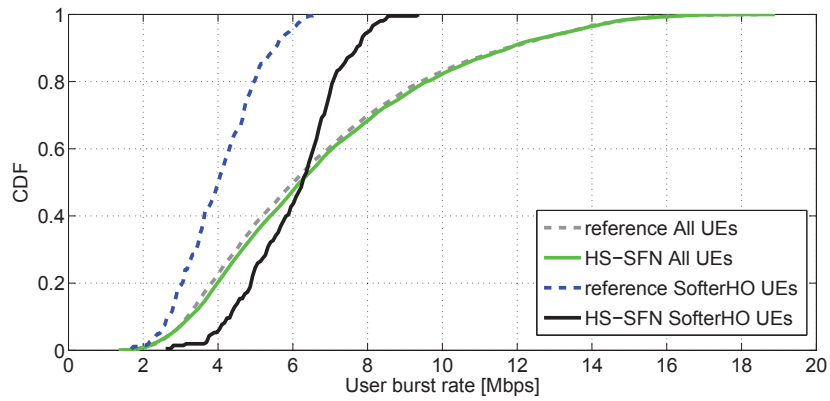

(b) Pedestrian B

(c) Vehicular A

FIGURE 46   CDF of HS-SFN with phase adjustment compared to non-HS-SFN operation for enhanced type3 receiver and 1UE per cell
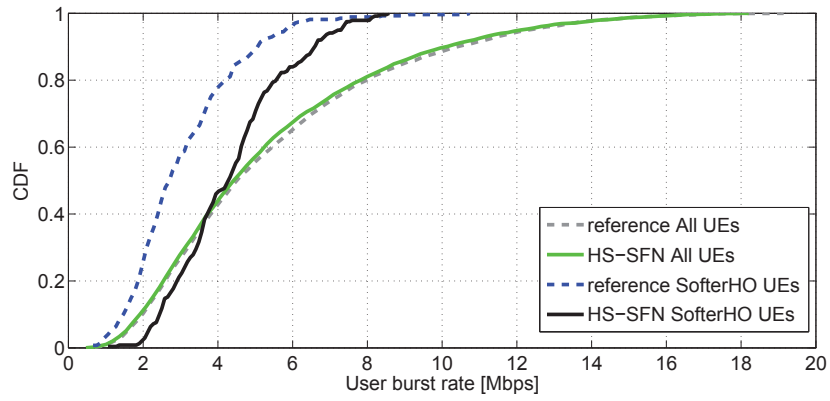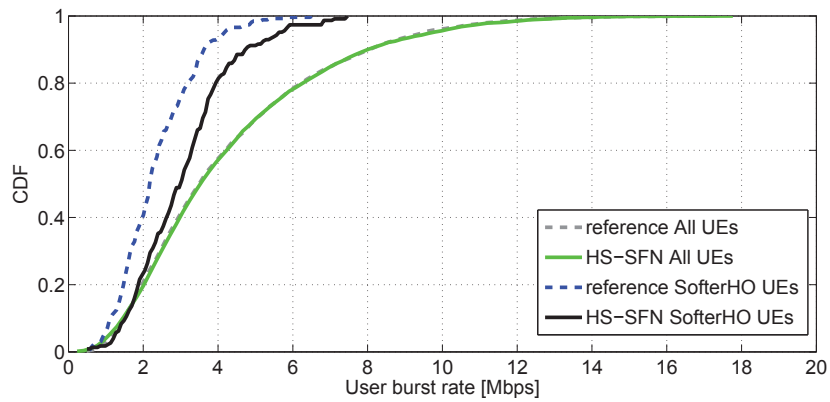
(a) Pedestrian A
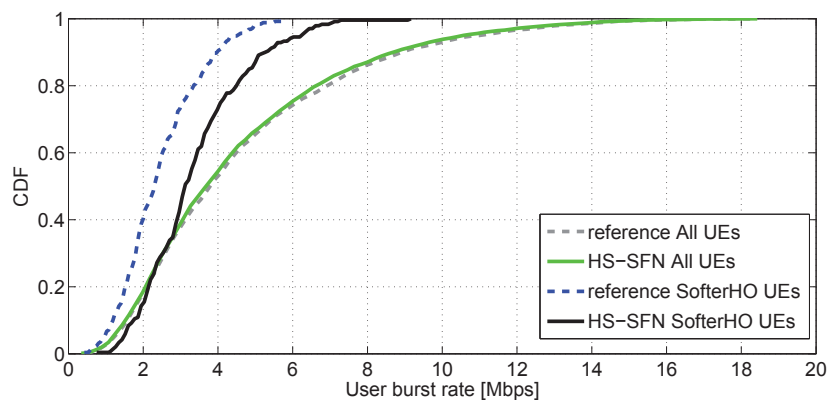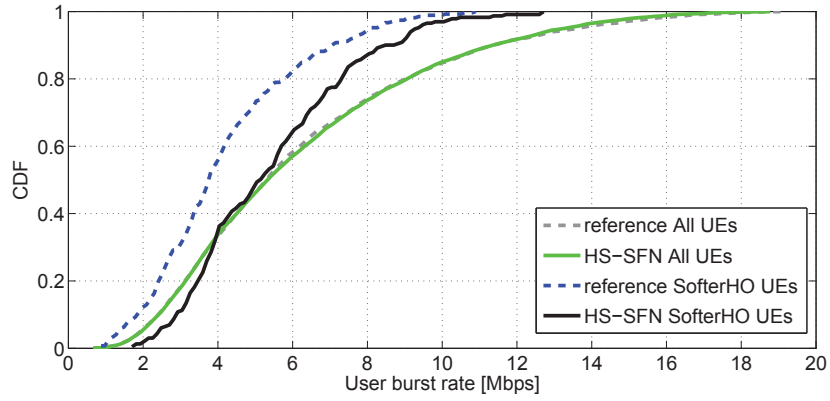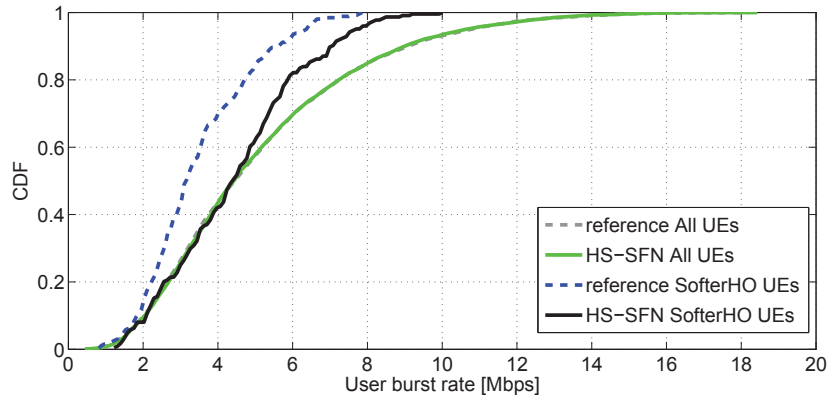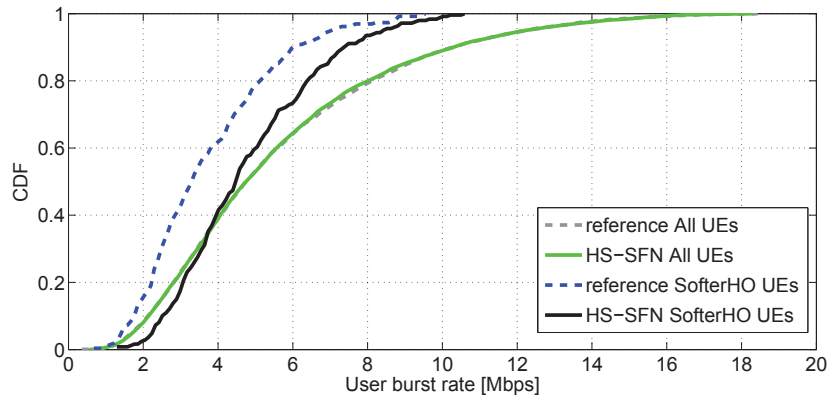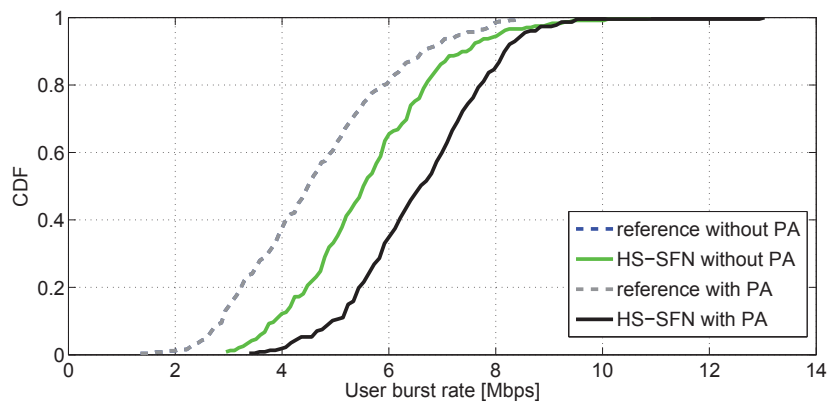

(b) Pedestrian B

(c) Vehicular A

FIGURE 47   CDF of HS-SFN with phase adjustment compared to non-HS-SFN operation for enhanced type3 receiver and 8UE per cell
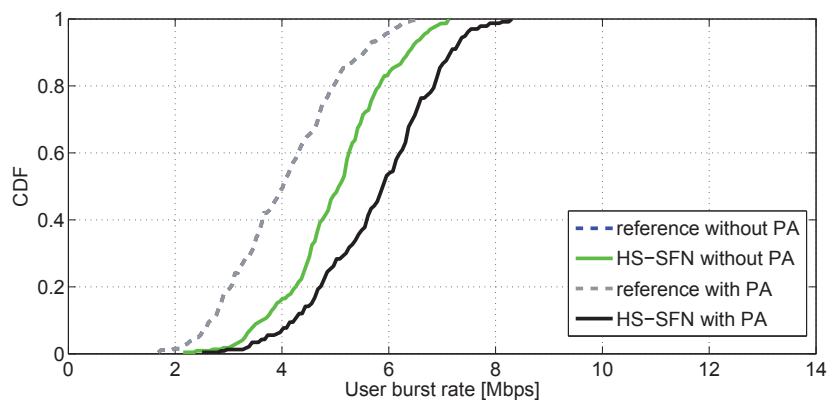
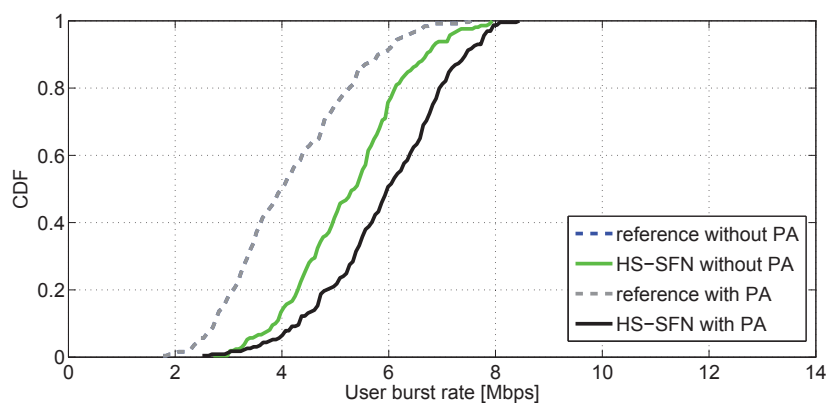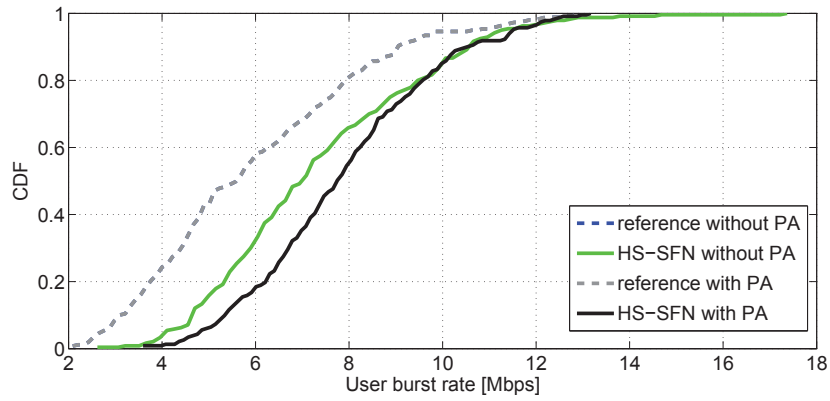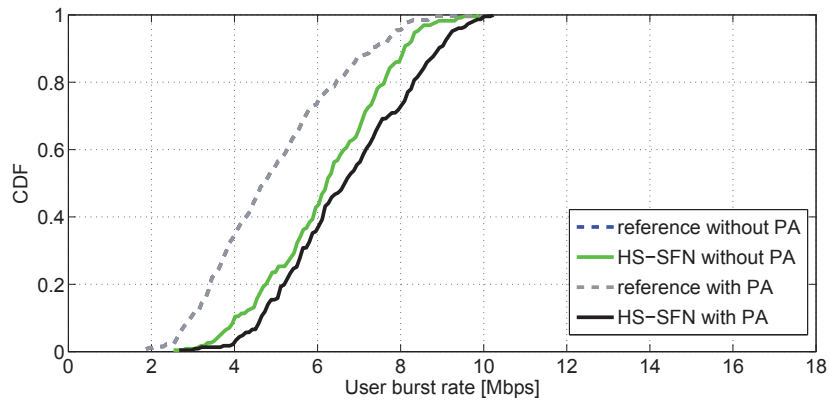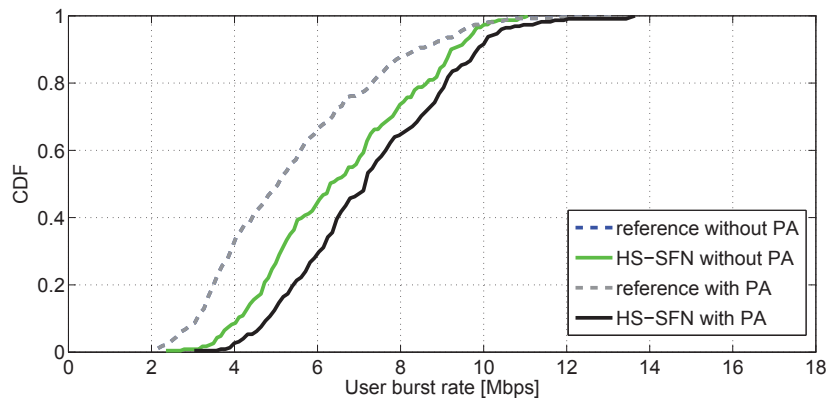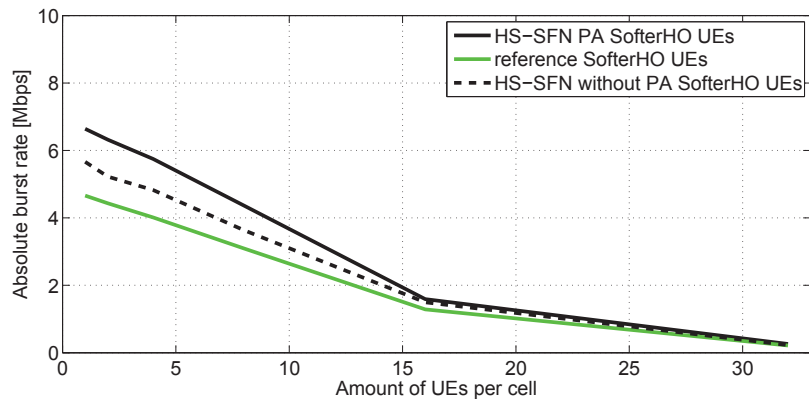(a) Pedestrian A

(b) Pedestrian B

(c) Vehicular A

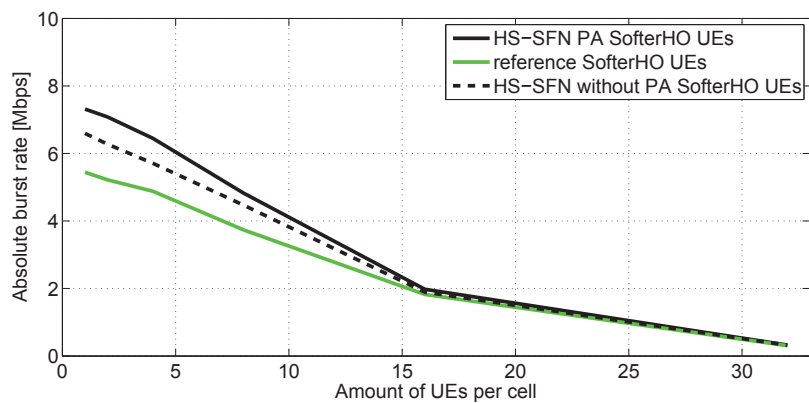FIGURE 48   Absolute burst rate of HS-SFN with phase adjustment for enhanced type3
receiver compared to pure HS-SFN and non-HS-SFN cases
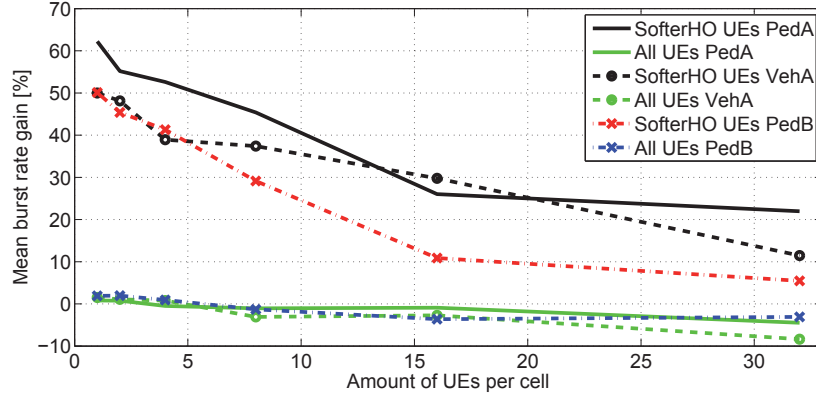
FIGURE 49   Burst rate gain of HS-SFN with enhanced type3 receiver and phase adjustment compared to non-HS-SFN operation with different ITU channels

Figure 46(a), Figure 46(b) and Figure 46(c) present CDF curves for the user burst rate of HS-SFN with the enhanced type3 receiver and phase adjustment as well as for the reference case for 1UE per cell. As can be seen from these figures, HS-SFN can increase the performance of the all softer handover UEs, i.e. the low burst rate UEs as well as the high burst rate UEs comprising the whole percentile of CDF. The performance of the all UEs in the network also gets a marginal improvement from the use of HS-SFN. The best performance can be achieved with the PedestrianA channel model. However, the difference between PedestrianB and VehicularA is marginal and cannot be seen properly from these CDF figures. The precise comparison between these channel models can be done from absolute burst rate or gain figures.

Figure 47(a), Figure 47(b) and Figure 47(c) show results similar to the previous figures but for 8UEs per cell. It can be seen from these figures that HS-SFN has smaller benefit than shown by the results with 1UE per cell. The same dependence can also be observed in the results of the previous subsections. The reference case for all UEs exhibits a slightly better performance than the HS-SFN results for all UES, however the difference is marginal.

Figure 48(a), Figure 48(b) and Figure 48(c) show an absolute burst rate comparison of HS-SFN transmission with phase adjustment and the enhanced type3 receiver, pure HS-SFN and the reference cases under the PedestrianA, PedestrianB and VehicularA channel models, respectively. These figures present the results only for the UEs in the softer handover area since the difference for the all UEs is marginal. It can be seen that phase adjustment and the enhanced type3 receiver can significantly increase the performance of HS-SFN, especially for the low-load cells. For high-load cells the benefit of HS-SFN, phase adjustment and the enhanced type3 receiver almost disappear. The same dependency as previously can be observed between different ITU channel models.

Figure 49 shows the results as burst rate gain of HS-SFN with phase adjustment and the enhanced type3 receiver over the reference case for the Pedes-

trianA, PedestrianB and VehicularA channel models. As can be seen from the figure, HS-SFN can have up to 62% gain for softer handover UEs with the PedestrianA channel model and 1UE per cell. This figure also shows that HS-SFN can perform better in a channel with smaller number of taps, i.e. PedestrianA; however, for other ITU channel models in low-load cells, HS-SFN can bring a 40-50% gain with marginal performance increasing for the all UEs. With 8UEs per cell, i.e. for average-load cells, HS-SFN can bring a gain of 27-45% for UEs in the softer handover area under the different ITU channel models, with a marginal impact for the performance of the all UEs. For the high-load cells, the gain from HS-SFN for softer handover UEs is decreasing, and the impact on overall performance becomes greater.

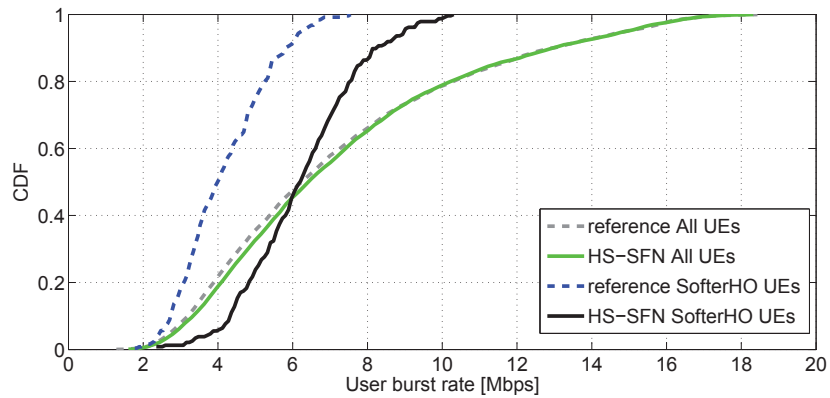### 4.2.5 HS-SFN with enhanced type3 receiver and phase adjustment 6 sector

This subsection presents the results for HS-SFN with phase adjustment and the enhanced type3 receiver and a comparison of these results to HS-SFN without phase adjustment with the type3 receiver (or pure HS-SFN) as well as to non-HS-SFN results for 6-sector site deployment. Similar results, but for 3-sector site are presented in the previous subsection. The main reason of consideration 6-sector site deployment with HS-SFN is that the number of HS-SFN UEs is increased from 4% to 6% compared to the simulations with 3-sector sites. It should be mentioned that, 6-sector site will double the load level of the network since we model certain number of UEs per cell. That is why these results show the network performance of only up to 16 UEs per cell. Nevertheless, the structure of this subsection is the same as that of Subsection 4.2.4. First, the results for 1 and 8 UEs per cell are presented as CDF of user burst rate. This is followed by an absolute burst rate comparison of HS-SFN with additions over pure HS-SFN and the reference cases, and then the burst rate gain of HS-SFN with phase adjustment and the enhanced type3 receiver over the reference case is presented.

Figure 50(a), Figure 50(b) and Figure 50(c) present CDF curves for the user burst rate of HS-SFN with the enhanced type3 receiver and phase adjustment as well as for the reference case for 1UE per cell under the PedestrianA, PedestrianB and VehicularA channel models, respectively. As can be seen from these figures, HS-SFN can increase the performance of UEs in the softer handover area over all percentiles of the CDF curve. The performance of the all UEs in the network also experiences marginal improvement from the usage of HS-SFN. The best performance can be achieved with the PedestrianA channel model; however, it is hard to see from these figures what the difference compared to the PedestrianB and VehicularA ITU channel models is.
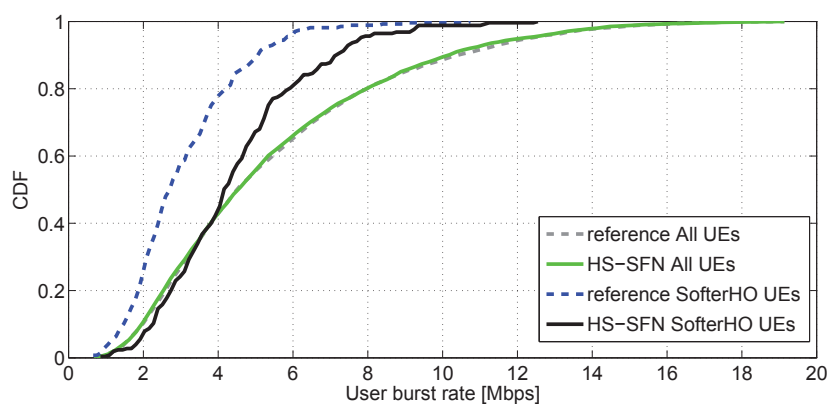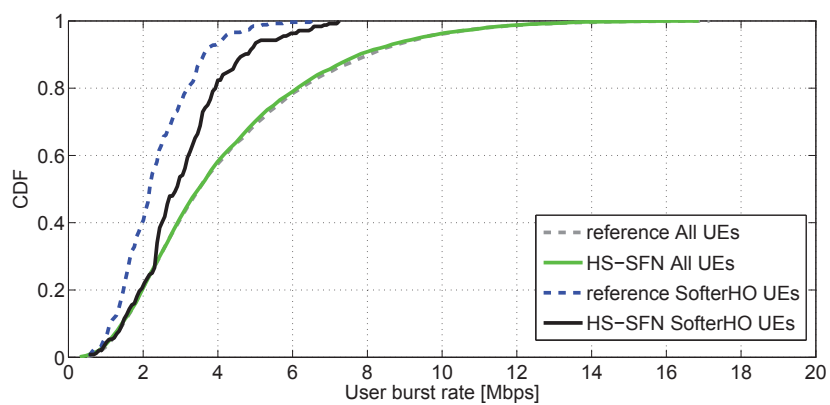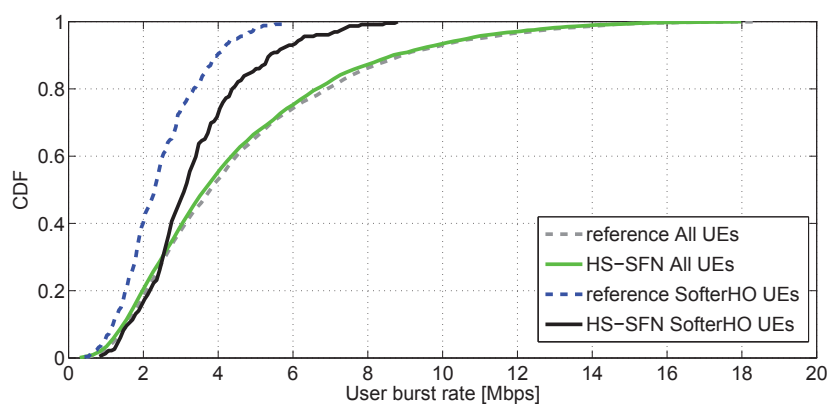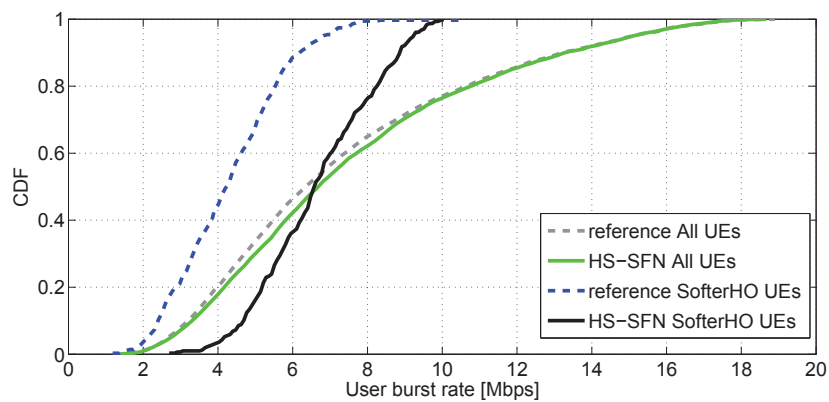
(a) Pedestrian A
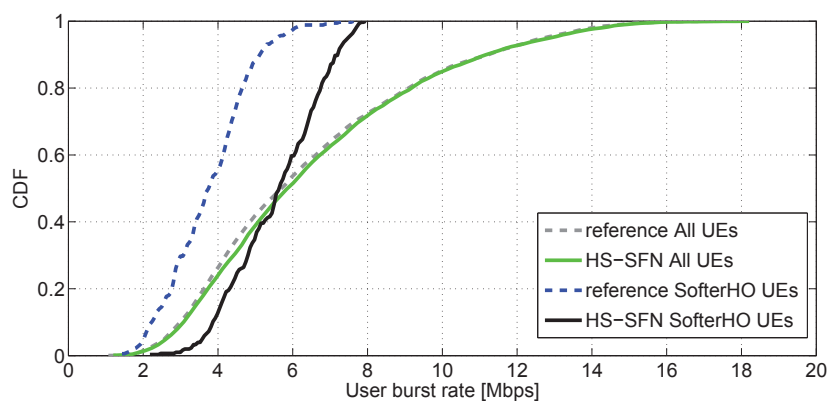
(b) Pedestrian B
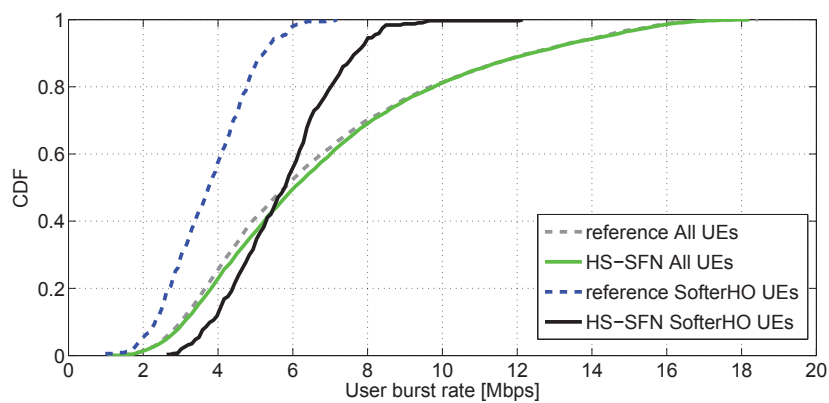
(c) Vehicular A

FIGURE 50   CDF of HS-SFN with phase adjustment compared to non-HS-SFN operation for enhanced type3 receiver with 1UE per cell and 6-sector site deployment
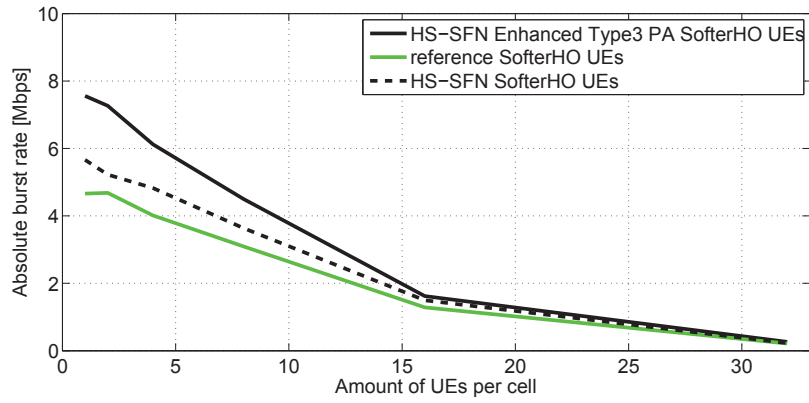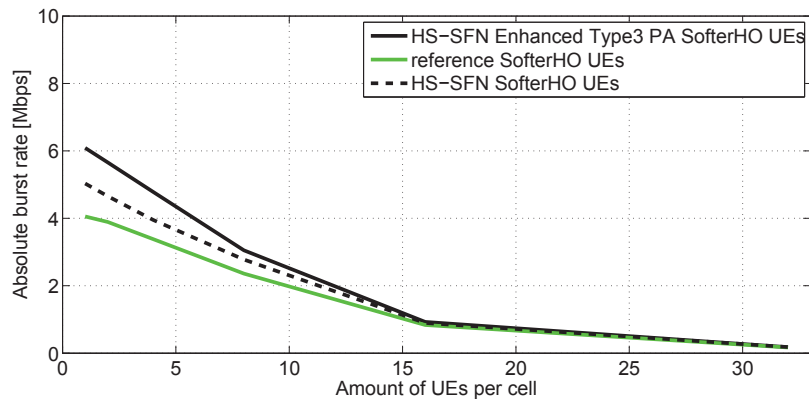
88
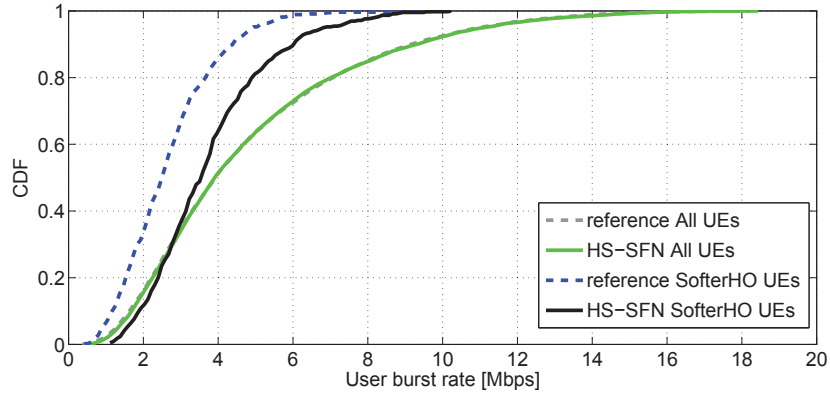
(a) Pedestrian A

(b) Pedestrian B

(c) Vehicular A
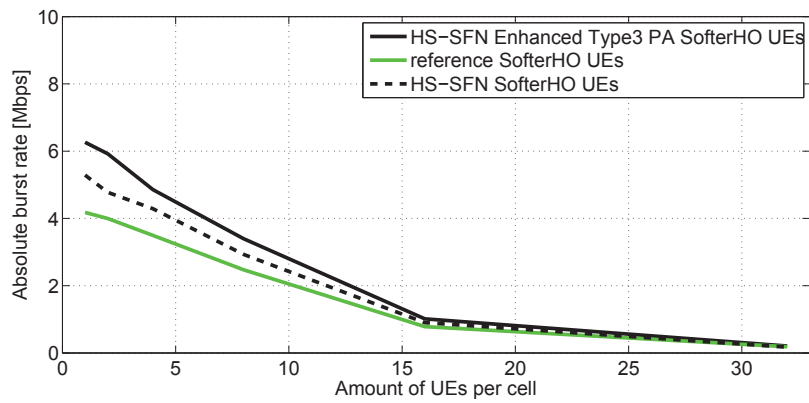
FIGURE 51   CDF of HS-SFN with phase adjustment compared to non-HS-SFN operation for enhanced type3 receiver with 8UE per cell and 6-sector site deployment
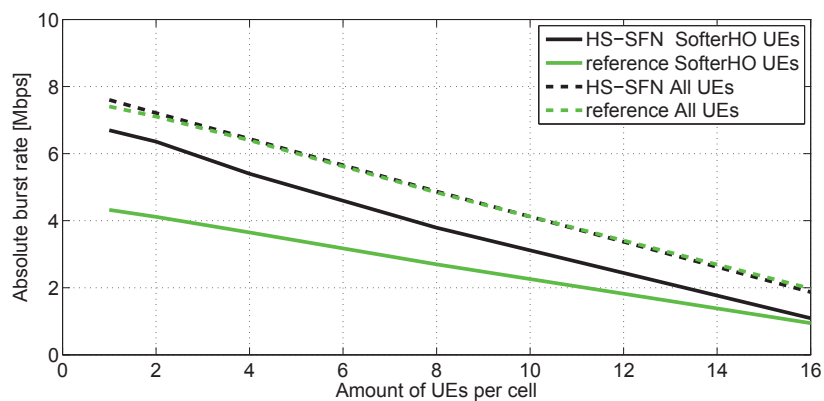
(a) Pedestrian A
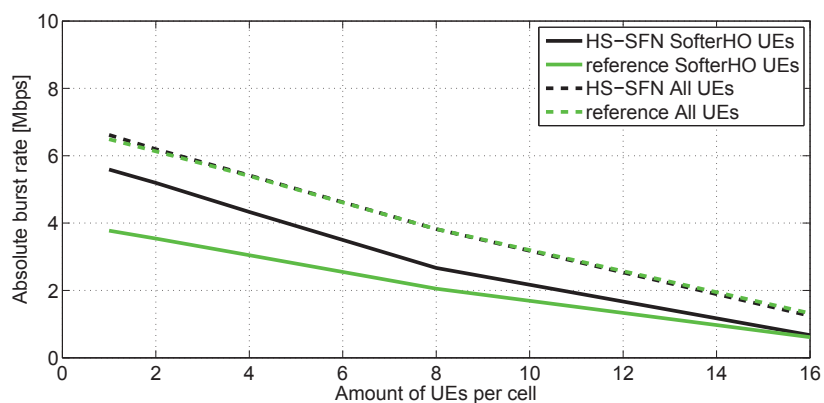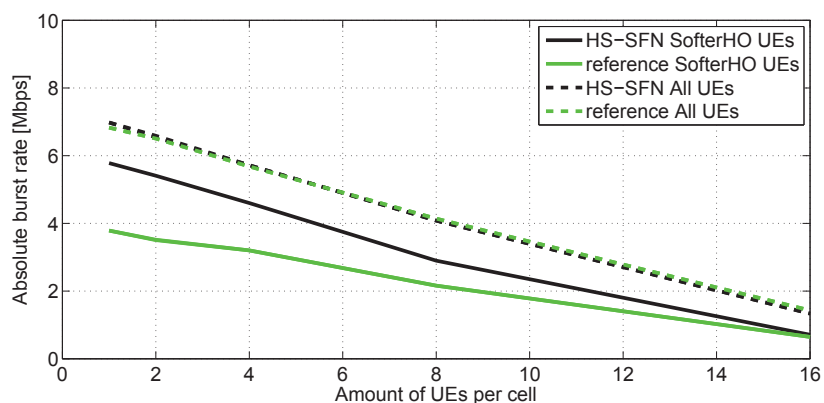
(b) Pedestrian B

(c) Vehicular A

FIGURE 52   Absolute burst rate of HS-SFN with phase adjustment for enhanced type3
receiver compare to pure HS-SFN and non-HS-SFN cases with PedestrianA
channel and 6-sector site deployment

Figure 51 shows the results for 8UEs per cell. As can be seen from this figure, compared to the results with 1UE per cell HS-SFN provides smaller improvement for UEs in the softer handover area; however, this effect can also be observed in the results of the previous subsections. There is almost no difference between the reference and HS-SFN cases for the all UEs.

Figure 52(a), Figure 52(b) and Figure 52(c) show an absolute burst rate comparison of HS-SFN transmission with phase adjustment and the enhanced type3 receiver, pure HS-SFN and the reference cases under the PedestrianA, PedestrianB and VehicularA channel models, respectively. These figures present the results not only for UEs in the softer handover area as previously, but also compare the absolute burst rate for the all UEs. The results for the UEs in the softer handover area are quite similar to the results with 3-sector site deployment. The impact of HS-SFN for all UEs is marginal.
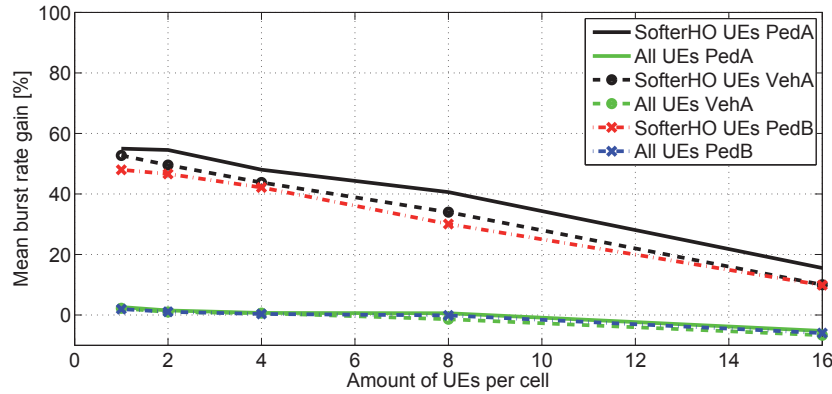
FIGURE 53   Burst rate gain of HS-SFN with enhanced type3 receiver and phase adjustment compared to non-HS-SFN operation with different ITU channels and 6-sector site deployment

Figure 53 shows the results for the burst rate gain of HS-SFN with phase adjustment and the enhanced type3 receiver over the reference case for the PedestrianA, PedestrianB and VehicularA channel models. As can be seen from the figure, the HS-SFN can bring a gain of up to 57% for the softer handover UEs with the PedestrianA channel model and 1-2 UEs per cell. It is slightly less than in the corresponding results for a 3-sector site; however, the decrease in gain with increasing cell loads occurs more linearly. The difference between the different ITU channel models is also more straightforward compared to 3-sector site. Here the logical dependence can be clearly seen. Of these three channel models, the best gain from HS-SFN can be achieved with PedestrianA; the gain is slightly worse with VehicularA; and it is the worst with PedestrianB. This can be easily explained by the number of taps in each channel, and their effect on phase adjustment. The marginal HS-SFN effect on the performance of all UEs for low-load and average-load cells also can be observed from this figure as a small impact with 16 UEs per cell.

4.2.6 Summary

This subsection presents summary of all the results in tabular form. The Table 7 presents mean burst rate gains comparison of HS-SFN transmission with different type of receivers and ITU channel model, phase adjustment and 3 and 6-sector site deployment. In total seven different HS-SFN schemes are summarized:

– HS-SFN with type3 receiver;
– HS-SFN with type3i receiver;
– HS-SFN with enhanced type3 receiver;
– HS-SFN with type3 receiver and phase adjustment;
– HS-SFN with type3i receiver and phase adjustment;
– HS-SFN with enhanced type3 receiver and phase adjustment;
– HS-SFN with enhanced type3 receiver and phase adjustment for 6-sector site deployment;

Comparing first two schemes, which represent pure HS-SFN with type3 and type3i receiver, it can be seen from the Table 7, that the gain from HS-SFN is quite similar for both types of receiver. Just to remind, that theoretically, HS-SFN gain should be bigger with type3 receiver, because HS-SFN remove the 70% of the interference from the second best interferer and type3i can already aware some the interference. That is why expected gain from type3i receiver should be lower than the gain with type3 receiver, however the absolute burst rate will be always higher for type3i receiver. The similarity of these results can be explained by the randomness in the simulation regarding the different UEs' position and fast fading, notwithstanding the big numbers of the simulation run. One more thing, that HS-SFN without phase adjustment might also decrease the signal strength via combining two signals. Looking at the third scheme, that show HS-SFN gain with enhanced type3 receiver, it can be seen that the gain from HS-SFN is bigger compare to type3 and type3i receiver. This can be explained by the new structure of the receiver, that can take into account combined data signals and separate control signals. Fourth and fifth schemes show HS-SFN with phase adjustment with type3 and type3i receivers. As can be seen from these schemes, the phase adjustment can almost double the gain from HS-SFN compared to HS-SFN without phase adjustment. Furthermore, the gain difference between type3 and type3i receiver looks as theoretically expected, i.e. the gain from HS-SFN is bigger with type3 receiver than with type3i. Finally, sixth and seventh schemes show HS-SFN with enhanced type3 receiver, phase adjustment and for 3 and 6-sector site deployment. These schemes show similar HS-SFN gain, however the gain with 3-sector site deployment is slightly better. It can be partly explained by increasing the percentage of HS-SFN candidates under 6-sector site deployment, different interference level (due to different antenna pattern and amount of sectors).

TABLE 7   Mean burst rate gain of HS-SFN compared to non-HS-SFN operation

HS-SFN scheme	Number of UEs per cell	SofterHO UEs			All UEs		
		PedA	PedB	VehA	PedA	PedB	VehA
Type3	1	21.52	24.1	26.58	1.28	-0.29	-0.33
	2	20.63	23.44	19.4	0.67	0.21	0.37
	4	20.30	16.76	22.69	-0.34	0.66	0
	8	17.44	17.63	18.53	-2.87	1.04	-1.81
	16	16.38	7.11	15.25	-3.75	0.62	-6.24
	32	5.01	7.35	-6.16	-2.43	-2.48	-6.57
Type3i	1	24.1	25.25	21.14	0.06	1.19	1.17
	2	22.69	20.66	20.21	-1.03	-0.08	1.65
	4	20.5	15.01	16.98	0.04	-0.2	0.04
	8	23.59	9.63	19.68	-1.11	-1.57	-0.82
	16	10.56	1.86	3.76	0.77	-1.58	0.16
	32	-3.04	-11.27	4.95	-7.89	-8.67	-3.1
Enhanced Type3	1	40.02	34.08	38.6	1.78	1.56	1.12
	2	38.9	29.42	37.66	0.31	-0.13	0.88
	4	35.13	27.13	31.48	-0.07	1.54	1.44
	8	23.15	28.67	28.01	-3.22	0.1	-2.58
	16	25.33	11.13	25.85	-3.74	-1.97	-2.77
	32	8.31	8.11	18.51	-3.66	0.1	-8.73
Type3, phase adjustment	1	42.55	43.09	42.62	0.37	1.35	1.03
	2	42.53	38.02	39.33	0.8	0.73	0.25
	4	43.31	38.43	34.42	1.1	0.44	1.37
	8	41.1	31.12	37.51	-2.37	0.7	-2.52
	16	23.6	9.46	23.18	-5.06	-1.14	-7.43
	32	21.26	7.83	17.58	-4.63	-6.8	-8
Type3i, phase adjustment	1	32.52	35.65	34.38	0.7	1.17	1.34
	2	30.88	35.62	35.7	-0.08	0.72	0.63
	4	31.7	29.48	32.13	0.32	1.08	0.46
	8	30.69	28.41	29.16	-0.13	0.01	-0.36
	16	18.88	20.63	8.3	-4.53	-3.97	-4.45
	32	4.08	2.33	5.9	-7.43	-1.74	-3.44
Enhanced Type3, phase adjustment	1	62.23	50.11	49.98	0.8	1.91	1.52
	2	55.18	45.39	48.13	0.76	1.96	1.06
	4	52.59	41.3	38.93	-0.47	0.93	0.77
	8	45.39	29.13	37.4	-1.05	-1.3	-3.08
	16	26.01	10.87	29.75	-0.9	-3.62	-2.7
	32	21.96	5.45	11.44	-4.48	-3.08	-8.38
Enhanced Type3, phase adjustment, 6-sector	1	54.97	47.99	52.72	2.63	1.96	2.23
	2	54.51	46.62	49.57	1.52	1.05	0.5
	4	48.03	42.16	43.8	0.68	0.36	0.61
	8	40.6	30.07	33.99	0.6	-0.1	-1.38
	16	15.54	9.88	10	-5.23	-5.96	-6.67

5   CONCLUSIONS AND FUTURE WORK

In this thesis, we have investigated one of the multipoint transmission schemes for HSDPA, referred to as HS-SFN, which can increase the performance of UEs in the softer handover area. In addition to the main research topic, this thesis also shows how HS-SFN performance can be increased with a new receiver type, the enhanced type3 receiver, and phase adjustment. The main results were obtained with a system level simulator; however, additional verification of these features as well as theoretical comparison with another multipoint transmission scheme, Multiflow, was done via a pseudo-random set of scripts in Matlab. The gain from pure HS-SFN, i.e. with the normal type3 receiver and without phase adjustment, for UEs in the softer handover area can be up to 25%, when compared to the simulations without HS-SFN. By leveraging upon the enhanced type3 receiver and phase adjustment, this gain can be increased further, with a marginal impact on overall network performance. However, this kind of gain can be achieved only for low-load cells. Gain degradation with the use of HS-SFN was observed with increasing cell load levels and can be explained by the decreasing amount of HS-SFN-scheduled TTIs. The amount of scheduled TTIs within HS-SFN is high for low-load cells because neighboring cells often do not have own users to schedule and a short-term load balancing effect, which can be observed there. For high-load cells, the load balancing effect disappears. There is no direct comparison between the type3 and type3i, however it is good to mention that type3i receiver provides better results than type3, as it should be. In terms of absolute burst rate type3i shows better results comparing to type3 receiver with or without HS-SFN. However, the gain of HS-SFN compare to non-HS-SFN for type3i is smaller than gain for type3 receiver. This can be explained by the fact that the gain from HS-SFN comes not only from two signals combining, but also from removing 70% of interference of the assisting cells. And since type3i can already be aware of some interference from the few best-interfering cells, the gain from HS-SFN is smaller. Enhanced type3 receiver was constructed, as can be seen from the name, from type3 receiver. The main difference from type3 receiver is that the channel from the own sector and from the second best interfering sector is assumed to be known for the enhanced type3 receiver and it can restore the orthogonality for the

combined signal (for data channel) and non-combined signal (for control channel). Type3i receiver can mitigate interference from several neighbouring cells, however it does not know the combined HS-SFN data channel. The enhanced type3i might be good topic for future research. As was seen from the results, the best performance with HS-SFN can be achieved under the PedestrianA channel, a bit lower under VehicularA, and the worst with PedestrianB. This can be explained by the number of taps for these channel models and by part of the gain from HS-SFN coming from combining the signals over the air. Moreover, the percentage of the HS-SFN UEs, or UEs in the softer handover area, can increase up to 6% with a 6-sector site deployment.

Although this thesis covers many issues regarding the multipoint transmission scheme for HSDPA and especially for HS-SFN, there are still a lot that has been left out of this thesis' scope and can be good subjects for further consideration and research. One of the major issues would be to compare HS-SFN to Multiflow on a system level because a theoretical comparison shows that HS-SFN can perform better than Multiflow for low-SINR UEs. Another good topic for future research is different softer handover thresholds. The impact of legacy UEs for HS-SFN and imperfect channel estimation might also be good subjects for further consideration. Since recent advances in HW computing allows to build HSPA system modules that control more than 3 cells, HS-SFN can be considered not only for softer handover, but also for areas between "sites" or soft handover area. In addition, even though HSPA does not have X2 interface like LTE, there can be the one (even proprietary) allowing for inter-site HS-SFN.

YHTEENVETO (FINNISH SUMMARY)

Tämä väitöskirja, jonka nimi on Nopeat HSDPA-yksitaajuusverkot, tutkii HS-SFN-monipistelähetystapaa HSDPA-verkoille, joka voi lisätä päätelaitteiden suorituskykyä softer handover -alueella. Tämän pääaiheen lisäksi tämä väitöskirja osoittaa myös, kuinka HS-SFN-lähetystavan suorituskykyä voidaan parantaa uudella vastaanotintyypillä, joka tunnetaan parannettuna 3-tyypin vastaanottimena sekä vaihesäädöllä. Päätulokset saatiin järjestelmätason tietoliikennesimulaatioilla. Lisävarmistuksia tuloksille saatiin ja teoreettinen vertailu Multiflow-monipistelähetystapaan tehtiin lisäksi matemaattisin keinoin Matlab-ympäristössä. Pelkästä HS-SFN-tekniikasta saatava etu voi olla jopa 25% softer handover -alueella. Suorituskykyä voidaan kasvattaa edelleen käyttämällä parannettuja 3-tyypin vastaanottimia ja vaihesäädöllä jopa 62% minimaalisin vaikutuksin muun verkon suorituskykyyn. Tällaiset parannukset voidaan kuitenkin saavuttaa vain kevyesti kuormitetuissa verkoissa. Kevyesti kuormitetuissa verkoissa naapurisolulla ei ole usein omia päätelaitteita, jolloin se voi auttaa HS-SFN-lähetyksessä palvelevaa solua. Raskaasti kuormitetuissa verkoissa naapurisoluilla ei ole paljon vapaita resursseja, jolloin HS-SFN-tekniikasta saatu hyöty pienenee. Myös lisääntyvät häiriöt vähentävät HS-SFN-tekniikan hyötyjä pienissä määrin. Parantuneen suorituskyvyn lisäksi HS-SFN-tekniikka tasoittaa solujen välisiä kuormia, mutta vain kevyesti kuormitetussa verkossa. Tuloksista nähdään, että suurin hyöty HS-SFN-tekniikasta saadaan PedestrianA-kanavalla ja pienin PedestrianB-kanavalla, VehicularA-kanavan sijoittuessa näiden väliin. Tämä selittyy kanavamallien tappien määrällä, joka on pienin PedestrianA-kanavassa. Lisäksi kuuden sektorin tukiasemilla softer handover -käyttäjien lukumäärä voi olla jopa 6% suurempi, mutta HS-SFN-tekniikan hyödyt eivät silti ole paljoa kolmen sektorin tilannetta suurempia.

REFERENCES

[3GPa]   3GPP home page. http://www.3gpp.org.

[3GPb]   3GPP R1-00-1395, Motorola. Adaptive Modulation and Coding (AMC), Motorola.

[3GPc]   3GPP R1-111141. Multiflow performance evaluation, Nokia Siemens Networks, Nokia.

[3GPd]   3GPP R1-111489. Text Proposal on the performance of HS-SFN, Nokia Siemens Networks, Nokia.

[3GPe]   3GPP R1-111775. Signaling and configuration for the multi-point transmission schemes, Nokia Siemens Networks, Nokia.

[3GPf]   3GPP R4-060369. Observations on Other-Cell Interference Modelling, Motorola.

[3GPg]   3GPP R4-060391. HSDPA Network Scenario and Associated Interference Profile for Evaluation of Generalized Interference Cancellation (IC) Receivers, Cingular Wireless.

[3GPh]   3GPP R4-060492. Interferer Statistics for the UE IC Study Item, Qualcomm Europe.

[3GPi]   3GPP R4-060512. Simulation results for scenario definition to interference mitigation studies, Nokia.

[3GPj]   3GPP RP-101439. Proposed study item on HSDPA multipoint transmission, Nokia Siemens Networks.

[3GPk]   3GPP TR 25.101. User equipment (UE) radio transmission and reception (FDD).

[3GPl]   3GPP TR 25.213. Spreading and modulation (FDD).

[3GPm]   3GPP TR 25.963. Feasibility study on interference cancellation for utra fdd user equipment (UE).

[3GPn]   3GPP TR 25.996. Spatial channel model for Multiple Input Multiple Output (MIMO) simulations.

[3GPo]   3GPP TR 36.814. Further advancements for E-UTRA physical layer.

[3GPp]   3GPP TR 36.819. Coordinated multi-point operation for LTE physical layer aspects.

[3GPq]   3GPP TS 25.211. Physical channels and mapping of transport channels onto physical channels (FDD).

[3GPr]   3GPP TS 25.211. Physical layer procedures (FDD).

[3GPs]   3GPP TS 25.306. UE Radio Access capabilities.

[3GPt]   3GPP TS 25.308. Overall description, stage 2.

[AKR$^+$01] M. Andrews, K. Kumaran, K. Ramanan, A. Stolyar, P. Whiting, and R. Vijayakumar. Providing quality of service over a shared wireless link. *Communications Magazine, IEEE*, Feb 2001.

[Bra83]   D.H. Brandwood. A complex gradient operator and its application in adaptive array theory. *Communications, Radar and Signal Processing, IEE Proceedings F*, 130(1):11 –16, Feb 1983.

[BZGA10]   S. Brueck, Lu Zhao, J. Giese, and M.A. Amin. Centralized scheduling for joint transmission coordinated multi-point in LTE-Advanced. In *Smart Antennas (WSA), 2010 International ITG Workshop on*, pages 177 –184, Feb 2010.

[dAKH$^+$09] D.M. de Andrade, A. Klein, H. Holma, I. Viering, and G. Liebl. Performance Evaluation on Dual-Cell HSDPA Operation. In *Vehicular Technology Conference Fall (VTC 2009-Fall), 2009 IEEE 70th*, pages 1 –5, Sep 2009.

[DAO01]   P. Darwood, P. Alexander, and I. Oppermann. LMMSE chip equalisation for 3GPP WCDMA downlink receivers with channel coding. In *Communications, 2001. ICC 2001. IEEE International Conference on*, volume 5, pages 1421 –1425 vol.5, 2001.

[DPSB10]   E. Dahlman, S. Parkvall, J. Skold, and P. Beming. *3G Evolution: HSPA and LTE for Mobile Broadband*. Academic Press, second edition edition, 2010.

[ERI99]   ERICSSON. Basic Concepts of HSPA. White Paper, 1999.

[FPD01]   P. Frenger, S. Parkvall, and E. Dahlman. Performance comparison of HARQ with Chase combining and incremental redundancy for HSDPA. In *Vehicular Technology Conference, 2001. VTC 2001 Fall. IEEE VTS 54th*, volume 3, pages 1829 –1833 vol.3, 2001.

[Gol05]   Goldsmith A. *Wireless Communications*. Cambridge University Press, second edition edition, 2005.

[GP06]   A. Gougousis and M. Paterakis. Scheduling with QoS Support for MultiRate Wireless Systems with Variable Channel Conditions. In *Wireless Conference 2006 - Enabling Technologies for Wireless Multimedia Communications (European Wireless), 12th European*, pages 1–8, 2006.

[Hol00]   J.M. Holtzman. CDMA forward link waterfilling power control. In *Vehicular Technology Conference Proceedings, 2000. VTC 2000-Spring Tokyo. 2000 IEEE 51st*, volume 3, pages 1663–1667 vol.3, 2000.

98

[Hol01]   Holtzman, J.M. Asymptotic analysis of proportional fair algorithm. In *Personal, Indoor and Mobile Radio Communications, 2001 12th IEEE International Symposium on*, volume 2, pages F–33–F–37 vol.2, 2001.

[Hol06]   Holma, H. and Toskala, A. Eds. *HSDPA/HSUPA for UMTS:High Speed Radio Access for Mobile Communications*. John Wiley & Sons, 2006.

[Hol07]   Holma, H. and Toskala, A. and Eds. *WCDMA for UMTS - HSPA evolution and LTE*. John Wiley & Sons, fourth edition edition, 2007.

[HPHC11]   V. Hytonen, O. Puchko, T. Hohne, and T. Chapman. High-speed single-frequency network for HSDPA. In *Communication Technologies Workshop (Swe-CTW), 2011 IEEE Swedish*, pages 1 –6, Oct 2011.

[HPHC12]   V. Hytonen, O. Puchko, T. Hohne, and T. Chapman. Introduction of Multiflow for HSDPA. In *New Technologies, Mobility and Security (NTMS), 2012 5th International Conference on*, pages 1–5, 2012.

[HSH$^+$12] H.T. Hoehne, A. Sayenko, V. Hytonen, O. Puchko, T. Chapman, F. Frederiksen, et al. CHANNEL QUALITY INDICATION (CQI) REPORTING IN A COMMUNICATIONS NETWORK, 2012. WO Patent 2,012,136,450.

[Hyt01]   Hytonen, T. . *Optimal Wrap-around Network Simulation*. Helsinki University of Technology, 2001.

[JPP00]   A. Jalali, R. Padovani, and R. Pankaj. Data throughput of CDMA-HDR a high efficiency-high data rate personal communication wireless system. In *Vehicular Technology Conference Proceedings, 2000. VTC 2000-Spring Tokyo. 2000 IEEE 51st*, volume 3, pages 1854–1858 vol.3, 2000.

[KPW$^+$03] T. Kolding, K. Pederson, J. Wigard, F. Frederiksen, and P. Mogensen. High Speed Downlink Packet Access: WCDMA Evolution. In *IEEE Vehicular Technology Society News*, Feb 2003.

[KZ00]   T.P. Krauss and M.D. Zoltowski. Oversampling diversity versus dual antenna diversity for chip-level equalization on CDMA downlink. In *Sensor Array and Multichannel Signal Processing Workshop. 2000. Proceedings of the 2000 IEEE*, pages 47 –51, 2000.

[KZL00]   T.P. Krauss, M.D. Zoltowski, and G. Leus. Simple MMSE equalizers for CDMA downlink to restore chip sequence: comparison to zero-forcing and RAKE. In *Acoustics, Speech, and Signal Processing, 2000. ICASSP '00. Proceedings. 2000 IEEE International Conference on*, volume 5, pages 2865 –2868 vol.5, 2000.

[MKW07]   M. Malkowski, A. Kemper, and Xiaohua Wang. Performance of Scheduling Algorithms for HSDPA. In *Communications and Networking in China, 2007. CHINACOM '07. Second International Conference on*, pages 1052–1056, 2007.

[MNK⁺07]   P. Mogensen, Wei Na, I.Z. Kovacs, F. Frederiksen, A. Pokhariyal, K.I. Pedersen, T. Kolding, K. Hugl, and M. Kuusela. LTE Capacity Compared to the Shannon Bound. In *Vehicular Technology Conference, 2007. VTC2007-Spring. IEEE 65th*, pages 1234 –1238, Apr 2007.

[Nih08]   Timo Nihtilä. *Performance of advanced transmission and reception algorithms for high speed downlink packet access*. PhD thesis, Faculty of Information Technology, University of Jyvaskyla, 2008.

[NKLR05]   T. Nihtila, J. Kurjenniemi, M. Lampinen, and T. Ristaniemi. WCDMA HSDPA network performance with receive diversity and LMMSE chip equalization. In *Personal, Indoor and Mobile Radio Communications, 2005. PIMRC 2005. IEEE 16th International Symposium on*, volume 2, pages 1245 –1249 Vol. 2, Sep 2005.

[NKV07]   T. Nihtila, J. Kurjenniemi, and E. Virtej. System Level Analysis of Interference Aware LMMSE Chip Equalization in HSDPA Network. In *Computers and Communications, 2007. ISCC 2007. 12th IEEE Symposium on*, pages 133 –138, Jul 2007.

[PDF⁺01]   S. Parkvall, E. Dahlman, P. Frenger, P. Beming, and M. Persson. The evolution of WCDMA towards higher speed downlink packet data access. In *Vehicular Technology Conference, 2001. VTC 2001 Spring. IEEE VTS 53rd*, volume 3, pages 2287 –2291 vol.3, 2001.

[PS07]   R. Patachaianand and K. Sandrasegaran. Performance Comparison of Adaptive Power Control in UMTS. In *Wireless Broadband and Ultra Wideband Communications, 2007. AusWireless 2007. The 2nd International Conference on*, page 81, Aug 2007.

[Puc12]   O. Puchko. Increasing the performance of HSDPA with high-speed single frequency network. In *Proceedings of the 15th ACM international conference on Modeling, analysis and simulation of wireless and mobile systems*, MSWiM '12, pages 47–54, New York, NY, USA, 2012. ACM.

[PWS⁺07]   J. Peisa, S. Wager, M. Sagfors, J. Torsner, B. Goransson, T. Fulghum, C. Cozzo, and S. Grant. High Speed Packet Access Evolution - Concept and Technologies. In *Vehicular Technology Conference, 2007. VTC2007-Spring. IEEE 65th*, pages 819 –824, Apr 2007.

[PZH⁺11]   O. Puchko, M. Zolotukhin, V. Hytonen, T. Hohne, and T. Chapman. Enhanced LMMSE equalizer for high-speed single frequency

network in HSDPA. In *Communication Technologies Workshop (Swe-CTW), 2011 IEEE Swedish*, pages 92 –97, Oct 2011.

[PZH+12]   O. Puchko, M. Zolotukhin, T. Hohne, T. Chapman, and V. Hytonen. Phase Adjustment in HS-SFN for HSDPA. In *New Technologies, Mobility and Security (NTMS), 2012 5th International Conference on*, pages 1–5, 2012.

[Rec97]   Recommendation ITU-R M.1225. Guidelines for the evaluation of radio transmission technologies for IMT-2000, 1997.

[SKM+10]   M. Sawahashi, Y. Kishiyama, A. Morimoto, D. Nishikawa, and M. Tanno. Coordinated multipoint transmission/reception techniques for lte-advanced [coordinated and distributed mimo]. *Wireless Communications, IEEE*, 17(3):26–34, 2010.

[XMX10]   Wang Xiaoyi, Kou Mingyan, and Qi Xin. Downlink System Performance of Cooperative Multiple Points Transmission with Realistic RRM Structure. In *Computer Modeling and Simulation, 2010. ICCMS '10. Second International Conference on*, volume 4, pages 467 –470, Jan 2010.

APPENDIX 1   MATLAB SCRIPTS OVERVIEW

1.1 Introduction

The purpose of this Appendix is to explain the Matlab scripts that were used to check the type 3, type 3i and enhanced type 3 receivers' implementation for HS-SFN in pseudo-random simulator. The following three scenarios are considered: standalone (SA), HS-SFN and HS-SFN with phase adjustment (PA).

1.2 List of files

`gen_script.m` – the main script that calculates filter coefficients and SINR values for three types of receivers in three cases: SA, COMP and PA;

`getSimulatorData.m` – the function returns the data obtained from system level simulations;

`construct_H.m` – the function constructs matrix H by concatenation of matrices h (matrices with complex multipath components of the link between Node B and rx-antennas of the UE);

`getwtype3.m` – the function calculates the weight for type 3 receiver;

`getwtype3i.m` – the function calculates the weight for type 3i receiver;

`getwtype3enh.m` – the function calculates the weight for enhanced type 3 receiver;

`testSimulatorvsMatlab.m` – the function compares the values of filter coefficients calculated in Matlab and values obtained from a system level simulator;

`getCoI_nonhssfn.m` – the function calculates SINR for the SA case;

`getCoI_hssfn.m` – the function calculates SINR for HS-SFN and PA;

`getColoredInterf.m` – the function returns the value of colored interference for SA and is used in SINR calculation;

`getColoredInterf_hs.m` – the function returns the value of colored interference for HS-SFN and PA and is used in SINR calculation.

1.3 The main script overview

All functions are called from this main script.

1.3.1 Auxiliary calculations

The first code block sets the display format for output, deletes the variables created, clears the command window and closes all opened figures. Test mode settings are used to indicate the cases for which filter coefficients and SINR values should be calculated. Note that the SA case will be considered in any case. To obtain results for other modes, the corresponding parameter must be changed to 1.

After that, the basic parameters for the following calculation are set up: receiver length (F), number of interfering base stations used to calculate the colored noise (N_i), relative power values for data channel ($P\_HSPDSCH$), CPICH channel (P_CPICH) and CPICH+other control channels (P_ctrl).

Then comes the data from system level simulations obtained using the function `getUpriseData.m`
The data which will be used in the following calculations consist of:

- $I0$ – white noise calculated when taken into account all interfering base stations except N_i base stations used for the calculation of colored noise,
- $Ithermal$ – thermal noise,
- $overallPgain$ – pathloss from the main base station to the UE,
- ha – matrix with complex multipath components of the link between the main transmitting base station and rx-antennas of the UE,
- hi – matrix with complex multipath components of the link between interfering Node B and rx-antennas of the UE,
- Pi – pathloss from base stations to the UE divided by pathloss from own Node B.

ha and hi are $N \times L$ matrices where N is the number of Rx antennas and L is delay spread. The number of interfering Node Bs and correspondingly the number of matrices hi are equal to Ni_total.

The next code block checks the white noise term $I0$. Besides, $NoAll$ (sum of noise from all interfering base stations and thermal noise; used for the SA case) and $NoAll\_hs$ (the same as $NoAll$ but for the first interfering Node B there is interference only from the control channel; used for HS-SFN and PA cases) are calculated.

After that, the matrix H_0 is constructed as a result of concatenation of matrix h_0 (see Appendix 1.5: `construct_H.m`). Similarly, matrices H_i are constructed. Also delay vector δ^D and delay matrix $\hat{\delta}$ are calculated.

For HS-SFN and PA cases matrices $H_{combined}$ must be constructed. For the HS-SFN case $H_{combined}$ is obtained as follows:

$$H_{combined} = H_0 + H_1\sqrt{\frac{L_1 P_{1,HS-PDSCH}}{L_0 P_{0,HS-PDSCH}}}. \tag{45}$$

Note that in these scripts $H_{combined} = H_C$, $H_0 = Ha$, $H_1 = Hi\{1\}$ and $\frac{L_1 P_{1,HS-PDSCH}}{L_0 P_{0,HS-PDSCH}} = Pi\{2\}$ ($P_{1,HS-PDSCH} = P_{0,HS-PDSCH} = P_{HS-PDSCH} = P\_HSPDSCH$).

For the PA case four $H_{combined}$ matrices must be calculated:

$$H_{combined,k} = H_0 + p_k H_1\sqrt{\frac{L_1 P_{1,HS-PDSCH}}{L_0 P_{0,HS-PDSCH}}}, \tag{46}$$

where p – the vector specifies the values of phase adjustment. It is determined as $p = [\frac{1+i}{\sqrt{2}}, \frac{1-i}{\sqrt{2}}, \frac{-1-i}{\sqrt{2}}, \frac{-1+i}{\sqrt{2}}]$ (in Matlab scripts it is denoted as ph_adj).

Matrix $Ct1$ is a thermal noise matrix constructed with thermal noise values ($Ithermal$) obtained from a system level simulator.

1.3.2 Receiver weight calculation

Next three code blocks implement the calculation of weights for different types of receivers, such as type3, type3i and enhanced type3 receivers. In the SA case, for the type 3 the covariance matrix takes into account interpath noise (matrix H_0 is used here), thermal noise and interference from all base stations. This covariance matrix is calculated as follows:

$$C_{rr,type3} = H_0^H H_0 + \frac{1}{L_0 P_0} C_{white,all}. \tag{47}$$

The receiver weight is calculated according to:

$$w_{type3} = C_{rr,type3}^{-1} H_0^H \delta_D, \tag{48}$$

where δ_D is the delay vector obtained before (see section `construct_H.m`, denoted as da). For cases HS-SFN and PA, there are only two small differences: matrix $H_{combined}$ (for HS-SFN) or $H_{combined,k}$ (for PA) instead of H_0 is used, and when calculating the interference only control channel must be taken into account for the first interfering Node B (the first term in the sum of interferences is multiplied by P_ctrl).

For type 3i receiver the covariance matrix takes into account (aside from interpath noise) noise from $N_{BS,interf}$ (in these scripts denoted as Ni) strongest paths calculated as colored noise (in these scripts denoted as $Crr1$):

$$C_{colored,3i} = \sum_{j=1}^{N_{BS,interf}} L_j P_j H_j^H H_j, \tag{49}$$

and noise from the remaining base stations calculated as white noise $C_{wh,all-ex-col}$ (in these scripts denoted as $Cw1$). Thus, the covariance matrix is calculated as follows:

$$C_{rr,type3i} = H_0^H H_0 + \frac{1}{L_0 P_0} C_{colored} + \frac{1}{L_0 P_0} C_{wh,all-ex-col} \tag{50}$$

The filter coefficient is calculated according to

$$w_{type3i} = C_{rr,type3i}^{-1} H_0^H \delta_D. \tag{51}$$

Similarly, for cases HS-SFN and PA matrix $H_{combined}$ (or $H_{combined,k}$) instead of H_0 is used, and when calculating colored noise only the control channel must be taken into account for the first interfering Node B.

For type 3, type 3i and enhanced type 3 receivers, interpath interference takes into account the relative values of power for data $P\_HSPDSCH$ and the control P_ctrl channels. Depending on implementation, it may take into account CPICH, or CPICH and other control channels of the neighboring cell. CPICH typically amounts to 10% of the total transmit power, and CPICH and other control channels to 30%. For the SA case, there are no differences between the values of receiver weight and enhanced receiver weight because there is no signal combining.

In the HS-SFN case due to signal combining, the weight of the enhanced type 3 receiver is calculated as:

$$w_{type3enh} = C_{rr,type3enh}^{-1} H_{combined}^H \delta_D, \tag{52}$$

where

$$C_{rr,type3enh} = P_{HS-PDSCH} H_{combined}^H H_{combined} + P_{ctrl} H_0^H H_0 + \frac{1}{L_0 P_0} C_{white,all,1}. \tag{53}$$

When calculating white noise $C_{white,all,1}$, only the control channel must be taken into account for the first interfering Node B (the first term in the sum of white noises is multiplied by P_ctrl). In the PA case, $H_{combined,k}$ are used instead of $H_{combined}$ for filter coefficients calculation.

1.3.3 SINR calculation

For the SA case the SINR value is calculated as follows:

$$\frac{C}{I} = \frac{P_{HS-PDSCH} \cdot \left| w^T H_0^T \delta_D \right|^2}{P_{HS-PDSCH} w^T H_0^T \hat{\delta} H_0^* w^* + P_{ctrl} w^T H_0^T \hat{\delta} H_0^* w^* + I_{colored} + \frac{1}{L_0 P_0} C_{thermal}} \quad (54)$$

Here the receiver weight w is calculated first, then $\hat{\delta}$ – delay matrix, $C_{thermal}$ – thermal noise. $I_{colored}$ is calculated as follows:

$$I_{colored} = \sum_{j=1}^{N_{BS,all}} \frac{L_j P_j}{L_0 P_0} w^T H_j^T H_j^* w^* \quad (55)$$

For the HS-SFN and PA cases, the following expression can be used to obtain SINR:

$$\frac{C}{I} = \frac{P_{HS-PDSCH} \cdot \left| w^T H_{combined}^T \delta \right|^2}{P_{HS-PDSCH} w^T H_{combined}^T \hat{\delta} H_{combined}^* w^* + P_{ctrl} w^T H_0^T \hat{\delta} H_0^* w^* + I_{colored,c} + I_{thermal}} \quad (56)$$

where

$$I_{colored,c} = P_{ctrl} \frac{L_j P_j}{L_0 P_0} w^T H_j^T H_j^* w^* + \sum_{j=2}^{N_{BS,all}} \frac{L_j P_j}{L_0 P_0} w^T H_j^T H_j^* w^* \quad (57)$$

and

$$I_{thermal} = \frac{1}{L_0 P_0} C_{thermal}. \quad (58)$$

In Matlab scripts $N_{BS,all} = NiTotal$.

1.3.4 Results display

For every case (SA, HS-SFN and PA), three values of SINR are displayed. These correspond to three different types of receivers: type 3, type 3i enhanced type 3. For clarity, all nine SINR values can be displayed as bar diagrams.

Also, using function `testSimulatorvsMatlab.m`, values of different receiver weights can be compared to each other and with the one that was calculated in a system level simulator.

1.4 getUpriseData.m

This function returns the data obtained from a system level simulator. There are no input arguments. The output arguments are:

– *I0* – white noise calculated when interfering base stations are taken into account. Excluded are N_i base stations used for the calculation of colored noise,

- *Ithermal* – thermal noise,
- *overallPgain* – pathloss from the main Node B to the UE,
- *ha* – matrix with complex multipath components of the link between the main transmitting Node B and rx-antennas of the UE,
- *W* – filter coefficient value obtained in a system level simulator,
- *hi* – matrix with complex multipath components of the link between interfering Node B and rx-antennas of the UE,
- *Pi* – pathloss from Node Bs to the UE divided by pathloss from own Node B,
- *Sum2* – covariance matrix from the system level simulator,
- *Inverse2* – inverse covariance matrix from the system level simulator,
- *Product3* – receiver coefficient from the system level simulator.

1.5 construct_H.m

This function constructs matrix H from matrix h with complex multipath components. Also it constructs delay vector δ^D and delay matrix $\hat{\delta}$.
Input arguments:

1. h – matrix with complex multipath components of the link between Node B and rx-antennas of the UE,
2. F – receiver length,
3. *mode* – type of antenna used: $mode = 1$ for interleaved antennas and $mode = 2$ for stacked antennas.

Output arguments:

1. H – resulting matrix,
2. d – delay vector,
3. dh – delay matrix.

h is an $N \times L$ matrix, where N is the number of Rx antennas and L is the delay spread value. For interleaved antennas case, H is constructed as follows:

$$H^i = \begin{pmatrix} h^T & 0 & \dots & 0 \\ 0 & h^T & \dots & 0 \\ \vdots & \vdots & \ddots & \vdots \\ 0 & 0 & \dots & h^T \end{pmatrix}. \tag{59}$$

For stacked antennas case, H is constructed as follows:

$$H^s = \begin{pmatrix} h_1^T & 0 & \dots & 0 & h_2^T & 0 & \dots & 0 & \dots & h_n^T & 0 & \dots & 0 \\ 0 & h_1^T & \dots & 0 & 0 & h_2^T & \dots & 0 & \dots & 0 & h_n^T & \dots & 0 \\ \vdots & \vdots & \ddots & \vdots & \vdots & \vdots & \ddots & \vdots & \dots & \vdots & \vdots & \ddots & \vdots \\ 0 & 0 & \dots & h_1^T & 0 & 0 & \dots & h_2^T & \dots & 0 & 0 & \dots & h_n^T \end{pmatrix}, \tag{60}$$

where $h_1, h_2, \ldots, h_n$ are rows of the matrix h.

d is constructed as the $(L + F - 1) \times 1$ unit vector with unit at some position, e.g. i_1. In this case, delay matrix dh is the unit matrix with diagonal element (i_1, i_1) equal to zero.

1.6 getwtype3.m

This function calculates the weight of type 3 receiver according to (48).

Input arguments:

- Cw – white noise matrix,
- H – matrix constructed from a matrix with multipath components,
- d – the delay vector.

Output argument w is the value of the receiver weight.

1.7 getwtype3i.m

This function calculates the weight of type 3i receiver according to (51).
Input arguments:

- Crr – colored noise matrix,
- Cw – white noise matrix,
- H – matrix constructed from matrix with multipath components,
- d – delay vector.

Output argument w is the value of the receiver weight.

1.8 getwtype3enh.m

This function calculates the weight of enhanced type 3 receiver according to (52).

Input arguments:

- P_data – relative power for data channel,
- P_ctrl – relative power for control channel,
- Cw – white noise matrix,
- H – matrix constructed from a matrix with multipath components (equal to H_0 for the CA case and $H_{combined}$ for HS-SFN and PA cases),

 – HH – matrix constructed from a matrix with multipath components (for all cases equal to H_0),
 – d – delay vector.

Output argument w is the value of the receiver weight.

1.9 testSimulatorvsMatlab.m

The function compares values of filter coefficients calculated in Matlab and those obtained from a system level simulator.
Function testSimulatorvsMatlab(w3, w3i, w3enh, wSimulator, figNo) Input arguments:

 – $w3$, $w3i$, $w3enh$ – receiver weight values calculated in Matlab,
 – $wSimulator$ – receiver weight value obtained from a system level simulator,
 – $figNo$ – number of the figure where the image will be displayed.

No output arguments.

For comparing weight values the following value is calculated:

$$ f = \sum_{k=1}^{F} N\left(|w| - |wUprise| \right), $$

where F – the receiver length, N – the number of Rx antennas and w is the receiver weight value calculated in Matlab (one of $w3$, $w3i$ or $w3enh$). The value f is displayed in the command window. Also real parts of all receiver weight values are plotted at the figure with number $figNo$.

1.10 getCoI_nonhssfn.m

The function calculates SINR for the SA case.
Input arguments:

 – w – receiver weight value,
 – H – matrix constructed from a matrix with multipath components of the link between the main transmitting Node B and rx-antennas of the UE,
 – Cw – thermal noise matrix,
 – $H\_interfs$ – matrix constructed from matrices with complex multipath components of the link between interfering Node B and rx-antennas of the UE,
 – Pj – pathloss from Node Bs to the UE divided by pathloss from own Node B,
 – d – delay vector,

- *dh* – delay matrix,
- *P_ctrl* – relative power of control channel,
- *P_data* – relative power of data channel.

Output arguments:

- *C* – signal power value,
- *I1* – interpath interference,
- *I2* – thermal interference,
- *I3* – colored interference.

The SINR value is calculated according to (54). Colored interference is calculated with the help of function `getColoredInterf.m.`

1.11 getCoI_hssfn.m

The function calculates SINR for the HS-SFN and PA cases.
Input arguments:

- *w* – receiver weight value,
- *H_C* – matrix $H_{combined}$,
- *H* – matrix constructed from a matrix with multipath components of the link between the main transmitting Node B and rx-antennas of the UE,
- *Cw* – thermal noise matrix,
- *H_interfs* – matrix constructed from matrices with complex multipath components of the link between interfering Node B and rx-antennas of the UE,
- *Pj* – pathloss from Node Bs to the UE divided by pathloss from own Node B,
- *d* – delay vector,
- *dh* – delay matrix,
- *P_ctrl* – relative power of control channel,
- *P_data* – relative power of data channel,

Output arguments:

- *C* – signal power value,
- *I1* – interpath interference,
- *I2* – thermal interference,
- *I3* – colored interference.

The SINR value is calculated according to (56). Colored interference is calculated with the help of function `getColoredInterf_c.m .`

1.12 getColoredInterf.m

The function returns the value of colored noise for the SA case.
Input arguments:

- w – receiver weight value,
- $H\_interfs$ – matrix constructed from matrices with complex multipath components of the link between interfering Node B and rx-antennas of the UE,
- Pj – pathloss from Node Bs to the UE divided by pathloss from own Node B.

The output argument is the value of colored noise in the SA case. Colored noise is calculated according to (21).

1.13 getColoredInterf_c.m

The function returns the value of colored noise for the SA case.

Input arguments:

- w – receiver weight value,
- $H\_interfs$ – matrix constructed from matrices with complex multipath components of the link between interfering Node B and rx-antennas of the UE,
- Pj – pathloss from Node Bs to the UE divided by pathloss from own Node B,
- P_ctrl – relative power of control channel.

The output argument is the value of colored noise in the HS-SFN and PA cases. Colored noise is calculated according to (57).